ANL-7488

ANL-7488
ANL-7488
ANL-7488
ANL-7488
ANL-7488
ANL-7488
ANL-7488
ANL-7488
ANL-7488
ANL-7488
ANL-7488
ANL-7488
ANL-7488
ANL-7488
ANL-7488
ANL-7488
ANL-7488
ANL-7488

The facilities of Argonne National Laboratory are owned by the United States Government. Under the terms of a contract (W-31-109-Eng-38) between the U. S. Atomic Energy

The facilities of Argonne National Laboratory are owned by the United States Government. Under the terms of a contract (W-31-109-Eng-38) between the U. S. Atomic Energy

The facilities of Argonne National Laboratory are owned by the United States Government. Under the terms of a contract (W-31-109-Eng-38) between the U. S. Atomic Energy

The facilities of Argonne National Laboratory are owned by the United States Government. Under the terms of a contract (W-31-109-Eng-38) between the U. S. Atomic Energy

The facilities of Argonne National Laboratory are owned by the United States Government. Under the terms of a contract (W-31-109-Eng-38) between the U. S. Atomic Energy

The facilities of Argonne National Laboratory are owned by the United States Government. Under the terms of a contract (W-31-109-Eng-38) between the U. S. Atomic Energy

The facilities of Argonne National Laboratory are owned by the United States Government. Under the terms of a contract (W-31-109-Eng-38) between the U. S. Atomic Energy

The facilities of Argonne National Laboratory are owned by the United States Government. Under the terms of a contract (W-31-109-Eng-38) between the U. S. Atomic Energy

The facilities of Argonne National Laboratory are owned by the United States Government. Under the terms of a contract (W-31-109-Eng-38) between the U. S. Atomic Energy

The facilities of Argonne National Laboratory are owned by the United States Government. Under the terms of a contract (W-31-109-Eng-38) between the U. S. Atomic Energy

ANL-7488
Engineering and
Equipment

ARGONNE NATIONAL LABORATORY
9700 South Cass Avenue
Argonne, Illinois 60439

FORCE-REFLECTING SERVOMECHANISMS WITH SIGNAL-TRANSMISSION TIME DELAY

by

William M. Thompson

Reactor Engineering Division

September 1968

Submitted in Partial Fulfillment of the
Requirements for the Degree of
Doctor of Philosophy in Electrical Engineering
in the Graduate School of
Illinois Institute of Technology

TABLE OF CONTENTS

	Page
SUMMARY	9
I. INTRODUCTION	11
A. Development of Remote Manipulators	11
B. Force-reflecting Servomechanisms	11
C. Signal-transmission Time Delay	12
D. Objective and Scope	13
E. Previous Research in Related Fields	13
F. Conventional Analytical Techniques and Their Limitations	14
G. Special Stability Problems of Force-reflecting Servomechanisms	15
H. Statement of the Specific Problem	16
I. The Pontryagin Stability Criterion	16
J. Other Techniques	17
K. Contributions of This Report	18
L. Outline of Report	18
II. DEVELOPMENT OF SYSTEM EQUATIONS	20
A. System Description	20
B. System Equations	21
C. The Transformed Equations	23
D. Form of Solutions of the System Equations	26
E. Network Representation	29
F. Characteristic Equation of Loaded System	30
G. Modification and Normalization of the Characteristic Equation	31
H. Other Terminal Conditions	33
I. Comments on the Characteristic Equation	34
J. Zeros at the Origin	35
K. Acceptable Location of Zeros for Stability	36
III. APPLICATION OF CONVENTIONAL TECHNIQUES	37
A. Application of Nyquist's Criterion	37
B. Satche Diagrams	39
C. Bode Diagrams	41
D. Analog Computer Setup	45
E. The System without Delay	49
IV. DEVELOPMENT OF A NEW METHOD OF APPLICATION OF PONTRYAGIN'S STABILITY CRITERION FOR FORCE-REFLECTING SERVOMECHANISMS	54
A. Introduction	54
B. Preliminary Considerations	55
C. The Pontryagin Criterion	56

TABLE OF CONTENTS

Page

D. Basis of the Criterion 58
E. Discussion of the Application of the Criterion. 61
F. The New Method of Application 62
G. Example of the Procedure. 63
H. Adjustment of the Parameters to Find Stability Boundaries. 67
I. Stability Diagrams. 68
J. Summary of the Procedure 71

V. EXTENSION OF THE CRITERION TO DETERMINE RELATIVE STABILITY 73

A. Contour with Radial Boundaries 73
B. The Composite Contour 76
C. Example of the Procedure. 78
D. Relative-stability Diagrams 80
E. Another Example. 82
F. Summary 83

VI. ANALYTICAL AND EXPERIMENTAL RESULTS 84

A. Analytical Results 84
B. Experimental Results. 85
C. Other Verification 90

VII. OTHER APPLICATIONS OF THE NEW TECHNIQUES 92

A. Load Effects. 92
B. Application to Classical Problems 94
C. An Alternate Procedure 96

VIII. CONCLUSIONS, EXTENSIONS, AND RECOMMENDATIONS . . 98

A. Summary and Conclusions. 98
B. Extension of Application of the Procedure 101
C. Recommendations for Future Research 102

APPENDIXES . . . .

A. Complete Nyquist Diagrams 103
B. Complete Satche Diagram 105
C. Asymptotic Zeros of System Equation 107
D. Adapting the Procedure for a Zero at the Origin 110

ACKNOWLEDGMENTS 111

REFERENCES 112

LIST OF FIGURES

No.	Title	Page
1.	Arrangement of Elements of Force-reflecting Servomechanism	20
2.	Block Diagram of Force-reflecting Servomechanism	25
3.	Network Representation of a Force-reflecting Servomechanism	29
4.	Nyquist Diagrams for the System with Different Time Delays	38
5.	Satche Diagram for System	40
6.	Block Diagram Showing Tandem, Single-loop Composition of the System	41
7.	Asymptotic Bode Plot for $\lvert G(j\omega)\rvert$	43
8.	Region of Unconditional Stability in the (k_1, k_2)-plane for $d_1 = d_2 = 0.9$	45
9.	Analog-computer Setup for Simulation of the System	48
10.	Stable Regions in (k_1, k_2)-plane for System with No Delay	52
11.	Root-locus Plots for System with No Delay	53
12.	Contour Used in Pontryagin Criterion	59
13.	G Functions for $\tau = 3\pi/4$ sec	64
14.	F Functions for $\tau = 3\pi/4$ sec	64
15.	Zeros of F and G for $\tau = 3\pi/4$ sec and $a = b = c = 0.8$	65
16.	Allowable F_2 Curves for $c = 0.9$ and $\tau = 3\pi/4$ sec	68
17.	Stability Diagram for a, b, and c with $\tau = 3\pi/4$ sec	69
18.	Stable Region in (k_1, k_2)-plane for $\tau = 3\pi/4$ sec and $d_1 = d_2 = 0.9$	70
19.	Stability Diagram for a, b, and c with $\tau = \pi/8$ sec	70
20.	Stable Region in (k_1, k_2)-plane for $\tau = \pi/8$ sec and $d_1 = d_2 = 0.9$	71
21.	First Contour for Determination of Relative Stability	73
22.	Composite Contour for Determination of Relative Stability	76
23.	Relative-stability F Functions for $\tau = \pi/8$ sec	78
24.	Relative-stability G Functions for $\tau = \pi/8$ sec	78

LIST OF FIGURES

No.	Title	Page
25.	Zeros of F and G along Relative-stability Contour for $a = b = c = 0.8$ and $\tau = \pi/8$ sec	79
26.	Relative-stability Diagrams for $\tau = \pi/8$ sec.	81
27.	Relative-stability F Functions for $\tau = 3\pi/4$ sec	82
28.	Relative-stability G Functions for $\tau = 3\pi/4$ sec	82
29.	Stability Regions in (k_1, k_2)-plane for $d_1 = d_2 = 0.9$ and Different Values of Time Delay	84
30.	Oscillograph Traces for Tests with $k_1 = k_2 = 0.9$, $d_1 = d_2 = 0.9$, and $\lambda = 0$	86
31.	Oscillograph Traces for Tests with $k_1 = k_2 = 0.9$, $d_1 = d_2 = 0.9$, and $\lambda = \pi/800$ sec	87
32.	Oscillograph Traces for Tests with $k_1 = k_2 = 0.9$, $d_1 = d_2 = 0.9$, and $\lambda = 3\pi/400$ sec	87
33.	Oscillograph Traces for an Unconditionally Stable System with $k_1 = k_2 = 1.0$, $d_1 = d_2 = 0$, and $\lambda = \pi/8$ sec	88
34.	Points in Stability Region That Were Tested Experimentally	89
35.	Complete Nyquist Diagrams	103
36.	Complete Satche Diagram	106

TABLE

No.	Title	Page
I.	Analog-computer Results for $\tau = \pi/8$ sec and $d_1 = d_2 = 0.9$	89

FORCE-REFLECTING SERVOMECHANISMS WITH SIGNAL-TRANSMISSION TIME DELAY

by

William M. Thompson

SUMMARY

The absolute and relative stability of a force-reflecting servomechanism with time delay in the signal-transmission channels is investigated by several methods. One method uses a stability criterion for time-lag systems due to Pontryagin. This criterion is adapted and extended for use in this study.

The servomechanism is the type that provides the connecting links in currently used, electrically connected, master-slave manipulators. The time delay is due to the time required for signals to traverse the distance between the master and slave arms, if they are separated by large distances. Two time delays of approximately 4 and 23 msec are used to illustrate the Pontryagin method. The latter delay corresponds to a separation distance of about 4000 miles.

The analog-computer simulation of the system indicated that the stability is very sensitive to the values of gain in the signal-transmission channels. Therefore, one objective was to determine the stable regions in gain-parameter space. Some stability information is developed by using conventional techniques, such as those of Nyquist, Satche, Bode, and Routh. However, the desired information cannot be obtained conveniently by any of these methods because of the number of parameters involved and the complexity of the system.

The stability information is obtained by using the Pontryagin criterion. This criterion gives the conditions under which exponential polynomials have zeros only in the left half complex plane. The characteristic equation of this system can be put into the form of an exponential polynomial. The criterion involves investigating the zeros of the real and imaginary parts of the exponential polynomial evaluated along the imaginary axis. These zeros must be real, simple, and alternating.

A new method of application of the criterion had to be developed. All earlier applications involved system equations of lower order for which simple trigonometric relations could be derived. This system is fourth order, and no such simple relations exist. The method uses the

convenience of digital computation and a simple graphical procedure to check the zeros. A procedure is also given for easily changing the location of the zeros of the real and imaginary parts by adjusting the parameters so that the limits of stability in gain-parameter space can be found.

The criterion is based on a fundamental theorem of complex variable theory, Cauchy's principle of the argument, and is explained in those terms. Adhering to this principle permits the criterion to be extended to give information on relative stability. By this means, zeros can be excluded from certain regions in the left half plane near the imaginary axis.

Examples of the procedures are given, and regions of stability and realtive stability are determined in gain-parameter space. The results were verified by analog-computer tests and by direct calculation of the zeros. A magnetic tape recorder was used to simulate the delay. The results show that there is some slight improvement in relative stability for delays up to about 4 msec. For the delay of 23 msec, however, the desired relative stability cannot be achieved for any reasonable values of gain.

Also discussed is the use of the new procedures to determine effects of loads on the system and to solve some classical problems of a more complicated form.

CHAPTER I

INTRODUCTION

Force-reflecting servomechanisms of the type studied in this report were developed along with, and for use in, electrically connected master-slave manipulators. Therefore, this introduction begins with a discussion of remote-manipulator development and its association with force-reflecting servomechanisms.

A. Development of Remote Manipulators

The need for remote manipulation has existed for many years in the nuclear-energy field where work must be carried out on highly radioactive material. Currently, a similar need is arising in the space and undersea programs. As a result of these continuing needs, different kinds of remotely controlled manipulators have been developed. Each, with various degrees of efficiency, allows a person to perform manipulations or experiments in a hazardous location while he is in a safe environment separated from the hazard by shielding or distance.

One kind of manipulator that has been very useful and popular, because it is easily and naturally controlled, is the master-slave manipulator. This type manipulator was invented about 20 years ago at Argonne National Laboratory where there has been a continuous manipulator development program ever since.[1]

A master-slave manipulator consists of two mechanical arms connected together either mechanically or electrically. The slave arm can be located in a remote or hazardous area, where it will follow almost exactly the motions of the master arm. A human operator controls the motion of the master arm by moving the control handle with his hand. A master-slave manipulator must have at least seven motions, that is, seven degrees of freedom. Three translational motions are necessary to move an object around in space, three rotational motions to orient it, and one grasping motion to hold it. If complex manipulations are to be carried out safely and efficiently, this manipulator must also have the feature of reflecting load forces back to the operator's hand; otherwise, uncontrolled and excessive forces could be applied at the slave without the immediate knowledge of the operator. A mechanically connected master-slave manipulator has this feature inherently because the two arms are coupled together tightly by linkages, steel cables, or steel tapes. An electrically connected one, however, requires a special system to achieve force reflection.

B. Force-reflecting Servomechanisms

The connecting links in an electrically connected master-slave manipulator are force-reflecting servomechanisms.[2,3] These systems simulate

mechanical connections by providing both positional correspondence and force reflection between input and output. Seven complete systems, one for each degree of freedom, are required for a manipulator. Force-reflecting servomechanisms, which were also developed at Argonne National Laboratory, have been successfully applied to several master-slave manipulators.[4-9]

A major advantage of using force-reflecting servomechanisms in master-slave manipulators is that they allow complete mechanical separation of the master and slave arms, while retaining the natural control features and much of the "feel" capability of mechanically connected manipulators. This advantage was only partially exploited in an application[10] where the slave arms were mounted on overhead movable bridges inside a sealed, shielded enclosure, and direct viewing was possible through shielding windows. Only direct wire connections were used between the arms. The signal cable lengths were relatively short, less than 100 ft to traverse take-up pulleys, penetrate shielding, and reach control amplifiers.

C. Signal-transmission Time Delay

Another possible extension of application of force-reflecting servomechanisms is to situations where direct wire connections are either not possible or not practical. A radio link is likely to be used in applications where distances are large, but it may also be advantageous for short distances to eliminate such problems as remote cable handling. The companion and necessary viewing system may require a radio link for similar reasons. If radio links are employed in a manipulator, the only limit to the amount of separation that can be achieved between master and slave is due to the effects of the signal-transmission time delay, that is, the finite time interval required for the signal to traverse the distance involved. This time delay may not be significant for most earth applications of manipulators. It can, however, become significant in many space applications. For example, the force-reflecting servomechanism used in the latest manipulator becomes unstable if the signal delay is only 23 msec. This corresponds to a separation distance of about 4000 miles.

Signal-transmission time delay may occur from many other causes besides the transmission time of wireless transmission systems. In any transmission system, if the number of signal channels is limited, signal multiplexing may be necessary. This could introduce a significant delay, especially if the signal must be digitized. Also, if any digital computations and modification were done with the signal, the computation time would add to the delay. Of course, if these delays are significant with respect to system time constants, the systems involved may have to be considered as sampled-data systems. In continuous systems, however, other delays can

also occur, for example, because of the use of hydraulic or pneumatic components. Even if short distances are involved, such systems can produce significant time delays that can accumulate at a rate as high as 1 msec/ft of connecting line.

D. Objective and Scope

The purpose of this investigation is to study the effects of signal-transmission time delay on force-reflecting servomechanisms, develop an analytical method for predicting their stability, and devise means for compensating for deleterious effects of the delay. The study is concerned with the type of force-reflecting servomechanism that has been successfully applied to manipulators. It is a continuous system to which will be added time delay in the signal-transmission channels. The signal channels will be assumed to have no effect on the signals except to delay them.

The term "signal-transmission time delay" has been used thus far in preference to other terms such as transport lag, because the delays under study occur only in the signal channels, as opposed to a delay in an output variable. Much of the analytical development, however, can be applied directly or with slight modification to any system with delay. The term "time delay" or just the word "delay," when the meaning is clear, shall be used as a convenient abbreviation of the above expression. The term "time lag" shall refer to the delay in time of any variable.

E. Previous Research in Related Fields

Systems with time lag have been studied extensively, and several excellent bibliographies exist. Those by Weiss[11] and Choksy[12] are comprehensive and easily available. Many pertinent references are contained in the bibliography of a thesis by Pierre.[13] A recent bibliography appears in a book by Oguztoreli.[14] Choksy[15] and Krall[16] have written review papers on stability criteria for time-lag systems.

Besides the continuing research and development program on force-reflecting servomechanisms for manipulators at Argonne National Laboratory, there have been research programs on these systems elsewhere.[17,18] Several of these have been sponsored by Argonne at nearby universities and have resulted in theses. Three were Ph.D. theses by Chalmers,[19] Weaver,[20] and Arzbaecher,[21] and one, a master's thesis by Schmidt.[22] A brief review of these follows.

Chalmers' thesis applies certain features of electrical network theory to force-reflecting servomechanisms by using electrical-mechanical analogies. He shows that under certain conditions a force-reflecting servomechanism can be represented by a passive, two-port mechanical

(or analogous electrical) network and, therefore, is stable for all passive load conditions. He develops a synthesis procedure, which provides for specified servomechanism characteristics while retaining the passivity conditions. Burnett has written a brief review of this network representation technique.[23]

Weaver's thesis develops a synthesis procedure for making a single-loop servomechanism containing a time lag have a specified response to a step input. He does not discuss the application to force-reflecting servomechanisms.

In the first part of his thesis,[21] Arzbaecher investigates the effects of positive- and negative-force feedback on servomechanisms. In a major section devoted to force-reflecting servomechanisms, he shows the possibilities of improving the sense of feel of such systems by using force feedback, which effectively reduces the inertia and friction of the system. He develops stability criteria for such systems based on network-theory stability concepts. Schmidt[22] did some preliminary work on inertia and friction reduction in single-loop systems.

Remote manipulation with transmission delay was studied extensively by Sheridan and Ferrell.[24-26] Their research was concerned mostly with the effects of transmission delay on the ability of the operator to perform certain manipulative tasks. The manipulator used in their experiments was a servo-driven master-slave positional system with two translation motions and one grasping motion. There was no force feedback to the operator. There have been some experiments on the above system with the addition of tactile force feedback in the grasping motion.[27] The force feedback was achieved by using signals from strain gauges to drive a motor on the master control. Instabilities occurred under certain conditions of force-feedback gain when contact was made with fixed loads. I have observed this kind of instability on systems of this type even without time delay. This is one of the reasons why force-reflecting servomachanisms of this type, using force transducers, have not been successfully applied to manipulators. Arzbaecher (Chapter 4 in Ref. 21) discusses this type of force-reflecting servomechanism.

F. Conventional Analytical Techniques and Their Limitations

The force-reflecting servomechanism under study in this investigation is a constant, multivariable, linear system with time lag. Bellman and Cooke showed that the response of such a system is determined by the location of the zeros of its characteristic equation.[28] It is a fourth-order system, and the characteristic equation for the system without delay is a fourth-order polynomial. With delay, the equation includes exponential functions, which make it transcendental, and, as a result, it has an infinite number of zeros. As for a system without delay, the system is stable if

no zeros are in the right half complex plane, and relatively unstable, or lightly damped, if the zeros in the left half plane are much closer to the imaginary axis than the real axis.

Of the various mathematical tools available for determing the stability or relative stability of systems with time lag, none was well suited to the system under study. Although some preliminary information was obtained using conventional techniques such as a generalized form of the Nyquist criterion, the dual-locus Satche diagrams, and Bode plots, these techniques were not tractable when the variation of more than one parameter was involved. Also, very little information concerning relative stability could be obtained by using these methods.

G. Special Stability Problems of Force-reflecting Servomechanisms

The stability and performance of the force-reflecting servomechanism under study depend on four parameters that are very susceptible to variation. These are the relative gains of the four signal-transmission channels that form the communication link between master and slave. Four separate channels are required, one each for position and velocity signals in each direction. Although the position and velocity signals could be combined for transmission, their gains would be independently adjustable, and therefore a separate channel is considered for each.

The effects of variation of the gain parameters were discovered while investigating the anomalous behavior of a model of the system that was set up on an analog computer. Without any time delay in the transmission channels, the system was unstable for many settings of the channel gains, both above and below their nominal values. The instability was manifested by an exponential, and sometimes oscillatory, growth of the error between the master and slave positions. When it was determined that the stability of the system depended on the relative gain settings of the transmission channels, rather than extraneous factors like computer-amplifier drift, it was decided to establish the stable regions in gain-parameter space before proceeding to the systems with time delay.

This instability due to gain variations does not occur in the currently used systems without delay because they are not arranged for a long-distance signal transmission. In such cases, a single error-in-position signal is generated at one end and is instantly transmitted to the other so that the same signal drives both the master and slave. When transmission delay is involved, however, there are two position-error signals, one generated at each end, and they are probably at least slightly different. A similar situation prevails for the velocity-error signals.

In a system with time delay, single error signals could be generated at one end and transmitted to the other. With this arrangement, one component of the signal at the far end would have twice the delay: one delay due to its original transmission, and another due to its return as part of the error signal. Because of the double delay in a loop where none existed before, investigation of this system was abandoned.

As the effect of variation of gain parameters on the stability of the system without delay was being investigated, difficulties in using conventional analytical techniques became apparent. Whereas complex plane plots had been employed earlier, they were not useful in this case, even without the delay, because of the large number of plots required to indicate the effects of parameter changes. Varying only one parameter at a time allowed some information to be produced by root-locus plots. The most useful technique, however, was employing Routh's criterion, and it was primarily by this means that the desired stability regions in parameter space were determined.

H. Statement of the Specific Problem

After the establishment of the stability regions in transmission-gain parameter space for force-reflecting servomechanisms without signal delay, it was appropriate to do the same for systems with delay. In addition, it was desirable to establish regions where a certain amount of relative stability exists and also to determine the effects due to the variation of other parameters. Therefore, the specific problem was to establish a means of obtaining this information. Of the well-known techniques, some, like the Routh criterion, could not be applied, and some, like root-locus plots could be applied only with considerable difficulty. A less well-known stability criterion, the Pontryagin Stability Criterion, seemed to show some promise, but it required modification in method of application and extension in scope. Through this criterion the desired results were obtained.

I. The Pontryagin Stability Criterion

Choksy[29] developed a stability criterion for control systems with time lags. It is based on work by Pontryagin which deals with the problem of determining if any zeros of exponential polynomials lie in the right half complex plane. The characteristic equation of the system under study can be put into the form of an exponential polynomial. Bellman[28,31] also summarized Pontryagin's results. Choksy gave his statement of the criterion in his review article.[15]

Although the Pontryagin criterion is basically not limited in application to systems of any order, in most published examples it was used only for systems of second order or less. (For example, see papers by Bhatt and Hsu.[32,33])

In addition, all examples, including one with a third-order characteristic equation,[34] were such that simple, explicit, analytical relations could be obtained among the trigonometric quantities involved. The system under study is fourth order, and no simple relationships could be evolved. Therefore, it was necessary to develop a new method of application for higher-order systems and in such a way that the effects of the variations of the gain parameters could be easily determined. To this end, a graphical technique with extensive use of digital computation was developed.

As established, the Pontryagin criterion is one for determining absolute stability. In this report, it is extended to provide information on relative stability.

J. Other Techniques

Other stability techniques were briefly investigated, but because of the successful results with the Pontryagin criterion they were not pursued exhaustively. The methods of Lyapunov have been applied to time-lag systems, but appear to offer more advantage for nonlinear systems or linear systems with time-varying parameters.[35] Even for linear constant systems, however, there is much computational difficulty with systems of first order.[36] The Laplace-transform techniques resulting in a transcendental characteristic equation are considered more productive. (For example, see the remark by Oguztoreli,[14] p. 112.) The results from the Pontryagin criterion give the necessary and sufficient conditions for stability. The results from Lyapunov methods are likely to be sufficient conditions, which would require more restrictive parameter settings.

Yuan-Shun[37] developed a technique for determining if a system with time lag is unconditionally stable, that is, stable for all values of time lag. He showed that a system is unconditionally stable if it is stable for no lag and there are no zeros of its characteristic equation along the imaginary axis. The second condition is transformed into one for finding if there are any real roots of an algebraic equation. A second-order system, however, results in a quartic algebraic equation, and the method becomes complicated. Chapter III of this report presents a method for finding similar information from Bode plots. The requirement for unconditional stability is usually too severe a restriction to put on a system.

Eisenberg[38] presented another technique for determining the absolute or relative stability of a linear system with time lag. He treated a system with two free parameters in linear combination; that is, no products of parameters occur. He transformed the real and imaginary parts of the system's characteristic equation into a form containing Chebyshev functions

and the parameters. Setting each part of the equation equal to zero, he could solve for each parameter, since he had two linear equations for the parameters. These equations define either a stability or a relative-stability boundary in the parameter plane, depending on the contour used for evaluting the characteristic equation. Chebyshev functions were used as a computational aid. This technique could not be applied directly to the system under study because more than two parameters are involved. Even when only two parameters are considered at a time, they do not occur linearly. In addition, the method depends on the relative-stability contour having radial lines as boundaries. Therefore, it would not apply to the main relative-stability boundary used here. Also, in this case there seems to be no special advantage in transforming to Chebyshev functions when the computations can be performed easily directly.

K. Contributions of This Report

This report has made the following contributions to the fields of remote and automatic controls:

1. The research on force-reflecting servomechanisms has been extended to include systems in which there is significant time delay in the signal channels. The effects of varying certain critical parameters are determined.

2. A new, graphical technique of application of Pontryagin's stability criterion for time lag systems has been developed. It uses the convenience of digital computation and provides the advantages that it can be applied to systems of any order and that the effects of the variations of certain parameters can be found easily.

3. The Pontryagin criterion has been extended to provide information about the relative stability of time-lag systems.

4. The basis of the proof of the Pontryagin criterion has been explained in terms more common to control engineers, with the possible result that a better understanding will promote a greater number of applications and extensions.

L. Outline of Report

The following is a brief outline of the material in the remaining chapters of this report.

Chapter II describes the basic force-reflecting servomechanism under study and develops the basic equations. From these, the normalized characteristic equation is produced. Chapter III describes the initial

investigations of the system, by the use of conventional analytical techniques. Here is given the analog computer setup on which the effects of the variation of gain parameters were noticed. This chapter also gives the conventional techniques used to provide the stability regions in gain-parameter space for systems without delay.

Chapter IV begins the discussion of the Pontryagin criterion. The first part of this chapter describes the criterion and its proof. Then the new method application is developed and illustrated. Chapter V extends the criterion to provide information about relative stability by restricting the regions in the complex plane wherein the zeros of the characteristic equation can lie. The proper region is developed, and the technique is illustrated.

Chapter VI contains the analytical results of the stability regions in gain-parameter space devloped from the Pontryagin criterion. Certain points are verified by analog-computer experiments. Chapter VII discusses other applications of the new techniques to determine load effects and solve classical problems. Chapter VIII contains the conclusions and possible areas of extended research.

For those interested only in the new techniques, the material has been arranged so that they may proceed directly to Chapter IV, where the discussion of Pontryagin's criterion begins.

CHAPTER II

DEVELOPMENT OF SYSTEM EQUATIONS

A. System Description

The system chosen for study in this investigation is the force-reflecting servomechanism with the arrangement of elements shown in Fig. 1. The system includes two separate mechanical assemblies each having a motor, a positional transducer, a velocity transducer, and an output shaft, connected together with gears. Each motor is controlled by an amplifier whose input is a combination of signals from the transducers. Four signal channels with transmission time delay transfer the signals between the two separated parts of the system. Although the system is completely symmetrical as shown and can operate equally well in either direction, the left shaft is usually referred to as the input of the system and the right as the output.

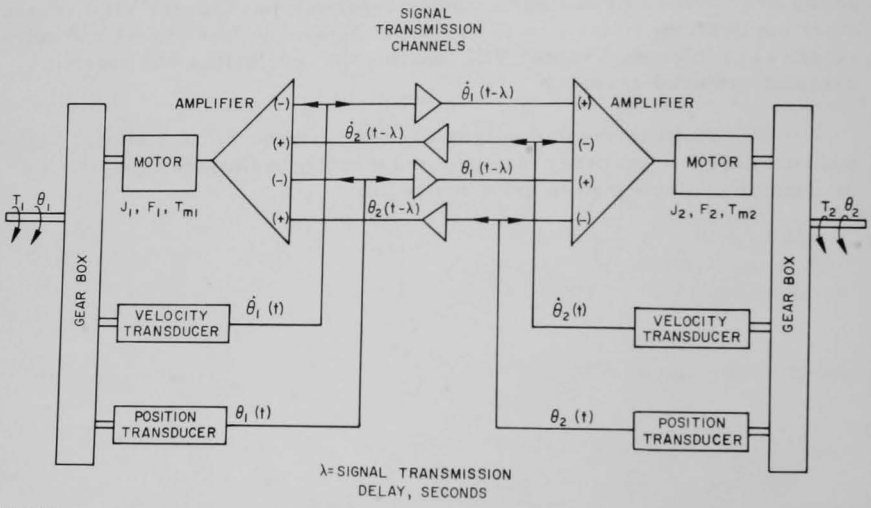

112-9486

Fig. 1. Arrangement of Elements of Force-reflecting Servomechanism

In the absence of time delay in the signal channels, this system is very effective as a force-reflecting servomechanism. It is essentially a combination of two positional servomechanisms, both operating to bring the input and output shafts into positional correspondence. If there is a positional difference, the same positional error signal appears at the input of each amplifier, and the motors tend to run in opposite directions with equal torques to correct this error. If this action is prevented by the externally applied torques, T_1 and T_2, they must also be equal and opposite to balance

the motor torques, thus giving torque reflection (force reflection in a linear-motion system). Effectively, the input and output shafts appear to be coupled together by a torsional spring. In addition, the system also tends to produce velocity correspondence between the two shafts by using the velocity error signal. Accurate torque reflection and position or velocity correspondence are achieved only under steady-state conditions of zero or constant velocity because of the time and the torque necessary to accelerate the inertia of the system. The situation is somewhat similar in the system with time delay, except that more time will lapse before steady-state conditions are achieved.

Although a force-reflecting servomechanism can be made up of other arrangements of elements[3] or have more elements such as force or torque transducers,[21] the system selected is the simplest type. Except for the time delay, it is the type that has been successfully applied in master-slave manipulators.[4,6,7,9,10] In future applications where the separation between the master and slave arms would result in significant transmission time delay for the signals, there would be a strong tendency to retain the same system. During this study, no reason developed to change the basic arrangement for the time delays considered. Furthermore, this system has the advantage of discouraging fast input motions that cannot be followed because of signal delay. Working at the input is like working into the output of a positional servomechanism until some signal returns from the far end; therefore the operator must exert considerable effort to produce fast motion.

B. System Equations

In most applications, the units on the gearbox shown in Fig. 1 would rotate at different speeds. In the equations below, however, all quantities are referred to the output shaft, and the gear ratios are included in the gain constants. Therefore, in the equations it appears that each unit rotates at the same speed. Also, the subscripts 1 and 2 refer to the input (left side) and output (right side) of the system, respectively, as shown in Fig. 1.

The basic torque equations, one for each side of the system, are

$$T_1(t) + T_{m1}(t) = J_1 \frac{d^2\theta_1(t)}{dt^2} + F_1 \frac{d\theta_1(t)}{dt} \tag{1}$$

and

$$T_2(t) + T_{m2}(t) = J_2 \frac{d^2\theta_2(t)}{dt^2} + F_2 \frac{d\theta_2(t)}{dt}, \tag{2}$$

where

T is an externally applied torque, ft-lb;

T_m is the torque developed by the motor, ft-lb;

J is the total rotary moment of inertia of the motor and its gearing, slug-ft^2 (ft-lb/rad/sec^2);

F is the coefficient of viscous friction of the motor and gearing, ft-lb/rad/sec;

and

θ is the position of the output shaft of the gearbox, radians.

The torques developed by the motors depend on the positions and velocity signals as follows:

$$T_{m1}(t) = -K_{11}\theta_1(t) + K_{12}\theta_2(t-\lambda) - D_{11}\frac{d\theta_1(t)}{dt} + D_{12}\frac{d\theta_2(t-\lambda)}{dt}, \tag{3}$$

and

$$T_{m2}(t) = K_{21}\theta_1(t-\lambda) - K_{22}\theta_2(t) + D_{21}\frac{d\theta_1(t-\lambda)}{dt} - D_{22}\frac{d\theta_2(t)}{dt}, \tag{4}$$

where

λ is the time delay of the signal transmission channel, seconds;

K_{ij} is the overall torque per unit of positional displacement constant that includes the transducer constant, amplifier gain, gearing ratio, and motor torque constant, ft-lb/rad;

and

D_{ij} is the overall torque per unit of velocity constant, similar to K, ft-lb/rad/sec.

The first subscript indicates the destination, and the second, the source of a signal.

The above equations represent a mathematical model of a force-reflecting servomechanism. The assumptions made in writing these equations are that the system is linear, the elements can be characterized by lumped constants, and the transmission channels have no other effects except that of pure delay. The motor (not necessarily an electric motor) is considered as a torque generator with linear speed-torque characteristics and with no time constant associated with torque buildup. These have proved to be reasonably good assumptions and approximations for previous studies of systems without signal delay and have resulted in good predictions of the behavior of actual systems in their normal working frequency range.

C. The Transformed Equations

The system equations are a set of linear differential-difference equations with constant coefficients. These equations can be solved by using the Laplace transformation.[28] The transforms of the functions with the delayed argument, $t - \lambda$, can be determined in the usual manner by multiplying by e^{-st} and integrating from zero to infinity. The requirements for initial conditions, however, are different. The functions must be specified for the initial period $-\lambda \leq t \leq 0$.

The initial conditions chosen in this case are

$$\left.\begin{aligned} \theta_1(t) &= A \\ \theta_2(t) &= \frac{d\theta_1(t)}{dt} = \frac{d\theta_2(t)}{dt} = 0 \end{aligned}\right\} \text{for } -\lambda \leq t \leq 0. \tag{5}$$

These are the initial conditions used in the analog-computer simulation tests. A magnetic tape recorder with separate record and playback heads was used to provide the time delay. With the tape recorder operating, the $\theta_1(t)$ variable was given a constant displacement at least one delay period before starting the problem.

Taking the Laplace transform of Eqs. 1-4 and using the above initial values gives

$$T_1(s) + T_{m1}(s) = J_1 s^2 \theta_1(s) - J_1 A s + F_1 s \theta_1(s) - F_1 A, \tag{6}$$

$$T_2(s) + T_{m2}(s) = J_2 s^2 \theta_2(s) + F_2 s \theta_2(s), \tag{7}$$

$$T_{m1}(s) = -K_{11}\theta_1(s) + K_{12} \int_0^\infty \theta_2(t-\lambda)\, e^{-st}\, dt - D_{11} s \theta_1(s)$$

$$+ D_{11} A + D_{12} \int_0^\infty \frac{d\theta_2(t-\lambda)}{dt} e^{-st}\, dt, \tag{8}$$

and

$$T_{m2}(s) = K_{21} \int_0^\infty \theta_1(t-\lambda)\, e^{-st}\, dt - K_{22}\theta_2(s)$$

$$+ D_{21} \int_0^\infty \frac{d\theta_1(t-\lambda)}{dt} e^{-st}\, dt - D_{22} s \theta_2(s), \tag{9}$$

where s is the Laplace transform variable.

The functions with the delayed argument are transformed by letting $\psi = t - \lambda$ and using the initial values. Thus, the first function becomes

$$\int_0^\infty \theta_2(t-\lambda)\, e^{-st}\, dt = \int_{-\lambda}^\infty \theta_2(\psi) e^{-s(\psi+\lambda)}\, d\psi$$

$$= e^{-s\lambda} \int_{-\lambda}^\infty \theta_2(\psi) e^{-s\psi}\, d\psi$$

$$= e^{-s\lambda} \int_0^\infty \theta_2(\psi) e^{-s\psi}\, d\psi$$

$$= e^{-s\lambda}\theta_2(s). \tag{10}$$

With the above result, the transform of the next function becomes

$$\int_0^\infty \theta_1(t-\lambda)\, e^{-st}\, dt = e^{-s\lambda}\left[\int_{-\lambda}^0 \theta_1(\psi) e^{-s\psi}\, d\psi + \theta_1(s)\right]$$

$$= e^{-s\lambda}\left[\int_{-\lambda}^0 Ae^{-s\psi}\, d\psi + \theta_1(s)\right]$$

$$= e^{-s\lambda}\left[-\frac{A}{s} + \frac{A}{s}e^{+s\lambda} + \theta_1(s)\right]$$

$$= e^{-s\lambda}\theta_1(s) + \frac{A}{s} - \frac{A}{s}e^{-s\lambda}. \tag{11}$$

The transform of the next function is found by using integration by parts as follows:

$$\int_0^\infty \frac{d\theta_2(t-\lambda)}{dt}\, e^{-st}\, dt = \theta_2(t-\lambda)\, e^{-st}\Big|_0^\infty + s\int_0^\infty \theta_2(t-\lambda)\, e^{-st}\, dt$$

$$= O - O + e^{-s\lambda} s\theta_2(s), \tag{12}$$

and, finally, the transform of the last function becomes

$$\int_0^\infty \frac{d\theta_1(t-\lambda)}{dt}\, e^{-st}\, dt = \theta_1(t-\lambda)\, e^{-st}\Big|_0^\infty + s\int_0^\infty \theta_1(t-\lambda)\, e^{-st}\, dt$$

$$= O - A + s\left[e^{-s\lambda}\theta_1(s) + \frac{A}{s} - \frac{A}{s}e^{-s\lambda}\right]$$

$$= se^{-s\lambda}\theta_1(s) - Ae^{-s\lambda}.$$

Using the above transforms in Eqs. 8 and 9 yields the following motor torque equations:

$$T_{m1}(s) = -K_{11}\theta_1(s) + K_{12}e^{-s\lambda}\theta_2(s) - D_{11}s\theta_1(s) + D_{12}e^{-s\lambda}s\,\theta_2(s) + D_{11}A, \tag{14}$$

and

$$T_{m2}(s) = K_{21}e^{-s\lambda}\theta_1(s) - K_{22}\theta_2(s) + D_{21}e^{-s\lambda}s\theta_1(s) - D_{22}s\theta_2(s) + K_{21}A(1 - e^{-s\lambda})/s - D_{21}Ae^{-s\lambda}. \tag{15}$$

If the system has no displacement during the initial period, that is, $A = 0$ for $-\lambda \geq t \geq 0$, Eqs. 6, 7, 14, and 15 can be used to produce the block diagram of the system shown in Fig. 2.

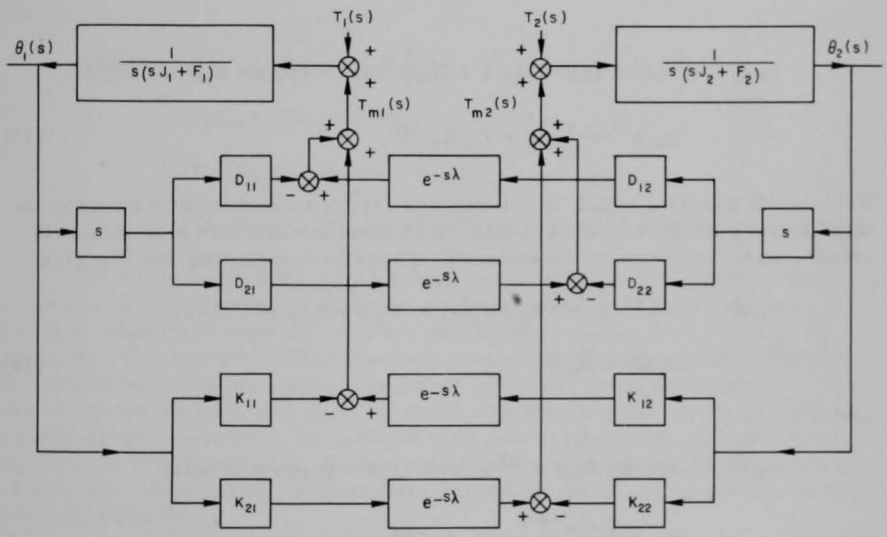

Fig. 2. Block Diagram of Force-reflecting Servomechanism

Figure 2 shows the signals that are combined to produce the motor torques. If there were no signal transmission delay and each of the K's and D's were equal to single constants, K and D, respectively, the motor torques would depend on the difference in position and the difference in velocity between the input and output shafts. These differences are the positional and velocity errors of the system. The motors are connected so that they tend to drive each side of the system in the direction to reduce these errors to zero. When there is signal-transmission delay, correct error signals generally are

not available instantaneously at either end. In addition, since the gain of each transmission channel cannot be set exactly or will not remain the same indefinitely, correct error signals may not be available at any time. The different K's and D's have been included in the equations to account for these unequal gains. As mentioned in the introduction, a major consideration of this report is determining the effects on the stability of the system due to using error signals that are modified by both the time delay and the unequal gains of the transmission channels.

After the substitution of the expressions for T_{m1} and T_{m2} from Eqs. 14 and 15 into Eqs. 6 and 7 and the rearrangement of terms, the system equations become

$$T_1(s) = \left[J_1 s^2 + (F_1 + D_{11})\, s + K_{11}\right] \theta_1(s) - (D_{12} s + K_{12})\, e^{-s\lambda} \theta_2(s) - J_1 A s - (F_1 + D_{11})\, A, \tag{16}$$

and

$$T_2(s) = \left[J_2 s^2 + (F_2 + D_{22})\, s + K_{22}\right] \theta_2(s) - (D_{21} s + K_{21})\, e^{-s\lambda} \theta_1(s) - K_{21} A \frac{1 - e^{-s\lambda}}{s} + D_{21} A e^{-s\lambda}. \tag{17}$$

Since each F-term, which is the viscous friction constant of its motor, is usually very small and always occurs in combination with a D-term, its effect can be included in the D-term. Therefore, dropping the F's gives

$$T_1(s) = (J_1 s^2 + D_{11} s + K_{11})\, \theta_1(s) - (D_{12} s + K_{12})\, e^{-s\lambda} \theta_2(s) - J_1 A s - D_{11} A, \tag{18}$$

and

$$T_2(s) = -(D_{21} s + K_{21})\, e^{-s\lambda} \theta_1(s) + (J_2 s^2 + D_{22} s + K_{22})\, \theta_2(s) - K_{21} A \frac{1 - e^{-s\lambda}}{s} + D_{21} A e^{-s\lambda}. \tag{19}$$

These equations represent the system shown in Figs. 1 and 2 in terms of input and output variables. To the extent that the previously made assumptions are valid, they can be used to determine the Laplace transform of the response of the system with or without external stimulation.

D. Form of Solutions of the System Equations

If the external torques $T_1(t)$ and $T_2(t)$ are considered as arbitrary forcing functions, Eqs. 18 and 19 can be solved for the transforms of the

angular positions of the shafts by using Cramer's rule. The results are

$$\theta_1(s) = \frac{J_2 s^2 + D_{22} s + K_{22}}{H(s)} [T_1(s) + J_1 As + D_{11} A]$$

$$+ \frac{(D_{12} s + K_{12})\, e^{-s\lambda}}{H(s)} \left[T_2(s) + K_{21} A \frac{1 - e^{-s\lambda}}{s} - D_{21} A e^{-s\lambda} \right] \tag{20}$$

and

$$\theta_2(s) = \frac{(D_{21} s + K_{21})\, e^{-s\lambda}}{H(s)} [T_1(s) + J_1 As + D_{11} A]$$

$$+ \frac{J_1 s^2 + D_{11} s + K_{11}}{H(s)} \left[T_2(s) + K_{21} A \frac{1 - e^{-s\lambda}}{s} - D_{21} A e^{-s\lambda} \right], \tag{21}$$

where

$$\begin{aligned} H(s) = {} & J_1 J_2 s^4 + (J_1 D_{22} + J_2 D_{11})\, s^3 \\ & + (J_1 K_{22} + J_2 K_{11} + D_{11} D_{22})\, s^2 \\ & + (K_{11} D_{22} + K_{22} D_{11})\, s + K_{11} K_{22} \\ & - \left[D_{12} D_{21} s^2 + (K_{12} D_{21} + K_{21} D_{12})\, s + K_{12} K_{21} \right] e^{-2s\lambda}. \end{aligned} \tag{22}$$

The inverse transforms of $\theta_1(s)$ and $\theta_2(s)$ give the complete time response of the system. If there is no delay, that is, $\lambda = 0$, these are rational, algebraic expressions, and taking the inverse transform is no problem. The nature of the time response depends on the poles of the expressions for θ. In this case, the poles can come from two sources. They are the poles of $T_1(s)$ and $T_2(s)$, if there are any, and the zeros of $H(s)$, the characteristic equation. In systems with delay, where the characteristic equation is transcendental, Bellman and Cooke have shown that the nature of the time response is likewise determined by the zeros of the characteristic equation.[28]

Just as for systems without delay, the time-domain solutions of the system equations consist of two parts. One is the complementary function or transient solution that depends on the initial values. The other is the particular or steady-state solution that depends only on the forcing functions T_1 and T_2. The transient solution indicates the stability or relative stability of the system. Therefore, attention can be limited to $T_1 = T_2 = 0$. In that case, Eq. 20 becomes

$$\theta_1(s) = \frac{P_1(s)}{H(s)}, \tag{23}$$

where

$$P_1(s) = (J_2 s^2 + D_{22} s + K_{22})(J_1 A s + D_{11} A)$$
$$+ (D_{12} s + K_{12})\, e^{-s\lambda}\left(K_{21} A \frac{1 - e^{-s\lambda}}{s} - D_{21} A e^{-s\lambda}\right). \tag{24}$$

The time-domain solution is the inverse Laplace transform of Eq. 23. This is

$$\theta_1(t) = \lim_{\omega \to \infty} \frac{1}{2\pi j} \int_{c-j\omega}^{c+j\omega} e^{st} \frac{P_1(s)}{H(s)}\, ds, \tag{25}$$

where the contour line of integration is to the right of all the singularities of the integrand. This integral can be evaluated by using the residue theorem. It is equivalent to an integral around a contour that encloses much of the left half plane. Therefore, many of the poles of the integrand, which are the zeros of H(s), are enclosed by that contour. Since there are an infinite number of zeros of H(s), no finite contour can enclose all of them. In this case, however, as shown later, the infinite chains of zeros of H(s) are in the left half plane. Therefore, successively larger contours, numbered N_k can be arranged so that the contour N_{k+1} encloses one more pole of the integrand than the contour N_k. Then the value of the integral becomes

$$\theta_1(t) = \lim_{k \to \infty} \left[\text{sum of the residues of } \frac{e^{st} P_1(s)}{H(s)} \text{ within the contour } N_k\right], \tag{26}$$

or

$$\theta_1(t) = \lim_{k \to \infty} \sum_{N_k} \exp(s_r t)\, p_r(t), \tag{27}$$

where $\exp(s_r t) p_r(t)$ is the residue of $e^{st} P_1(s)/H(s)$ at the zero, s_r, of H(s). The function $p_r(t)$ is a polynomial of one degree less than the multiplicity of s_r. Because the zeros can be put into a definite order and they have a certain limiting distance between them, $\theta_1(t)$ can be expressed as a convergent infinite series as follows:

$$\theta_1(t) = \sum_{r=1}^{\infty} \exp(s_r t) p_r(t). \tag{28}$$

If H(s) has no multiple zeros,

$$\theta_1(t) = \sum_{r=1}^{\infty} C_r \exp(s_r t), \tag{29}$$

where

$$C_r = \frac{P_1(s_r)}{H'(s_r)} \text{ and } H' = \frac{dH(s)}{ds}. \tag{30}$$

The expression for $\theta_2(t)$ is the same, except for the subscripts.

Similar series expansions can be obtained even when the system is forced. Therefore, for the system considered in this study, the response is determined by the zeros of the characteristic equation of the system. For example, if its characteristic equation has any zeros with positive real parts, the time response of the system to any disturbance will be a growing exponential and, therefore, the system is unstable. Much attention will be devoted to determining the regions in the complex plane where there are no zeros of the characteristic equation

$$H(s) = 0. \tag{31}$$

E. Network Representation

A force reflecting servomechanism can be represented by a four-terminal, two-port network. This representation has been useful in previous studies[19,21] and in this case provides a convenient device for discussing load effects or terminal conditions. Although the input and output variables are mechanical rotations and torques, the techniques of electric-network theory are applicable either directly or by using a suitable electrical-mechanical analog. The current-torque, voltage-velocity analog has been the more useful one for these systems and is employed here. Figure 3 shows analogous electrical and mechanical networks and their common admittance parameters. The equations, in transformed form, for the electric network with zero initial values, in terms of the admittance parameters are

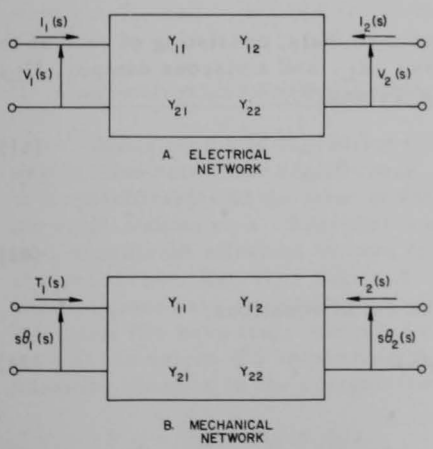

Fig. 3. Network Representation of a Force-reflecting Servomechanism

$$I_1(s) = Y_{11}(s)V_1(s) + Y_{12}(s)V_2(s), \tag{32}$$

and

$$I_2(s) = Y_{21}(s)V_1(s) + Y_{22}(s)V_2(s). \tag{33}$$

The equations for the mechanical network are

$$T_1(s) = Y_{11}(s)s\theta_1(s) + Y_{12}(s)s\theta_2(s), \tag{34}$$

and

$$T_2(s) = Y_{21}(s)s\theta_1(s) + Y_{22}(s)s\theta_2(s). \tag{35}$$

The Y-terms in Eqs. 34 and 35 are the mechanical-admittance parameters of the mechanical network. They can be manipulated in any way that is permitted for the admittance parameters of the electric network. Comparison with Eqs. 18 and 19 for the situation with zero initial values, that is, A = 0, gives the mechanical-admittance parameters for the force-reflecting servomechanism under study. These are

$$Y_{11}(s) = J_1 s + D_{11} + K_{11}/s, \tag{36}$$

$$Y_{12}(s) = -(D_{12} + K_{12}/s)\, e^{-s\lambda}, \tag{37}$$

$$Y_{21}(s) = -(D_{21} + K_{21}/s)\, e^{-s\lambda}, \tag{38}$$

and

$$Y_{22}(s) = J_2 s + D_{22} + K_{22}/s. \tag{39}$$

F. Characteristic Equation of Loaded System

A force-reflecting servomechanism must be stable for various conditions of load. The first requirement is that it be stable for no load. This involves investigating the zeros of the characteristic equation. The characteristic equation can also be written in terms of the admittance parameters. From Eqs. 34 and 35 for $T_1(s) = T_2(s) = 0$, it is

$$H(s) = s^2[Y_{11}(s)Y_{22}(s) - Y_{12}(s)Y_{21}(s)]. \tag{40}$$

This reduces to Eq. 22 when Eqs. 36-39 are substituted for the Y's.

For a passive load on the output terminals, consisting of each of the three elements, an inertia, J_L, a spring, K_L, and a viscous damper, D_L, there is an additional equation relating T_2 and θ_2,

$$-T_2(s) = Y_L(s) s \theta_2, \tag{41}$$

where

$$Y_L(s) = J_L s + D_L + K_L/s. \tag{42}$$

Substituting Eq. 41 into Eq. 35 gives the set of equations

$$T_1(s) = Y_{11}(s) s\theta_1(s) + Y_{12}(s) s\theta_2(s), \tag{34}$$

and

$$0 = Y_{21}(s) s\theta_1(s) + [Y_{22}(s) + Y_L(s)]\, s\theta_2(s). \tag{43}$$

The characteristic equation for this set is

$$H(s) = s^2\{Y_{11}(s)[Y_{22}(s) + Y_L(s)] - Y_{12}(s)Y_{21}(s)\}. \tag{44}$$

As can be seen by comparison to Eq. 40, this characteristic equation is modified by the addition of Y_L to Y_{22}. Since Y_{22} has been maintained as a separate term, different from Y_{11}, the effects of loading can be included in Y_{22}. If the base system is assumed to be symmetrical, then any variation from symmetry can be considered as partially due to loading. With the following substitutions

$$\left.\begin{aligned} J_1 &= J, \quad J_2 = J(1+\alpha); \\ D_{11} &= D, \; D_{22} = D(1+\beta); \\ K_{11} &= K, \; K_{22} = K(1+\gamma); \end{aligned}\right\} \tag{45}$$

the characteristic equation becomes

$$\begin{aligned} H(s) = {} & J^2(1+\alpha)\, s^4 + 2JD(1+0.5\alpha+0.5\beta)\, s^3 \\ & + 2JK(1+0.5\alpha+0.5\gamma)\, s^2 \\ & + [D^2(1+\beta) - D_{12}D_{21}e^{-2s\lambda}]\, s^2 \\ & + [2KD(1+0.5\beta+0.5\gamma) - K_{12}D_{21} + K_{21}D_{12})\, e^{-2s\lambda}]\, s \\ & + [K^2(1+\gamma) - K_{12}K_{21}e^{-2s\lambda}], \end{aligned} \tag{46}$$

where α, β, and γ are the variations from symmetry that include load effects.

G. Modification and Normalization of the Characteristic Equation

Some terms in Eq. 46 have been combined in a slightly different way to illustrate their significance. For an unloaded system, the magnitudes of the coefficients of the first-order and zero-order terms are close to zero for small values of s. Therefore, small changes in the coefficients could have significant effect on system behavior. As discussed earlier, the constituent terms, K_{12}, K_{21}, D_{12}, and D_{21}, which include the signal-transmission channel gains, are very likely to vary from their nominal values of K and D. When the K's have their nominal value, the characteristic equation has a zero at the origin. To emphasize the variations from nominal values, the following changes in the designation of the parameters are used:

$$\begin{aligned} K_{12} &= k_1K, \quad D_{12} = d_1D; \\ K_{21} &= k_2K, \quad D_{21} = d_2D; \end{aligned} \tag{47}$$

where the lower-case k's and d's have the nominal value of one. After substitution of these into Eq. 46 and rearrangement of the order, the equation becomes

$$
\begin{aligned}
H(s) \doteq\ & J^2(1+\alpha)\, s^4 + 2JD(1+0.5\alpha+0.5\beta)\, s^3 \\
& + 2JK(1+0.5\alpha+0.5\gamma)\, s^2 + D^2(1+\beta)\, s^2 \\
& + 2KD(1+0.5\beta+0.5\gamma)\, s + K^2(1+\gamma) \\
& - [D^2 d_1 d_2 s^2 + KD(k_1 d_2 + k_2 d_1)\, s + K^2 k_1 k_2]\, e^{-2s\lambda}.
\end{aligned}
\tag{48}
$$

Since the zeros of Eq. 48, the characteristic equation, are to be investigated, numerical values must be substituted for some of the parameters to keep the problem tractable. The values chosen are approximately those of a system used in a manipulator application without signal time delay. The facility for load changes and signal-channel gain changes is retained. The values used are

$$
\left.
\begin{aligned}
J &= 0.05 \text{ slug-ft}^2, \\
D &= 5 \text{ ft-lb-sec}, \\
\text{and} \quad & \\
K &= 250 \text{ ft-lb/rad.}
\end{aligned}
\right\}
\tag{49}
$$

After substitution of these values, Eq. 48 becomes

$$
\begin{aligned}
H(s) =\ & 0.0025(1+\alpha)\, s^4 + 0.5(1+0.5\alpha+0.5\beta)\, s^3 \\
& + 25(1+0.5\alpha+0.5\gamma)\, s^2 + 25(1+\beta)\, s^2 \\
& + 2500(1+0.5\beta+0.5\gamma)\, s + 62{,}500(1+\gamma) \\
& - [25 d_1 d_2 s^2 + 1250(k_1 d_2 + k_2 d_1)\, s + 62{,}500 k_1 k_2]\, e^{-2s\lambda}.
\end{aligned}
\tag{50}
$$

Because of the range of values of the coefficients, it is desirable to normalize this equation. The undamped natural frequency of the system with all nominal values and no signal delay is

$$
\omega_n = \sqrt{\frac{2K}{J}} = 100 \text{ rad/sec.} \tag{51}
$$

This factor is used to change the complex frequency and the time variables as follows:

$$\left.\begin{aligned} s &= 100\hat{s} \\ \lambda &= \tau/100 \end{aligned}\right\}. \tag{52}$$

The equation in terms of the new variables is

$$\begin{aligned} H(s) = 2.5 \times 10^5 \{&(1+\alpha)\,\hat{s}^4 + (2+\alpha+\beta)\,\hat{s}^3 \\ &+ (2+0.5\alpha+\beta+0.5\gamma)\,\hat{s}^2 \\ &+ (1+0.5\beta+0.5\gamma)\,\hat{s} + 0.25(1+\gamma) \\ &- [d_1d_2\hat{s}^2 + 0.5(k_1d_2+k_2d_1)\,\hat{s} + 0.25k_1k_2]\,e^{-2\hat{s}\tau}\}. \end{aligned} \tag{53}$$

Since only the zeros in this equation are of interest, the constant multiplying factor can be dropped. Also, since the normalized equation can be identified by the τ, the circumflex over the s is dropped. In addition, another substitution is convenient:

$$\left.\begin{aligned} a &= d_1d_2, \\ b &= k_1k_2, \\ \text{and} \quad & \\ c &= 0.5(k_1d_2+k_2d_1). \end{aligned}\right\} \tag{54}$$

After these changes, the characteristic equation is in its final general form,

$$\begin{aligned} H(s) = &(1+\alpha)\,s^4 + (2+\alpha+\beta)\,s^3 + (2+0.5\alpha+\beta+0.5\gamma)\,s^2 \\ &+ (1+0.5\beta+0.5\gamma)\,s + 0.25(1+\gamma) \\ &- (as^2+cs+0.25b)\,e^{-2s\tau}. \end{aligned} \tag{55}$$

H. Other Terminal Conditions

The other terminal conditions to be considered are those with one or both shafts locked so that they cannot move. This is equivalent to grounding or shorting the input or output terminals. If it is assumed that the output shaft is locked, $s\theta_2(s) = 0$, and Eqs. 34 and 35 become

$$T_1(s) = Y_{11}s\theta_1(s), \tag{56}$$

and

$$T_2(s) = Y_{21}s\theta_1(s). \tag{57}$$

The response of θ_1 to an input torque is, from Eq. 56,

$$\theta_1(s) = \frac{1}{sY_{11}(s)} T_1(s). \tag{58}$$

Therefore, the system characteristic equation is

$$H_{sc}(s) = sY_{11}(s). \tag{59}$$

Equation 57 merely relates T_2 to θ_1. T_2 cannot exist without θ_1 because Y_{21} has no finite poles, whereas θ_1 can exist without T_1 because $1/Y_{11}$ does have finite poles.

The details of the characteristic equation are found by substituting Eq. 36 into Eq. 59 and obtaining

$$H_{sc}(s) = J_1 s^2 + D_{11} s + K_{11}. \tag{60}$$

This equation contains no delayed-signal terms. Since motion is prevented at the output end, no signals are generated there. The zeros of this equation are obviously in the left half complex plane. Therefore, this terminal condition need not be considered any further with regard to stability and the effects of signal delay. Similar conclusions can be drawn for the input shaft locked or both shafts locked.

The more important case is that of imperfect grounding, that is, locking a shaft through a resilient member. This is equivalent to connecting a stiff spring across the output terminals. No further development is necessary, however, because this case is included in Eqs. 46 and 55 as another load condition.

The effects of a human operator on the system are not considered to any extent in this investigation. It is tacitly assumed that he is lightly coupled to the input. Therefore, he is equivalent to a force generator with almost infinite internal impedance (zero admittance) connected to the input terminals. For a manipulator with seven motions in operation, this is the case for several of the motions much of the time, especially when the operator is positioning the arm or handling very light loads. Therefore, this study was limited to the stability of a system itself without any effects due to the operator. However, to the extent that the dynamic characteristics of a human operator can be described as a linear, lumped-constant impedance, he can be considered as another load on the system.

I. Comments on the Characteristic Equation

As pointed out in Section H above, Eq. 55 is the system characteristic equation that is most significant. It is the one to be studied at length. Much

of the study, however, is done on the unloaded system since that form of the equation is sufficient to illustrate most of the techniques employed. Also, the first requirement of any force-reflecting system is that it be stable for no load. For the no-load case, $\alpha = \beta = \gamma = 0$, and Eq. 55 becomes

$$H(s) = s^4 + 2s^3 + 2s^2 + s + 0.25 - (as^2 + cs + 0.25b)\, e^{-2s\tau}. \tag{61}$$

This is the equation for a fourth-order system with time delay. In the absence of time delay, this reduces to a fourth-order polynomial. The delay causes the exponential terms, making the equation transcendental; that is, it cannot be written as an algebraic equation with a finite number of terms. Because of the exponential terms, the equation has an infinite number of zeros. For a stable system, none of these are in the right half complex plane.

J. Zeros at the Origin

If, in Eq. 61, $b = 1$, the characteristic equation has a zero at the origin. This is an acceptable location for a zero. Consider, for example, the solution indicated by Eq. 28 or 29 for the system excited by an initial fixed displacement of A units. If $K_{11}K_{22} = K_{12}K_{21}$, the characteristic equation has a simple zero at the origin. Calculating the residue of $\theta_1(s)$ at the origin shows the first term of the solution to be

$$R_1 = \frac{K_{22}D_{11}A - K_{12}D_{21}A + \lambda A K_{12}K_{21}}{K_{11}D_{22} + K_{22}D_{11} - K_{12}D_{21} - K_{21}D_{12} + 2\lambda K_{12}K_{21}}. \tag{62}$$

If the system has gain parameters with the nominal values of K and D, this first term reduces to $A/2$. If all the remaining zeros of the characteristic equation are in the left half plane, R is the final position of the input shaft. There would be a similar response if the system had been excited by an impulse of torque. This is a desirable response for a force-reflecting servomechanism. It means that there is no special rest position, such as zero, and the system can be placed anywhere within its working range.

If b is not equal to one, there is no zero at the origin, and the system has the "home" position of $\theta_1 = \theta_2 = 0$. If all the zeros of the characteristic equation are in the left half plane, the system will return to that position when all external torques are removed. If b is very close to one, there is a zero on the real axis close to the origin. (This can be shown by using a series expansion of H(s) for small s.) The rate at which the system moves with respect to the "home" position is approximately proportional to the distance of this zero from the origin. If b is less than one, the zero is to the left of the origin and the system returns to "home"; if b is greater than one, the zero is to the right of the origin, and the system

diverges from "home." In the first case, the motion appears to be a slow drift and can be tolerated. The latter case, however, is technically unstable and is considered as such in this study. Even if the divergent velocity is small at the beginning, it increases exponentially with time.

A force-reflecting servomechanism without signal time delay can be stable and have a characteristic equation with a double zero at the origin. If $a = b = c = 1$ and $\tau = 0$, Eq. 61 reduces to

$$H(s) = s^2(s^2 + 2s + 2). \tag{63}$$

This system, when excited by an impulse and after the transient subsides, continues to move with a constant velocity. During this motion, the system does not dissipate any energy. For a system with signal delay, the series expansion for its characteristic equation, Eq. 61, is

$$H(s) = 0.25(1 - b) + (1 - c + 0.5b\tau)\, s$$
$$+ (2 - a + 2c\tau - 0.5b\tau^2)\, s^2 + \text{higher terms}. \tag{64}$$

This indicates that a double zero at the origin occurs when $b = 1$ and $c = 1 + 0.5\tau$. Whether the system is unstable under these conditions due to the location of the other zeros must be investigated.

K. Acceptable Location of Zeros for Stability

The above discussion leads to the conclusion that, for a force-reflecting servomechanism to be stable, all the zeros of the characteristic equation must be in the left half complex plane except for either one or two at the origin. Zeros on the imaginary axis, except at the origin, are not acceptable because they indicate a response of sustained oscillation.

CHAPTER III

APPLICATION OF CONVENTIONAL TECHNIQUES

Several conventional techniques were used early in this study to obtain preliminary stability information about the force-reflecting servomechanism described in Chapter II both with and without time delay. This information helped in the formulation of the problem. The techniques used and some of the results are described briefly in this chapter.

A. Application of Nyquist's Criterion

One of the initial investigations of the stability of the system involved making complex-plane plots of its characteristic equation for values of the independent variable along the imaginary axis and then applying a stability criterion similar to that of Nyquist. The Nyquist criterion is usually applied to the plot of an open-loop transfer function composed of a ratio of polynomials. (A reprint of Nyquist's paper appears in a collection of classical papers.[39]) However, the application of essentially the same criterion to transcendental characteristic equations is brought out in a paper by Dzung.[40] In the discussion of that paper, Tizard refers to such application as the use of a "generalized Nyquist criterion." As Hoffman pointed out,[41] the resulting plots are conformal maps of a region that includes most of the right half complex plane, and these criteria are based on Cauchy's principle of the argument. The criterion used in Chapter IV of this report is an application of the same principle.

The normalized characteristic equation of the system considered here is, from Eq. 61,

$$H(s) = s^4 + 2s^3 + 2s^2 + s + 0.25 - (s^2 + s + 0.25)\, e^{-2s\tau}. \tag{65}$$

The system considered has no load (that is, $\alpha = \beta = \gamma = 0$) and has the nominal values of transmission gains, $a = b = c = 1$. The equation was plotted for values along the positive imaginary axis, that is, for $s = j\omega$ for $\omega \geq 0$, and several different values of τ. The equation was split into its real and imaginary parts as follows:

$$H(j\omega) = F(\omega) + jG(\omega), \tag{66}$$

where

$$F(\omega) = \omega^4 - 2\omega^2 + 0.25 + (\omega^2 - 0.25)\cos 2\omega\tau - \omega \sin 2\omega\tau, \tag{67}$$

and

$$G(\omega) = -2\omega^3 + \omega - \omega \cos 2\omega\tau - (\omega^2 - 0.25)\sin 2\omega\tau. \tag{68}$$

Each part was calculated on a digital computer for incremental values of ω and then plotted. Figure 4A shows these plots for real time-delay values of λ = 0, 0.01, and 0.25 sec (τ = 0, 1.0, and 2.5 sec); Fig. 4B, for λ = 0.05 sec (τ = 5 sec). The plots for λ = 0 and 0.01 sec indicate stable systems; the plots for λ = 0.025 and 0.05 sec indicate unstable systems. The stability is determined in the usual manner by counting encirclements of the origin, taking into account the entire contour. In this case, since the characteristic equation has no poles in the right half plane, there must be no encirclements for stability. The entire contour in the s-plane consists of the usual infinite-radius semicircle and the imaginary axis with an indentation to miss the zero at the origin. Appendix A gives the details of the contours and the stability determination.

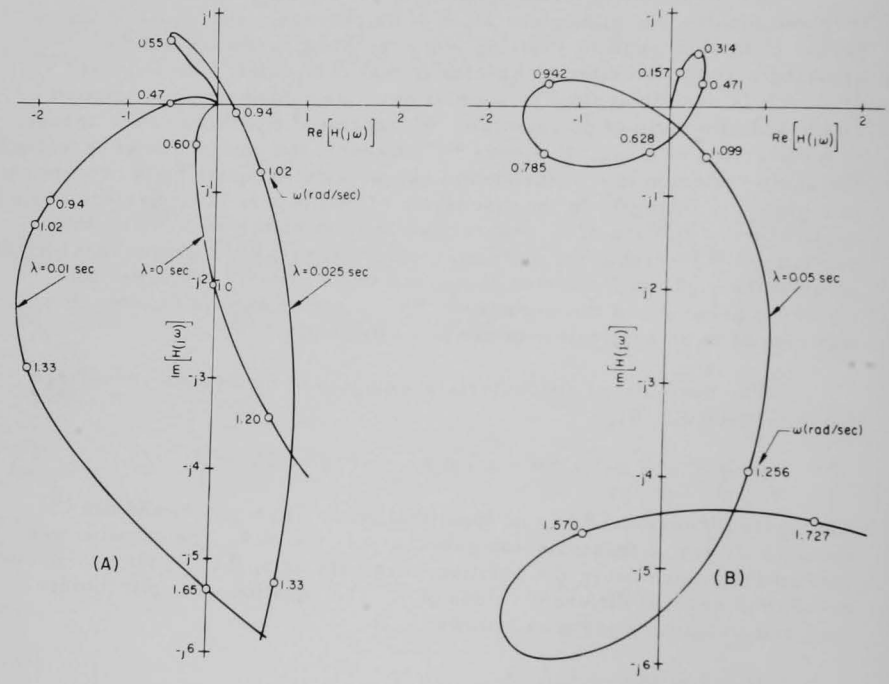

Fig. 4. Nyquist Diagrams for the System with Different Time Delays

Although stability of a system with a particular set of parameters can be determined by this method, it is not very useful when the parameters vary. Each new set would require a completely new plot, since the effects of varying individual parameters are not apparent. In fact, it is not evident from the plots that this system will be unstable for all time delays greater than 0.025 sec.

B. Satche Diagrams

Another graphical technique for determining stability, due to Satche, is particularly suited to systems with time lag.[42,43] It involves splitting the characteristic equation into two parts so that one consists only of the exponential term. Each part is plotted for the values on the contour that encloses the right half plane, the same contour as in Section A above. The plot of the exponential term is simple. It consists of the unit circle for values of s along the imaginary axis, and points within the unit circle for values of s along the large semicircle. A vector joining the two plots at points corresponding to the same values of s will change in magnitude and angle as the contour in the s-plane is traversed. If no poles in the right half plane have been introduced, the total change in angle of this vector must be zero for stable systems. If, for each value of s, the tail of this vector was placed at the origin, its head would describe a locus similar, but not identical, to the Nyquist plots of Section A above. Therefore, the requirement of zero change in angle is the same as the requirement of no encirclements.

To apply the Satche technique, the system characteristic equation, Eq. 65, was split as follows:

$$H(s) = (s^2 + s + 0.25)\left(\frac{s^4 + 2s^3 + 2s^2 + s + 0.25}{s^2 + s + 0.25} - e^{-2sT}\right). \tag{69}$$

Then, if

$$F_1(s) = \frac{s^4 + 2s^3 + 2s^2 + s + 0.25}{s^2 + s + 0.25} \tag{70}$$

and

$$F_2(s) = e^{-2sT}, \tag{71}$$

the characteristic equation becomes

$$H(s) = (s^2 + s + 0.25)\,[F_1(s) - F_2(s)]. \tag{72}$$

Since the zeros of $s^2 + s + 0.25$ are in the left half plane, $F_1(s)$ has no poles in the right half plane. Then, if

$$F(s) = F_1(s) - F_2(s), \tag{73}$$

the functions $F(s)$ and $H(s)$ have the same zeros, if there are any, in the right half plane. Therefore, it is sufficient to examine the function $F(s)$ to determine stability.

Figure 5 shows plots of the functions $F_i(j\omega)$ and $F_2(j\omega)$ for $\omega \geq 0$. The function $F(j\omega)$ can be represented by a vector drawn from the locus of $F_2(j\omega)$, the unit circle, to the locus of $F_1(j\omega)$. The ends of the vector are at points on each locus that have the same value of ω. The locus $F_1(j\omega)$ represents the function of Eq. 70 with that set of parameters. The shape of the locus of $F_2(j\omega)$, however, is the same for any value of τ. As τ changes, only the value of ω associated with each point on the unit circle changes. Therefore, Fig. 5 can be used to determine the effects of all values of time delay.

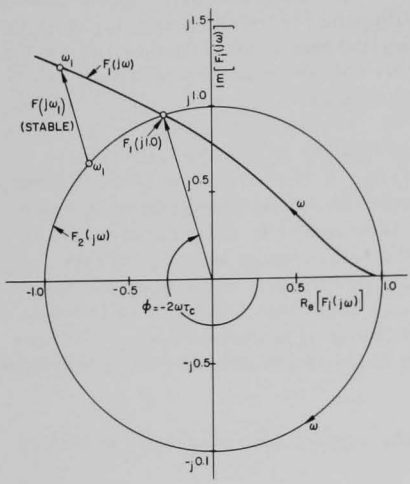

Fig. 5. Satche Diagram for System

The critical value of time delay, that is, the one for which the system just becomes unstable, is determined by the intersection of the two loci in the second quadrant. $F_1(j\omega)$ intersects the unit circle for $\omega = 1$. The apparent intersection at the point $+1 + j0$ is due to the characteristic equation having the zero at the origin. Appendix B discusses the details of stability determination involving the complete contour. However, if τ is less than the critical value, the point on F_2 for $\omega = 1$ will not have reached the point of intersection, and the direction of F is generally upward as ω increases in this region. On the other hand, for τ greater than the critical value, the $\omega = 1$ point on F_2 is beyond the intersection and the vector F will make an extra rotation as ω increases in this region. This, along with a similar rotation for the negative frequencies, results in a change of angle of F of 4π, which indicates two zeros in the right half plane and instability for the system.

The critical value of time delay for the system can be determined from Fig. 5. For that value of τ, the angle of F_2 is such that the point for $\omega = 1$ also falls on the point of intersection. In this case, $-2\omega\tau = -2\tau_c = -\phi = -4.42$ rad and $\tau_c = 2.21$ sec for the normalized system and $\lambda = 0.022$ sec for the real time system.

The use of the Satche diagram results in a great improvement in determining the effects of time delay for this system. The diagram indicates that increasing the time delay beyond the critical value will result only in more rotations of F and, therefore, greater instability. If other parameters vary, however, this method is less helpful. For example, $F_1(j\omega)$ might have to be replotted for many changes in signal-transmission gain or load to discover any trends. Any modification of F_1

that advances the point of intersection to the right probably would increase stability, but each case would have to be checked. If, however, F_1 can be modified so that it always remains outside the unit circle and never intersects it, the system so represented would never become unstable regardless of the time delay; it would be unconditionally stable. The technique for accomplishing this is more easily achieved by the method discussed in Section C below.

C. Bode Diagrams

The equations for the system can be rearranged so that an open-loop-type transfer function appears. In that case, the usual analytical techniques using Nyquist and Bode diagrams can be applied. If no external torques are applied and the initial values are zero, Eqs. 19 and 18 can be written as

$$\theta_2(s) = \frac{(D_{21}s + K_{21})\, e^{-s\lambda}}{J_2 s^2 + D_{22}s + K_{22}}\, \theta_1(s), \tag{74}$$

and

$$\theta_1(s) = \frac{(D_{12}s + K_{12})\, e^{-s\lambda}}{J_1 s^2 + D_{11}s + K_{11}}\, \theta_2(s). \tag{75}$$

Figure 6 is a block diagram representing these equations, where

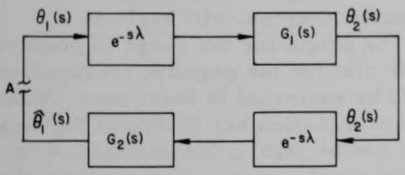

Fig. 6. Block Diagram Showing Tandem, Single-loop Composition of the System

$$G_1(s) = \frac{D_{21}s + K_{21}}{J_2 s^2 + D_{22}s + K_{22}}, \tag{76}$$

and

$$G_2(s) = \frac{D_{12}s + K_{12}}{J_1 s^2 + D_{11}s + K_{11}}. \tag{77}$$

The entire system is essentially composed of two second-order positional systems connected in tandem in a loop and with time delays in the connecting signal links. If the loop is opened at point A, $\hat{\theta}_1(s)$, the output of the $G_2(s)$ block, is

$$\hat{\theta}_1(s) = G_2(s)\, e^{-s\lambda}\, \theta_2(s), \tag{78}$$

and

$$\theta_2(s) = G_1(s)\, e^{-s\lambda}\, \theta_1(s). \tag{79}$$

Combining these equations gives

$$\frac{\hat{\theta}_1(s)}{\theta_1(s)} = G_1(s)\, G_2(s)\, e^{-2s\lambda}. \tag{80}$$

When the loop is closed, $\hat{\theta}_1(s)$ and $\theta_1(s)$ are identical.

If this system is compared to a standard single-loop system with negative feedback, the equivalent open-loop transfer function is

$$W(s) = -G_1(s)\, G_2(s)\, e^{-2s\lambda}, \tag{81}$$

and the stability of the system depends on the roots of the equation

$$1 + W(s) = 1 - G_1(s)\, G_2(s)\, e^{-2s\lambda} = 0. \tag{82}$$

Equation 82 gives the same characteristic equation as before.

With the equations in this form, the usual Nyquist diagrams for the open-loop transfer function W(s) can be drawn. Similar information for this system can be found more easily from Bode diagrams. Nevertheless, a necessary condition for stability can be derived from a consideration of the Nyquist diagram. The zero-frequency point will be located at $s = -K_{12}K_{21}/K_{11}K_{22}$, and the infinite-frequency point at the origin. If the magnitude of $K_{12}K_{21}/K_{11}K_{22}$ is greater than one, the Nyquist diagram will begin at a point to the left of the -1 point and go to the origin for the range of positive frequencies, and there will be a conjugate plot for the negative frequencies. Under these conditions, the -1 point must be encircled at least once. When $K_{12}K_{21}/K_{11}K_{22}$ equals one, the characteristic equation has a zero at the origin as previously mentioned, and the system can be stable, for example, with no delay as discussed in Section II.J. Therefore, a necessary condition for stability is

$$\frac{K_{12}K_{21}}{K_{11}K_{22}} \leq 1. \tag{83}$$

A sufficient condition for stability can also be derived from the Nyquist diagram. If $|W(j\omega)|$ is less than one for all frequencies greater than zero, the -1 point cannot be encircled and the system is stable. Since $|e^{-j\omega 2\lambda}| = 1$ for any value of λ, the equivalent condition is $|G_1(j\omega)G_2(j\omega)| < 1$. Therefore, a sufficient condition for stability for any value of time delay is

$$|G_1(j\omega)G_2(j\omega)| < 1, \quad \text{for } \omega > 0, \tag{84}$$

in addition to the condition of Eq. 83.

The system can be examined for this condition by using a Bode diagram.[44] After the substitution of the normalization factors and component values of Eqs. 47 and 49, the transfer function becomes

$$W(s) = G_1(s)\, G_2(s)\, e^{-2sT}, \tag{85}$$

where

$$G_1(s) = \frac{d_2 s + 0.5\, k_2}{s^2 + s + 0.5} \tag{86}$$

and

$$G_2(s) = \frac{d_1 s + 0.5\, k_1}{s^2 + s + 0.5}. \tag{87}$$

If it is assumed that the two systems are identical, that is, $k_1 = k_2 = k$ and $d_1 = d_2 = d$, the individual transfer functions become

$$G_1(s) = G_2(s) = G(s) = \frac{ds + 0.5\, k}{s^2 + s + 0.5}, \tag{88}$$

and the condition of Eq. 84 becomes $|G^2(j\omega)| < 1$, which is the same as $|G(j\omega)| < 1$. Figure 7 is an asymptotic plot of the Bode diagram for $|G(j\omega)|$ for $k = 1$ and $d = 1$. Since the magnitude is greater than one for a large range of frequency, the condition is not met.

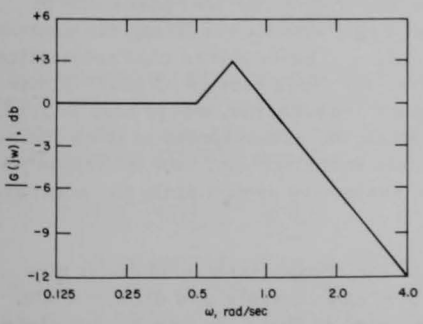

Fig. 7. Asymptotic Bode Plot for $|G(j\omega)|$

In this case, values of d and k that will provide unconditional stability can be found relatively easily. This is because the damping ratio of the denominator term is 0.707 and $|G(j\omega)|$ has no resonant peaking due to this term. The condition $|G(j\omega)| < 1$ becomes, for all $\omega > 0$,

$$\sqrt{0.25 + \omega^4} > \sqrt{\omega^2 d^2 + 0.25\, k^2}, \tag{89}$$

or, when rearranged,

$$\omega^4 - \omega^2 d^2 + 0.25\,(1 - k^2) > 0. \tag{90}$$

The condition is satisfied when

$$d^4 + k^2 < 1, \tag{91}$$

which can be found by equating Eq. 90 to zero, solving for ω, and finding the conditions for which the solutions are imaginary.

Equation 91 indicates that the condition can be satisfied with either k or d equal to zero. Each of these, however, would basically change the system by eliminating these signals. If k = 0, there would be no positional coupling between master and slave. Such a system could not hold a steady load unless there was a velocity difference between the two ends. This would be undesirable for most applications. Making d = 0 would eliminate the signal that has been most effective in improving the impulse response of systems without delay. Such improvement increases the operator's sense of feel of changing load forces. It could be expected to do the same for systems with delay, at least for some range of delays. If k = d, condition 91 becomes

$$k = d < 0.787, \tag{92}$$

which shows that both k and d can be reasonably sized even for unconditional stability. If the load or other parameters change so that the damping ratio of the denominator of Eq. 88 becomes different from 0.707, the analytical computation becomes much more complicated.

Another method of achieving unconditional stability is to add one or more compensation networks in tandem in the loop. For example, low-pass filters could be used to compensate for any magnitude increases due to either the numerator or denominator of $G(j\omega)$ without requiring the position coupling, k, to be reduced to a small value. The required characteristics of these filters could be determined from the Bode plot of $|G(j\omega)|$. These filters, however, by attenuating the higher frequencies, would also degrade the dynamic response of the system. Since the achievement of unconditional stability is not a primary objective of this investigation, this technique was not pursued. An unconditionally stable system is used mainly for comparison in later sections.

A system that is used as a basis for comparison throughout this report is one with a fixed d, equal to 0.9, and variable and different k's, k_1, and k_2. Stability boundaries will be found in the k_1, k_2 parameter plane using different techniques. The unconditional stability boundary can be found by using the technique discussed in this section. From Eqs. 86 and 87 with a fixed d, by algebraic manipulation, the condition of Eq. 84 becomes

$$\omega^8 + \omega^4(0.5 - d^4) + 1/16 > (k_1^2 k_2^2/16) + (k_1^2 + k_2^2)\, d^2\omega^2/4. \tag{93}$$

For d = 0.9, Eq. 93 becomes

$$\omega^8 - 0.1561\ \omega^4 + 0.0625 > 0.2025(k_1^2 + k_2^2)\ \omega^2 + 0.0625\ k_1^2 k_2^2. \qquad (94)$$

The boundaries of this inequality can be determined graphically. With a change in variable, $\Omega = \omega^2$, each side of the equation can be plotted as a function of Ω. The right side will be a straight line whose location depends on the values of k_1 and k_2. The inequality boundary occurs when the straight line is tangent to the curve of the left side of the equation. All other lines below the tangent line satisfy the inequality. Thus, the allowable ranges of values of the slopes and intercepts of these lines can be found. From this information the allowable values of k_1 and k_2 can be determined. Figure 8 shows the unconditional stability boundary in the (k_1, k_2)-plane determined by this process.

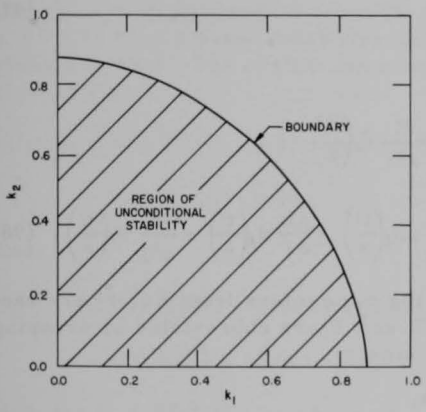

Fig. 8. Region of Unconditional Stability in the (k_1, k_2)-plane for $d_1 = d_2 = 0.9$

Although the unconditional stability boundary above could be determined with only moderate difficulty, it becomes much more difficult to use this method to determine the actual stability boundaries for systems with fixed delays. In that case, both magnitude and phase of the open-loop transfer function must be considered simultaneously and both are complicated functions of the k's and d's. Additional complication would be introduced by adding a load to the system, by changing other parameters, or by using a compensation network. Also, very little information concerning relative stability can be derived from Bode plots. Therefore, other methods were sought to obtain both absolute and relative stability boundaries.

D. Analog Computer Setup

The system under study was simulated on an analog computer first to investigate its behavior as the various parameters were varied and later to verify some of the conclusions established analytically. For this purpose the system equations, Eqs. 1-4, were reduced and rearranged as follows:

$$J_1\ddot{\theta}_1(t) = T_1(t) - K_{11}\theta_1(t) + K_{12}\theta_2(t-\lambda) - D_{11}\dot{\theta}_1(t) + D_{12}\dot{\theta}_2(t-\lambda), \qquad (95)$$

and

$$J_2\ddot{\theta}_2(t) = T_2(t) + K_{21}\theta_1(t-\lambda) - K_{22}\theta_2(t) + D_{21}\dot{\theta}_1(t-\lambda) - D_{22}\dot{\theta}_2(t). \tag{96}$$

After one makes the substitutions of Eq. 45, makes provisions for a time-scale change by letting t' = at, and rearranges the terms, the above equations become

$$\ddot{\theta}_1\left(\frac{t'}{a}\right) = \frac{1}{a^2J}\,T_1\left(\frac{t'}{a}\right) - \frac{K}{a^2J}\,\theta_1\left(\frac{t'}{a}\right) + \frac{k_1K}{a^2J}\,\theta_2\left(\frac{t'-a\lambda}{a}\right)$$

$$- \frac{D}{aJ}\,\dot{\theta}_1\left(\frac{t'}{a}\right) + \frac{d_1D}{aJ}\,\dot{\theta}_2\left(\frac{t'-a\lambda}{a}\right), \tag{97}$$

and

$$\ddot{\theta}_2\left(\frac{t'}{a}\right) = \frac{1}{a^2J}\,T_2\left(\frac{t'}{a}\right) + \frac{k_2K}{a^2J}\,\theta_1\left(\frac{t'-a\lambda}{a}\right) - \frac{K}{a^2J}\,\theta_2\left(\frac{t'}{a}\right)$$

$$+ \frac{d_2D}{aJ}\,\dot{\theta}_1\left(\frac{t'-a\lambda}{a}\right) - \frac{D}{aJ}\,\dot{\theta}_2\left(\frac{t'}{a}\right) - \alpha\ddot{\theta}_2\left(\frac{t'}{a}\right) - \frac{\beta D}{aJ}\,\dot{\theta}_2\left(\frac{t'}{a}\right) - \frac{\gamma K}{a^2J}\,\theta_2\left(\frac{t'}{a}\right). \tag{98}$$

The numerical values for the nonvarying parameters from Eq. 49 are used. Also, the arguments of the functions T and θ are abbreviated by dropping the symbol a. Thus, the equations become:

$$\ddot{\theta}_1(t') = \frac{20}{a^2}\,T_1(t') - \frac{5000}{a^2}\,\theta_1(t') + \frac{5000\,k_1}{a^2}\,\theta_2(t'-a\lambda)$$

$$- \frac{100}{a}\,\dot{\theta}_1(t') + \frac{100\,d_1}{a}\,\dot{\theta}_2(t'-a\lambda), \tag{99}$$

and

$$\ddot{\theta}_2(t') = \frac{20}{a^2}\,T_2(t') + \frac{5000\,k_2}{a^2}\,\theta_1(t'-a\lambda) - \frac{5000}{a^2}\,\theta_2(t') + \frac{100\,d_2}{a}\,\dot{\theta}_1(t'-a\lambda)$$

$$- \frac{100}{a}\,\dot{\theta}_2(t') - \alpha\ddot{\theta}_2(t') - \frac{100\,\beta}{a}\,\dot{\theta}_2(t') - \frac{5000\,\gamma}{a^2}\,\theta_2(t'). \tag{100}$$

Three time scales were used in this study. The first, a = 100, provided for the normalization used in Chapter II and defined $\tau = 100\,\lambda$. In most of the stability determinations, two values of τ were used, $\pi/8$ and $3\pi/4$. These correspond to the real time delays of $\pi/800 = 3.93$ msec and $3\pi/400 = 23.6$ msec. With this value of a, the system equations become

$$\ddot{\theta}_1(t') = 0.002\ T_1(t') - 0.5\ \theta_1(t') + 0.5\ k_1\theta_2(t' - \tau) - \dot{\theta}_1(t') + d_1\dot{\theta}_2(t' - \tau), \quad (101)$$

and

$$\ddot{\theta}_2(t') = 0.002\ T_2(t') + 0.5\ k_2\theta_1(t' - \tau) - 0.5\ \theta_2(t') + d_2\dot{\theta}_1(t' - \tau) - \dot{\theta}_2(t')$$

$$- \alpha\ddot{\theta}_2(t') - \beta\dot{\theta}_2(t') - 0.5\,\gamma\theta_2(t'). \quad (102)$$

The other time scales were necessary because of the fixed time delays available from the magnetic tape recorder used in this simulation. The delays available were 0.14, 1.4, and 14 sec, but only the first two were used. The 0.14-sec delay was used to simulate $\tau = \pi/8$ or $\lambda = \pi/800$. In this case, a is determined from the relation $a\lambda = 0.14$ sec which gives $a = 35.7$. The 1.4-sec delay was used for $\tau = 3\pi/4$ or $\lambda = 3\pi/400$. This gives $a = 59.3$. The system equations with these time scales are, for $t' = 35.7\ t$,

$$\ddot{\theta}_1(t') = 0.016\ T_1(t') - 3.92\ \theta_1(t') + 3.92\ k_1\theta_2(t' - 0.14) - 2.80\ \dot{\theta}_1(t')$$

$$+ 2.80\ d_1\dot{\theta}_2(t' - 0.14), \quad (103)$$

and

$$\ddot{\theta}_2(t') = 0.016\ T_2(t') + 3.92\ k_2\theta_1(t' - 0.14) - 3.92\ \theta_2(t') + 2.80\ d_2\dot{\theta}_1(t' - 0.14)$$

$$- 2.80\ \dot{\theta}_2(t') - \alpha\ddot{\theta}_2(t') - 2.80\ \beta\dot{\theta}_2(t') - 3.92\,\gamma\theta_2(t'); \quad (104)$$

and, for $t' = 59.3\ t$,

$$\ddot{\theta}_1(t') = 0.057\ T_1(t') - 1.42\ \theta_1(t') + 1.42\ k_1\theta_2(t' - 1.4) - 1.68\ \dot{\theta}_1(t')$$

$$+ 1.68\ d_1\dot{\theta}_2(t' - 1.4), \quad (105)$$

and

$$\ddot{\theta}_2(t') = 0.057\ T_2(t') + 1.42\ k_2\theta_1(t' - 1.4) - 1.42\ \theta_2(t') + 1.68\ d_2\dot{\theta}_1(t' - 1.4)$$

$$- 1.68\ \dot{\theta}_2(t') - \alpha\ddot{\theta}_2(t') - 1.68\ \beta\dot{\theta}_2(t') - 1.42\,\gamma\theta_2(t'). \quad (106)$$

The two major items of equipment used in this simulation were an analog computer and a magnetic tape recorder. The analog computer consists of conventional, patchable amplifiers and integrators made of solid-state components and having a dynamic voltage range of 100 V. Different summing and feedback components can be chosen to give amplifier and integrator gains of one to ten. The tape recorder has eight separate channels, each with FM modulating and detecting amplifiers and, therefore, with a signal frequency bandwidth from dc up to at least 100 Hz, depending

on an output filter. The unit has separate record and playback heads so the recorded signal can be played back after the time required for a point on the tape to move from one head to the other. The signal voltage range is about 2 V.

Figure 9 shows the analog-computer component arrangement used for this study. With the gain of ten chosen, either set of equations, Eqs. 103 and 104 or Eqs. 105 and 106, could be simulated by merely resetting the potentiometers at the inputs of amplifiers No. 5 and 11 and changing the tape speed of the tape recorder. Balancing the recorder amplifiers, however, was necessary after a speed change. The potentiometers and amplifiers in each tape-recorder channel were necessary, first to attenuate 100-V range signals to a 1.5-V range suitable for recording and then amplifying back to the 100-V range. Because of the filtering of the integrators, noise generated in the tape-recorder channels, although very apparent in oscilloscope patterns, proved to be no problem.

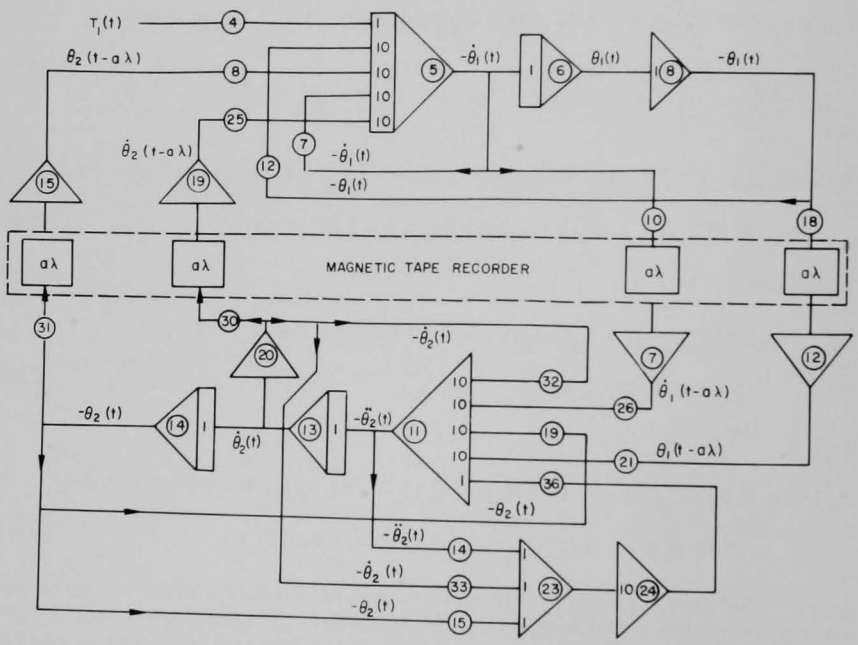

Fig. 9. Analog-computer Setup for Simulation of the System

Extra amplifiers were used to make it convenient for changing load conditions. In Eqs. 104 and 106, the terms containing α, β, and γ were written separately although they could have been included in other terms.

Amplifiers No. 23 and 24 simulate these terms. Amplifier No. 11 is not an integrator, so that the variable $\ddot{\theta}_2(t)$ is available. With this arrangement, each potentiometer at the input to amplifier No. 23 has independent control over one of the load parameters, α, β, and γ.

During most of the testing, the system was excited by setting in an initial condition on amplifier No. 6 for $\theta_1(t)$. No external excitation was used. The variable $\theta_1(t)$ was recorded, and $\theta_1(t) - \theta_2(t)$ was generated and recorded. The latter term is the error in position between the two ends of the system. The transmission-gain parameters k_1, k_2, d_1, and d_2 were changed by adjusting potentiometers No. 8, 21, 25, and 26, respectively. Chapter VI gives the results of some of these tests.

As mentioned in the Introduction, during the initial tests, there seemed to be some anomalous behavior of the system. Even when the tape-recorder channels were bypassed, eliminating the delay, unstable operation occurred for most settings of the transmission-gain parameters. Reducing the position-gain parameters, k_1 and k_2, did not seem to help. Section E below describes the investigation of this anomaly.

E. The System without Delay

To resolve the anomalous behavior of the analog-computer simulation of the system mentioned in Section D above, the stability of the system was investigated analytically. Since no time delay was involved and only absolute stability was to be determined, straightforward application of conventional techniques was appropriate. The desired results were obtained primarily by using Routh's criterion. Some information was obtained using the root-locus techniques.

The system characteristic equation considered in this section is that of Eq. 55 with $\tau = 0$ and no load on the system. Under these conditions and with the use of Eq. 54, Eq. 55 becomes

$$H(s) = s^4 + 2s^3 + (2 - d_1d_2)\, s^2 + [1 - 0.5(k_1d_2 + k_2d_1)]\, s + 0.25(1 - k_1k_2). \tag{107}$$

In the standard form, the equation is

$$H(s) = a_4s^4 + a_3s^3 + a_2s^2 + a_1s + a_0, \tag{108}$$

where

$$a_4 = 1, \quad a_3 = 2, \quad a_2 = 2 - d_1d_2,$$

$$a_1 = 1 - 0.5\,(k_1d_2 + k_2d_1), \quad \text{and} \quad a_0 = 0.25(1 - k_1k_2). \tag{109}$$

The Routh array for this equation is

$$\left.\begin{array}{lll} a_4 & a_2 & a_0 \\ a_3 & a_1 & \\ b_1 & a_0 & \\ c_1 & & \\ a_0 & & \end{array}\right\}, \tag{110}$$

where

$$b_1 = a_2 - \frac{a_1 a_4}{a_3}, \tag{111}$$

and

$$c_1 = a_1 - \frac{a_0 a_3}{b}. \tag{112}$$

For the equation to have no zeros with positive real parts, Routh's criterion[44] requires that all the a's be positive (since a_4 and a_3 are positive) and that there be no sign changes in the first column of the array.

One case that gave anomalous behavior of the system was that for $d_1 = d_2 = 1$. For that case, the various elements become:

$$\left.\begin{aligned} a_2 &= 1, \\ a_1 &= 1 - 0.5(k_1 + k_2), \\ b_1 &= 0.5 + 0.25(k_1 k_2), \\ c_1 &= \frac{0.25(k_1 - k_2)^2}{1 + 0.5(k_1 + k_2)}, \\ \text{and} \quad & \\ a_0 &= 0.25(1 - k_1 k_2). \end{aligned}\right\} \tag{113}$$

The only nonnegative value of c_1 occurs when $k_1 = k_2$, making $c_1 = 0$. All other values of k_1 and k_2 produce an unstable system. Also, $c_1 = 0$ indicates a pair of imaginary zeros, and, therefore, the response of the system would be a sustained oscillation. The system is stable for only one condition, that of $k_1 = k_2 = 1$. In this case, a_0 and a_1 both are zero, and the system characteristic equation reduces to one with two zeros at origin and two in the left half plane, the stable configuration discussed in Chapter II.

Since only one point in the (k_1, k_2)-plane represents a stable system, it becomes apparent why it was difficult to obtain a stable system with the analog computer. This situation would also prevail in the systems that have been applied to manipulators. Stability in those cases, however, is not difficult to achieve for two reasons. First, because only a single positional error, $e(t) = K[\theta_1(t) - \theta_2(t)]$, is generated, the different values of the K's do not exist and $k_1 = k_2 = 1$. In addition, every practical system has some friction so that the F-terms in Eqs. 16 and 17 are not zero. Also, since there is only one velocity error, all the D's in those equations are equal. Therefore, effectively, $D_{11} = D + F > D_{12} = D$ and $D_{22} = D + F > D_{21} = D$. This makes both d_1 and d_2 less than one, and, as is shown below, increases the stable region for the system.

When the d's are less than one, the stability requirements are less stringent. (The system is always unstable when the d's are each greater than one.) For all the zeros to be in the left half plane, all the a's in the equation and all the terms in the first column of the Routh array must be positive. Since all the a's must be positive, $c_1 > 0$ includes the condition $b_1 > 0$. Also, $c_1 > 0$ can be reduced to the condition

$$a_1a_2a_3 - a_1^2a_4 - a_0a_3^2 > 0. \tag{114}$$

After substitution of the fixed values, the conditions for stability are

$$\left.\begin{aligned} &a_2 = 2 - d_1d_2 > 0 \quad \text{(this is assured since } d_1d_2 < 1 \text{ by assumption)},\\ &a_1 = 1 - 0.5(k_1d_2 + k_2d_1) > 0,\\ &a_0 = 0.25(1 - k_1k_2) > 0,\\ &\text{and}\\ &2a_1a_2 - a_1^2 - 4a_0 > 0. \end{aligned}\right\} \tag{115}$$

For the case used for comparison, in which $d_1 = d_2 = 0.9$, the conditions become

$$\left.\begin{aligned} &(1)\quad 1 - 0.45(k_1 + k_2) > 0,\\ &(2)\quad 1 - k_1k_2 > 0,\\ &\text{and}\\ &(3)\quad 1.52 - 0.684(k_1 + k_2) + 2.38\, k_1k_2 - 0.81(k_1^2 + k_2^2) > 0. \end{aligned}\right\} \tag{116}$$

Figure 10A is a plot of the stable region of the (k_1, k_2)-plane. Each of the three conditions above contributes to part of the boundary. Condition 1 provides the straight-line sections; Condition 2, the part of the hyperbola that passes through the 1, 1 point; Condition 3, the side sections, which are also conic sections. Only positive values of k_1 and k_2 are considered in this report, although the stable region extends into the other quandrants.

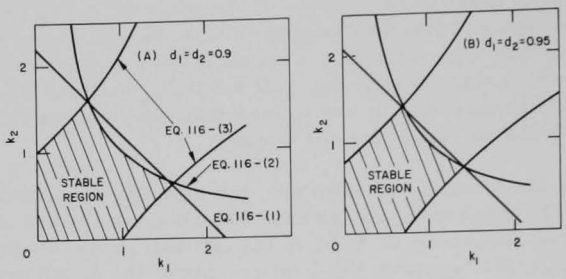

Fig. 10. Stable Regions in (k_1, k_2)-plane for System with No Delay

In a similar manner, the stable region for the case of $d_1 = d_2 = 0.95$ was determined, as is shown in Fig. 10B.

Some information about the zeros in the stable regions of Fig. 10 was determined from root-locus plots. For $d_1 = d_2 = 0.9$, the system equation is

$$s^4 + 2s^3 + 1.19\, s^2 + [1 - 0.45(k_1 + k_2)]\, s + 0.25(1 - k_1 k_2) = 0. \tag{117}$$

To put this equation in standard form, one of the parameters had to be eliminated. This was done by assigning a specific value to it. With the substitution $k_1 = 1$, the equation becomes

$$s^4 + 2s^3 + 1.19\, s^2 + 0.55\, s + 0.25 - 0.45\, k_2 s - 0.25\, k_2 = 0. \tag{118}$$

When put into the open-loop form, the equation is

$$1 - \frac{0.45\, k_2(s + 0.56)}{s^4 + 2s^3 + 1.19\, s^2 + 0.55\, s + 0.25} = 0. \tag{119}$$

To put the open-loop term in factored form required finding the zeros of the denominator. When these are used, the equation becomes

$$1 - \frac{0.45\, k_2(s + 0.56)}{(s + 0.70)(s + 1.29)(s + 0.0011 + j0.52)(s + 0.0011 - j0.52)} = 0. \tag{120}$$

The root loci in Fig. 11A were made using the above equation. The asymptotes intersect the real axis at -0.48. The stable range of k_2, from

application of Routh's criterion, is $-0.07 < k_2 < 1$. In a similar manner, the root loci in Fig. 11B were made for $k_1 = 0.5$. In Figs. 11C and 11D are root loci for $d_1 = d_2 = 0.95$ and the same values of the k's as above.

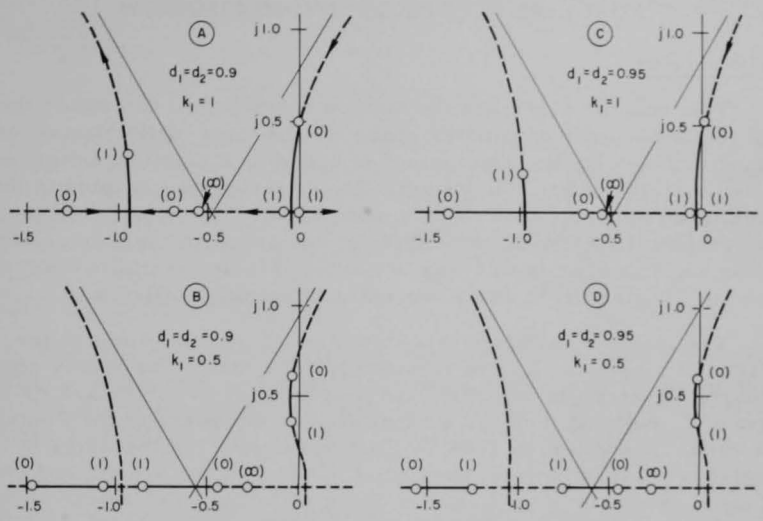

Fig. 11. Root-locus Plots for System with No Delay. (Only the top half of the s-plane is shown. Values of k_2 are in parentheses.)

As can be seen in Figs. 11A and 11B, when either of the k's is about 0.5 or less, the system is lightly damped. Although Fig. 10A shows a large stable region, part of it is a region of low relative stability. Similar comments apply to $d_1 = d_2 = 0.95$, except that the stable region is even smaller. This is another indication that it is desirable to have a means of determining relative stability in addition to absolute stability.

Although the above methods produced the desired results for the system without delay, their extension to systems with delay is difficult or impossible. The Routh criterion, as it exists, cannot be applied. Root-locus techniques have been applied to time-lag systems,[45] but the application would require much computation and many plots. Even in the above case without delay, putting the system equation into the standard form was difficult. It was accomplished only by fixing the value of three of the parameters and allowing the fourth to vary. In addition, although the general form of the plots could be determined beforehand, most of the zeros had to be obtained on a computer. For some of these reasons, another stability-determining technique was desired like the Pontryagin criterion discussed in Chapter IV. That criterion has been referred to as an extension of Routh's criterion to transcendental equations.

CHAPTER IV

DEVELOPMENT OF A NEW METHOD OF APPLICATION OF PONTRYAGIN'S STABILITY CRITERION FOR FORCE-REFLECTING SERVOMECHANISMS

A. Introduction

This chapter describes the method developed to determine the stable regions in gain-parameter space for the force-reflecting servomechanism under study. The method is based on a stability criterion for time-lag systems due to Pontryagin. The criterion was adapted to the problem and then applied by using a new graphical technique. By means of this graphical technique, the effects of variations of the gain parameters could be found easily. In this way, we avoided the main difficulties, described in Chapter III, in using conventional stability criteria.

The stability criterion is a statement of the conditions under which the zeros of a certain class of transcendental functions have only negative real parts. Pontryagin presented the proofs of the criterion and its basic theorems.[30] Bellman included a short English summary of the Pontryagin paper in his monograph in 1954.[31] Choksy restated the theorems in control-system terminology, gave brief outlines of the proofs, and also gave some examples of applications of the criterion to classical problems.[29] In their book, published in 1963, Bellman and Cooke devoted a chapter to the criterion and its application to classical problems.[28] The theorems were not proved; instead, the reader was referred to Pontryagin's paper.

Although the Pontryagin criterion has been available for more than 10 years, there have been a few published discussions and extensions of it. Since the main source of information regarding the basic proofs of the criterion is Pontryagin's original paper, its mathematically rigorous presentation may partially account for this situation by making it appear that the proofs are difficult to understand. Therefore, a different approach is used here. The bases of the proofs are explained with more emphasis on concepts and terms familiar to control engineers. In addition, rather than a general development being given, the particular characteristic equation of the system under study is used throughout the discussion.

To obtain the desired results from this criterion required the development of a new method of application. The criterion has been used often to determine stability boundaries in parameter space. Before this study, however, there have been no known published applications in which the equation of main consideration could not be reduced to one with only one trigonometric term. Such a reduction was not possible in this case because of the complexity of the system. Furthermore, the classical equations discussed by Choksy and Bellman and by Bhatt and Hsu[32,33] are second order or less. The only other exception, besides the one in this study, is a third-order equation discussed by Jeffrey.[34] For the type of systems under study, the application of the criterion can be extended to equations of any order.

The transcendental equation to which the criterion is applied in this chapter is the characteristic equation of the force-reflecting servomechanism system described in Chapter II. The equation is the one for the system with no load. It is Eq. 61, which is repeated and renumbered here for convenience:

$$H(s) = s^4 + 2s^3 + 2s^2 + s + 0.25 - (as^2 + cs + 0.25b)\, e^{-2s\tau}. \tag{121}$$

The objective of this chapter is to find the values of the parameters, a, b, and c, for which the zeros of H(s) are in the left half plane, except for possibly one at the origin. If, as explained in Chapter II, the zeros of H(s) are so located, the system is stable. These parameters, a, b, and c, are related to the transmission gain parameters of the system by Eq. 54.

B. Preliminary Considerations

The Pontryagin criterion gives the necessary and sufficient conditions for an exponential polynomial to have zeros only in the left half plane. Exponential polynomials are members of a class of transcendental functions of the form $P(z) = p(z, e^z)$, where $p(z,q)$ is a polynomial.

The characteristic equation of the system, Eq. 121, can be put into the form of an exponential polynomial. Since it cannot have negative exponents, Eq. 121 is divided by $e^{-2s\tau}$. This gives

$$H_p(s) = (s^4 + 2s^3 + 2s^2 + s + 0.25)\, e^{2s\tau} - (as^2 + cs + 0.25b). \tag{122}$$

This equation has the same finite zeros as Eq. 121, because the divisor, $e^{-2s\tau}$, has no finite zeros. After the substitution of $z = s\tau$, where $z = x + jy$, the equation becomes

$$P(z) = \left(\frac{1}{\tau^4} z^4 + \frac{2}{\tau^3} z^3 + \frac{2}{\tau^2} z^2 + \frac{1}{\tau} z + \frac{1}{4}\right) e^{2z} - \left(\frac{a}{\tau^2} z^2 + \frac{c}{\tau} z + \frac{1}{4} b\right). \tag{123}$$

In this equation, the powers of τ are considered as parts of the constant coefficients of the exponential polynomial in z and $q = e^z$. Since τ is a positive constant, the real part of a particular value of s has the same sign as that of the corresponding z. Therefore, the stable zeros of Eq. 123 are also stable zeros of Eq. 122.

The first question with regard to the exponential polynomial is whether it has a principal term. A polynomial of the form

$$p(z,q) = \sum_{m,n} a_{mn} z^m q^n \tag{124}$$

has a principal term if and only if the maximum values of the exponents m and n each occur together in the same term. Although other terms may contain one of the maximum exponents, only the principal term contains both. In Eq. 123, $a_{42}z^4q^2$ is the principal term, where $a_{42} = 1/\tau^4$. Pontryagin's first theorem states that, if the function $p(z,q)$ has no principal term, the function $P(z,e^z)$ in Eq. 123 has an unbounded number of zeros with positive real parts. Therefore, a necessary condition for stability is that the exponential polynomial derived from the system characteristic equation have a principal term.

Pontryagin's proof of this theorem involves seeking solutions for the general equation $P(z,e^z) = 0$ that have positive real parts and finding that the equation must not have a principal term for the solutions to exist. However, the presence or lack of a principal term in an equation of this type determines whether the zeros of large magnitude are in the left or right half plane. But asymptotic values for these zeros can be found, as shown in Pinney[46] and in Bellman and Cooke.[28] The zeros far from the origin lie in a finite number of chains extending to infinity. If the equation does not have a principal term, these chains are in the right half plane. The asymptotic zeros of Eq. 123 are shown in Appendix C to be in chains in the left half plane. The stability of the system represented by an equation with a principal term, such as Eq. 123, is determined by the location of a finite number of zeros near the origin.

The requirement for having a principal term is easily achieved for the equations considered here. In fact, it is difficult to produce an equation without a principal term unless unusual changes are made in the system. One way is to change the sign of τ. Then, no division of Eq. 121 is necessary and the substitution of $z = s\tau$ yields the highest powers of z and $q = e^z$ in the different terms, z^4q^0 and z^2q^2, respectively. With this change, the motor torques would depend on the future values of position and velocity. Such a system, of course, is not physically possible. Another way of changing the system to eliminate the principal term is to take successive derivatives of the signals so that an s^5 term occurs after the negative sign in Eq. 122. This, while possible, is not reasonable. Therefore, the major consideration will be with the equation with the principal term.

C. The Pontryagin Criterion

If the system function $P(z)$, an exponential polynomial, has a principal term, the stability of the system is determined by the behavior of the

equation along the imaginary axis, that is, $P(z)$ for $z = jy$. Splitting the function $P(jy)$ into its real and imaginary parts gives

$$P(jy) = F(y) + jG(y). \tag{125}$$

The following theorem gives the most often used form of Pontryagin's criterion:

Theorem 1a. If $P(z)$ is an exponential polynomial with a principal term, then, in order that all its zeros lie to the left of the imaginary axis, it is sufficient that one of the following conditions be satisfied:

a. All the zeros of the functions $F(y)$ and $G(y)$ are real, simple, and alternate, and, for at least one value of y,

$$G'(y)\,F(y) - G(y)\,F'(y) > 0, \tag{126}$$

where

$$G'(y) = \frac{dG(y)}{dy}, \text{ and } F'(y) = \frac{dF(y)}{dy}.$$

b. All the zeros, y_0, of $F(y)$ are real and simple, and for each zero, the condition of Eq. 126 is satisfied; that is,

$$G(y_0)\,F'(y_0) < 0. \tag{127}$$

c. All the zeros, y_0, of $G(y)$ are real and simple, and for each zero, the condition of Eq. 126 is satisfied; that is,

$$G'(y_0)\,F(y_0) > 0. \tag{128}$$

Theorem 1b. Conversely, if all the zeros of $P(z)$ lie to the left of the imaginary axis, then the zeros of $F(y)$ and $G(y)$ are real, simple, and alternating, and the condition of Eq. 126 exists for each y.

A second theorem that states another form of the criterion is:

Theorem 2a. Let $P(z)$ be an exponential polynomial with the principal term $a_{rv}z^r q^v$ $(q = e^z)$. Also, let the vector $W = P(jy)$ for all real y, and $W \neq 0$ for any value of y. Then, if the vector W subtends an angle $4k\pi v + \pi r + \delta_1$, where

$$\lim_{k\to\infty} \delta_1 = 0,$$

when y ranges over the interval $-2k\pi \leq y \leq 2k\pi$, then the zeros of $P(z)$ lie to the left of the imaginary axis. It also follows that W rotates in the positive direction with positive velocity, which is the same as the condition in Eq. 126.

Theorem 2b. Conversely, if all the zeros of $P(z)$ lie to the left of the imaginary axis, W rotates in a positive direction with a positive velocity, and when y is in the interval $-2k\pi \leq y \leq 2k\pi$, the vector W subtends an angle $4\pi kv + \pi r + \delta_1$. The statement in Theorem 2a relating the positive velocity of W to Eq. 126 can be verified by differentiating the argument of W with respect to y. Let $\phi = \text{Arg } W$; then

$$\phi = \tan^{-1} \frac{G(y)}{F(y)}, \tag{129}$$

and

$$\frac{d\phi}{dy} = \frac{G'(y)\,F(y) - F'(y)\,G(y)}{F^2(y) + G^2(y)}. \tag{130}$$

Therefore, the signs of $d\phi/dy$ and of the numerator of the right side of Eq. 130 are the same.

D. Basis of the Criterion

The basis of the criterion is Cauchy's principle of the argument.[47] Each of the above theorems can be derived from this principle. The principle states that if a meromorphic function, $P(z)$, of the complex variable z is considered for values of z that lie on a simple, closed contour in the z-plane, the change in the argument of $P(z)$ as z traverses the contour depends on the difference between the number of zeros and the number of poles of $P(z)$ enclosed by the contour. In particular, the change in argument of $P(z)$ equals $2\pi(N_z - N_p)$, where N_z is the number of zeros of $P(z)$ and N_p is the number of poles enclosed as z traverses the contour in a counterclockwise direction. No singularities of $P(z)$ are permitted on this contour. If $N_p = 0$, as it is in the case being considered, the variation in argument gives the number of zeros. The variation in argument is an integral multiple of 2π. Therefore, if the function $P(z)$ is plotted in the $P(z)$-plane for values of z on the contour, the number of encirclements of the origin in the positive (counterclockwise) direction by the plot of $P(z)$ is equal to the number of zeros of $P(z)$ inside the contour.

The contour in the z-plane used in this case is the rectangle determined by the values $0 \leq x \leq a$ and $-2k\pi + \epsilon \leq y \leq 2k\pi + \epsilon$, as shown in Fig. 12. This contour encloses the entire right half plane as $k \to \infty$ and $a \to \infty$. The value of ϵ is chosen so that the functions $F(y)$, $G(y)$, and e^{2z}, considered later, are not zero on the horizontal parts of the contour.

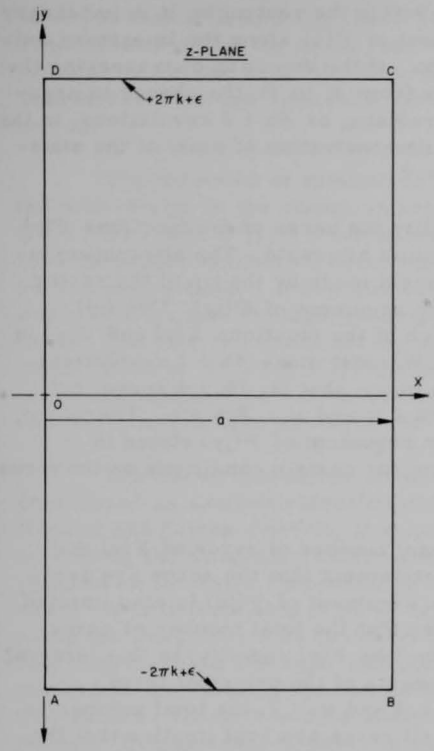

Fig. 12. Contour Used in Pontryagin Criterion

An unusual situation occurs when the argument principle is applied to exponential polynomials. The different parts of the contour contribute a large, but countable, number of encirclements of the origin. For a stable system, however, the net number must be zero. For example, the change in argument as z traverses ABCD, the three sides of the contour, must be cancelled by change as z traverses DA, the imaginary axis. The change in argument due to ABCD is relatively easy to determine as described below.

To evaluate the change in argument of P(z) for the contour ABCD, it is necessary to separate the term with the maximum power of z and rewrite Eq. 123 as

$$P(z) = \frac{1}{\tau^4} z^4 q^2 + \sum_{\substack{m < 4 \\ n \leq 2}} a_{mn} z^m q^n \tag{131}$$

Dividing out the first term gives

$$P(z) = \frac{1}{\tau^4} z^4 q^2 [1 + \delta(z)]. \tag{132}$$

The value of ϵ is chosen so there is no division by zero, but, since $|q^2| = e^{2x} \geq 1$ on the contour, any ϵ will do. Also, since $\delta(z)$ contains only negative powers of z, $\delta(z) \to 0$ as $k \to \infty$ and $a \to \infty$. Therefore, the change in argument of P(z) on this part of the contour approaches that of $(1/\tau^4)\, z^4 e^{2z}$ as k and a increase. The change in argument for $z^4 e^{2z}$ is the sum of changes for z^4 and e^{2z}. For z^4, as Arg z varies from $-\pi/2$ to $\pi/2$, the change is 4π. For the function e^{2z}, the change along the upper side of the contour cancels the change along the lower side because

$$\exp\{2[x + j(\epsilon + 2k\pi)]\} = \exp\{2[x + j(\epsilon - 2k\pi)]\} = \exp\{2[x + j\epsilon]\},$$

and these sides are traversed in opposite directions. The change along the right side is $8k\pi$. Thus, the total change in argument of P(z) as z traverses the three sides approaches $8k\pi + 4\pi = 2\pi(4k+2)$ radians, or $4k + 2$

In order that there be no zeros within the rectangle, it is necessary and sufficient that the change in argument of $P(z)$ along the imaginary axis from D to A cancel the above variation. If the direction of traversing the imaginary axis is reversed so that it is from A to D, the change in argument of $P(z)$ must approach $8k\pi + 4\pi$ radians, or $4k + 2$ revolutions, in the positive direction as $k \to \infty$. This is a demonstration of most of the statements of Theorem 2 for $r = 4$ and $v = 2$.

Theorem 1 states that for stability the zeros of the functions $F(y)$ and $G(y)$ must be real and simple and must alternate. The alternation is an indication of encirclements of the origin made by the tip of the vector $W = P(jy)$, and, therefore, the change in argument of $P(jy)$. One full revolution of W requires two zeros each of the functions $F(y)$ and $G(y)$ in alternating order. Since, in this case, W must make $4k + 2$ revolutions, $F(y)$ and $G(y)$ each must have twice as many, that is, $8k + 4$ zeros that alternate in the range between $y = -2\pi k + \epsilon$ and $y = 2\pi k + \epsilon$. Therefore, the requirement for a certain change in argument of $P(jy)$ stated in Theorem 2 is related to the requirement for certain conditions on the zeros of $F(y)$ and $G(y)$ stated in Theorem 1.

Although it is not stated, the exact number of zeros of $F(y)$ and $G(y)$ in this interval is implied by the statement that the zeros are real and simple. Thus, a specific change in argument of $P(jy)$ is also implied. Another of Pontryagin's theorems states that the total number of zeros (including nonreal ones) of each function like $F(y)$ and $G(y)$ in this interval is $4kv + r$, where v and r are the exponents of the principal term, $a_{rv}z^r q^v$, of $P(z)$. In this case, for $r = 4$ and $v = 2$, the total number is $8k + 4$. Therefore, the statement that all zeros are real implies that the number of real zeros is also $8k + 4$. In addition, if all the zeros are simple, the proper number of revolutions of W follows.

The above theorem can be explained with reference to the analytical expressions for the function $P(jy) = F(y) + jG(y)$. Therefore, substituting $z = jy$ into Eq. 123, applying De Moivre's theorem, and combining terms gives

$$F(y) = \left(\frac{y^4}{\tau^4} - \frac{2y^2}{\tau^2} + \frac{1}{4}\right)\cos 2y + \left(\frac{2y^3}{\tau^3} - \frac{y}{\tau}\right)\sin 2y + a\frac{y^2}{\tau^2} - \frac{1}{4}b, \qquad (133)$$

and

$$G(y) = \left(-\frac{2y^3}{\tau^3} + \frac{y}{\tau}\right)\cos 2y + \left(\frac{y^4}{\tau^4} - \frac{2y^2}{\tau^2} + \frac{1}{4}\right)\sin 2y - c\frac{y}{\tau}. \qquad (134)$$

For large values of k and most values of ϵ in $y = \pm 2\pi k + \epsilon$, the ends of the interval, $F(y)$ and $G(y)$ have dominant terms $(y^4/\tau^4)\cos 2y$ and $(y^4/\tau^4)\sin 2y$, respectively. By application of Rouche's theorem,[47] it can

be shown that F(y) and G(y) each have the same number of zeros as their dominant terms for the same range of y. For each dominant term there are four zeros due to y^4 and 8k zeros due to the trigonometric functions. Therefore, F(y) and G(y) each have 8k + 4 zeros, some of which may not be real.

The direction of rotation of the vector W must be positive to give the proper sign to the change in argument. The direction is positive if $G'(y)\,F(y) - G(y)\,F'(y) > 0$ for at least one value of y. If F(y) and G(y) have the proper number of zeros, the direction remains the same throughout the entire range. If it did not remain the same, the tip of the vector W would cross a line through the origin of the W-plane more than 8k + 4 times. But this is impossible because it requires a function that is a linear combination of F(y) and G(y) and has a number of zeros greater than the maximum number, 8k + 4, determined by its dominant term. The dominant term would have the form $Ay^4 \cos(2y + \psi)$.

The above discussion shows that the Pontryagin criterion can be considered as another extension of the principle of the argument. Like the Nyquist and Satche criteria, it requires investigation of a system function only along the imaginary axis. Whether the zeros of F(y) and G(y) are checked or the angle subtended by P(jy) is found, the objective is the same. It is determining if there is enough change in the argument of P(z) along the imaginary axis to cancel the change due to the rest of the contour that encloses the right half plane when extended to its limits. The method of determining the change in argument is arbitrary; any method will suffice: Often it is done analytically if the functions are simple enough. In this case, however, a partially graphical procedure is used.

E. Discussion of the Application of the Criterion

The procedure used in this investigation is to plot certain forms of the functions F(y) and G(y) to determine if the conditions of the Pontryagin criterion are met. First, however, a return to the original variables is made by substituting $z = s\tau$ for z. Since $z = x + jy$ and $s = \sigma + j\omega$, the substitution gives $x = \tau\sigma$ and $y = \tau\omega$. When these substitutions are made, Eqs. 133 and 134 become

$$F(\tau\omega) = (\omega^4 - 2\omega^2 + 0.25)\cos 2\tau\omega + (2\omega^3 - \omega)\sin 2\tau\omega + a\omega^2 - 0.25b, \tag{135}$$

and

$$G(\tau\omega) = (-2\omega^3 + \omega)\cos 2\tau\omega + (\omega^4 - 2\omega^2 + 0.25)\sin 2\tau\omega - c\omega, \tag{136}$$

where

$$H_p(j\omega) = F(\tau\omega) + jG(\tau\omega), \tag{137}$$

and $H_p(s) = 0$ is Eq. 122, essentially the characteristic equation of the system. In this form, the changes in τ can be more easily accommodated. In the present study, different values of time delay are considered, so it is convenient not to have the algebraic parts of the functions depend on τ. This is basically only a coordinate scale change and does not affect the number of zeros of the functions F and G or their alternation.

Before a graphical method was selected, attempts were made to simplify Eqs. 135 and 136 so that the zeros could be determined analytically. In all published applications of the criterion, one function could be reduced to an equation with only one trigonometric quantity, usually the tangent. It is possible in this case, only if either c or both a and b are zero. The sine and cosine terms in each function can be combined, but the resulting sine (or cosine) term has a phase angle that is a complicated function of ω.

Plotting the functions F and G directly against ω can give the necessary information for determining stability for particular cases, but this method has the same disadvantage of the conventional techniques discussed in Chapter III. Almost every case, for different values of the parameters a, b, and c would have to be plotted. This difficulty was overcome by the development of the method of application described in Section F below.

F. The New Method of Application

A useful extension of the application of the criterion is developed here. The method developed consists of splitting each function F and G into two parts, one containing all the trigonometric terms, the other, only algebraic terms and the parameters. Then, the effects of variation of the parameters on stability can be found by a simple graphical procedure. The two parts are

$$F(\tau\omega) = F_1(\tau,\omega) - F_2(\omega), \tag{138}$$

and

$$G(\tau\omega) = G_1(\tau,\omega) - G_2(\omega), \tag{139}$$

where

$$F_1(\tau,\omega) = (\omega^4 - 2\omega^2 + 0.25)\cos 2\tau\omega + (2\omega^3 - \omega)\sin 2\tau\omega, \tag{140}$$

$$F_2(\omega) = 0.25b - a\omega^2, \tag{141}$$

$$G_1(\tau,\omega) = (-2\omega^3 + \omega)\cos 2\tau\omega + (\omega^4 - 2\omega^2 + 0.25)\sin 2\tau\omega, \tag{142}$$

and

$$G_2 = c\omega. \tag{143}$$

The advantage of the splitting may be seen by examining the parts above. F_1 and G_1 are complicated trigonometric functions, but they can be easily computed on a digital computer for suitable ranges of ω and different values of τ. The parts that depend on the parameters F_2 and G_2 are relatively simple functions and are easily calculated by hand. Moreover, they represent simple geometric curves that can be easily plotted and adjusted for changes in parameters. For example, G_2 is a straight line (passing through the origin) whose slope depends on c. The zeros of F can be determined by the intersections between a plot of F_1 and a plot of F_2. That is, when $F_1 = F_2$, $F = F_1 - F_2 = 0$. The zeros of G can be determined similarly.

Therefore, the following procedure was developed:

1. Compute F_1 and G_1 for each desired value of τ. Some preliminary computation may be necessary to determine the range of ω. A suitable range for this system is $0 \leq 2\tau\omega \leq n\pi$, where n is 2, 3, or 4, for the chosen values of τ. As will be shown, only a few cycles of the functions need be plotted. In addition, only positive values of ω are necessary since F_1 is an even function of ω and G_1 is odd. Similarly, F is even and G is odd.

2. Plot each function F_1 and G_1 for a particular value of τ on separate graphs. Then, plot F_2 for some nominal values of a and b, such as a = 1 and b = 1, on the same graph as F_1. Similarly, plot G_2 on the graph of G_1 with c = 1.

3. Examine the points of intersection between F_1 and F_2 and those between G_1 and G_2. These are the zeros of F and G, respectively. Check that the proper number of zeros are present and they alternate as required by the Pontryagin criterion. Also check that the direction of change of the argument of $H_p(j\omega)$ is positive as ω increases. If these conditions are met, the system is stable.

4. If the system is not stable, or on the boundary of stability, adjust the graphs of F_2 and G_2 to obtain the desired intersections by changing the values of the parameters a, b, and c.

The detailed mechanics of the procedure and some short cuts are best illustrated by the example given in Section G below.

G. Example of the Procedure

Figures 13 and 14 are examples of typical graphs of the F and G functions for $\tau = 3\pi/4 = 2.35$ sec. Because of the time-scale factor of 100, this corresponds to a real time delay of 23.5 msec. In Fig. 13, the oscillatory curve is G_1; the straight lines are G_2 for different values of c. The

line for c = 1 does not intersect the second peak. Therefore the number of real roots of this G is two less than the G's for the other cases. As will be shown, this demonstrates an obvious case of instability. No adjustment of the other parameters, a and b, can correct this instability.

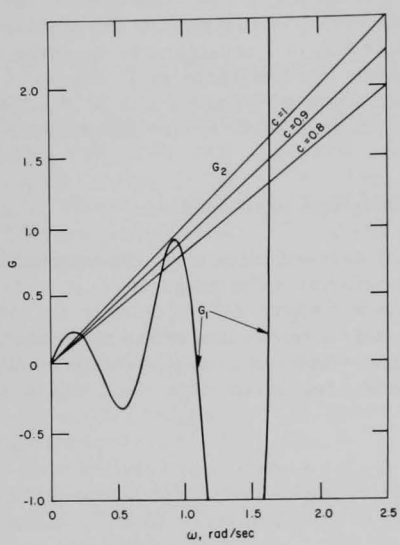

Fig. 13. G Functions for $\tau = 3\pi/4$ sec

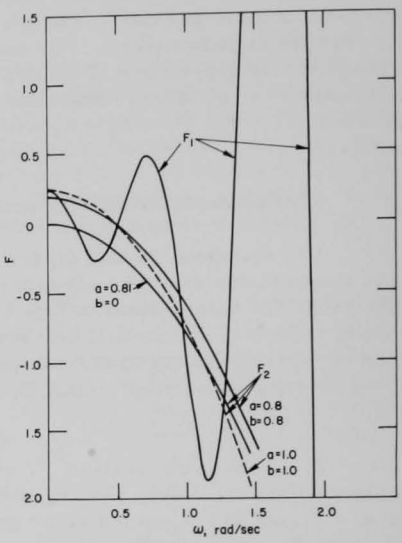

Fig. 14. F Functions for $\tau = 3\pi/4$ sec

In Fig. 14, F_1 is shown with a few F_2 curves for different values of a and b. The F_2 curve for a = 1, b = 1 intersects F_1 at $\omega = 0$. This indicates a zero of F at $\omega = 0$. However, Fig. 13 shows that G always has a zero at $\omega = 0$. This combination indicates a zero of H(s) on the imaginary axis at the origin. Because of this, the zeros of F and G do not alternate, and that condition of the criterion is not met. This is the situation with the zero at the origin discussed in Chapter II. For the present, this difficulty will be avoided by considering curves an incremental amount below this one. This curve actually indicates a stability boundary because an F_2 curve slightly above this one misses intersecting this peak of F_1. This results in nonreal zeros of F and denotes instability. In Appendix D it is shown that this zero at the origin can be accommodated by indenting the contour of Fig. 12 around it with a small semicircle, as is often done when applying the Nyquist criterion.

Another general point mentioned earlier is illustrated in these figures. The amplitude of each function F_1 and G_1 increases rapidly with ω because of the ω^4 term as compared to F_2 and G_2, which increase with ω^2 and ω^1, respectively. Therefore, intersections are assured beyond a

certain value of ω for any reasonable changes in a, b, or c. As can be seen, the intersections beyond $\omega = 2$ occur at points where the F_1 and G_1 curves are almost vertical. Therefore, the zeros of F and G are practically the zeros of F_1 and G_1 beyond $\omega = 2$. Also, for larger values of ω the functions become approximately

$$F_1 \simeq \omega^4 \cos 2\tau\omega, \tag{144}$$

and

$$G_1 \simeq \omega^4 \sin 2\tau\omega. \tag{145}$$

These functions are 90° out of phase with respect to each other; therefore, the alternation of zeros is assured. As a result, after the existence of a sufficient number of zeros has been determined, the investigation of the effects of adjusting the parameters can be confined to a small range of ω (in this case, for ω from zero to about two).

The procedure for determining if F and G have the proper number of alternating zeros is demonstrated for a = b = c = 0.8. For this set of parameters, the zeros of F and G can be tabulated from Figs. 13 and 14 and the digital-computer data for the values of the functions beyond the range of the figures. These zeros are marked off on the ω-axes in Fig. 15. Oscillating curves are drawn through these zeros to roughly indicate the form of F and G. These curves have a distorted ordinate scale and serve only to indicate the location of the zeros of the functions and their sign between the zeros. Figure 15 shows that for values of ω greater than about two, the distance between zeros is almost constant and approximately equal to $\pi/2\tau = 2/3 = 0.67$.

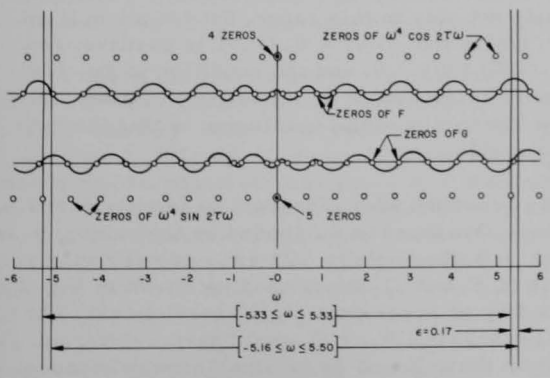

Fig. 15

Zeros of F and G for $\tau = 3\pi/4$ sec and a = b = c = 0.8

The range of ω in which zeros are counted is, from Fig. 12 for $y = \omega\tau$, $-2\pi k + \epsilon \le \omega\tau \le 2\pi k + \epsilon$. The index k must be large enough so that

every increase of the index by one results in the appearance of the same number of new zeros in the range. This occurs when the zeros of the functions F and G are almost periodic, and, for Fig. 15, it occurs before $\omega = 5$. With this value of ω, the approximate value of k can be determined from $k = \tau\omega/2\pi = 15/8$. Since k must be an integer, $k = 2$ is chosen. One-half the range of ω is $2\pi k/\tau = 16/3 = 5.33$. Therefore, the total range of ω is $-5.33 + \epsilon \leq \omega \leq 5.33 + \epsilon$.

Counting the zeros of the functions F and G is a method of determining if all the zeros are real. This is also accomplished by comparing the number of zeros of each function with that of its dominant term for the same suitable range of independent variable. For all the zeros to be real, the number must be the same, as discussed at the end of Section D of this chapter.

The end points of a suitable range of ω are selected by the proper choice of ϵ. Figure 15 also shows the zeros of $\omega^4 \sin 2\tau\omega$, the dominant term of G. For very large values of ω, the zeros of each function and its dominant term approach each other, and they can be matched on a one-to-one basis. The zeros of G at $\omega = \pm 5.4$ correspond to those of the dominant term at $\omega = \pm 5.33$. The range of ω should include the corresponding zeros of each function. Also, the ends of the range should be sufficiently far from any zeros so there is no confusion as to whether a zero is within the range. The value $\epsilon = 0.17$ provides the suitable range of $-5.16 \leq \omega \leq 5.50$ as shown in Fig. 15. In addition, this choice is well suited to the function F since the ends of the range are away from the zeros of F.

In the above range of ω, the functions F and G each have 20 zeros. Notice, for example, that $\omega^4 \sin 2\tau\omega$ has a quintuple zero at $\omega = 0$. As a consequence, the zeros of F and G are all real and simple, and, as indicated in Fig. 15, they alternate not only in this range, but for all ω from $-\infty$ to $+\infty$. Finally, at $\omega = 0$, notice that $G(0) = 0$, $G'(0)$ is positive, and $F(0)$ is positive; therefore, $G'(0)\,F(0) > 0$, and the condition of Eq. 126, concerning the positive velocity of the vector W, is satisfied. Thus, all the conditions of Theorem 1a are met, and the conclusion is that the system with $a = b = c = 0.8$ is stable.

The same conclusion is reached when Theorem 2a is considered. For $v = 2$ and $r = 4$, the angle that must be subtended by the vector W is $8k\pi + 4\pi + \delta_1$ radians. For $k = 2$, the angle is $20\pi + \delta_1$, or very nearly 10 revolutions. The 20 zeros of F and G, distributed as shown in Fig. 15, also indicate an angle of $20\pi + \delta_2$ or approximately 10 revolutions. The value of δ_2 is less than $\pi/2$; otherwise F or G would have a different number of zeros. This limit on the value of δ_2 is small enough because the only errors possible in determining the angle subtended by W are integral multiples of 2π. The tip of W describes a closed contour in the

W-plane and makes either full encirclements of the origin or none at all. Therefore, the value of angle deduced from Fig. 15 sufficiently matches that required by Theorem 2a, and this again indicates a stable condition.

The detailed attention given to the behavior of the functions F and G beyond the range of Figs. 13 and 14 is necessary only when an unknown system is being considered. If some prior information about the stability of the system is known, shortcuts are possible. For example, in the system under study, if all the signal-transmission channels are disconnected, the system is obviously stable. In this case, $a = b = c = 0$, the curves F_2 and G_2 in Figs. 13 and 14 coincide with the horizontal axis, and the zeros of F and G are the zeros of F_1 and G_1. Thus, the number and order of zeros that represent a stable system are the same as the number and order of the zeros of F_1 and G_1.

Similarly, since the system with $a = b = c = 0.8$ is stable, any change in the number of zeros of the functions F or G or their order will result in instability. For example, increasing the value of c to 1.0 does this by reducing the number of zeros of G by two. These two zeros become nonreal. Adjusting the curves of F_2 and G_2 from a stable to an unstable configuration enables the limits of stability to be found in terms of the parameters a, b, and c.

H. Adjustment of the Parameters to Find Stability Boundaries

The adjustment of the F_2 and G_2 curves in Figs. 13 and 14 to find the stability boundaries can be done in many ways. The procedure used depends often on which parameters have major interest. The method chosen here is more for illustrative purposes than efficiency. First, the stability conditions are found for the parameters a, b, and c, and then these results are used to determine the stable regions in gain-parameter space.

Since certain values of the parameter c cause unconditional instability, this parameter is adjusted initially. It is adjusted incrementally to permit stability. Then, for each value of c, the allowable values of a and b are found. Figure 13 shows G_2 lines for three different values of c. As stated before, since the line for $c = 1$ does not intersect the second peak of G_1, the system is unstable, regardless of the values of a and b. For each of the other two lines, five intersections with G_1 are shown, including two at the second peak and one at the origin. These are the zeros of the function G. The location of these zeros can be shown as points on a graph of F. For example, four of the zeros of G for the line $c = 0.9$ are shown as the points A, B, C, and D in Fig. 16. The abscissa values of these points are the locations of the zeros of G. For alternation of the zeros of F and G and hence stability, the F_2 curves must intersect the F_1 curve once and only once between each pair of adjacent points.

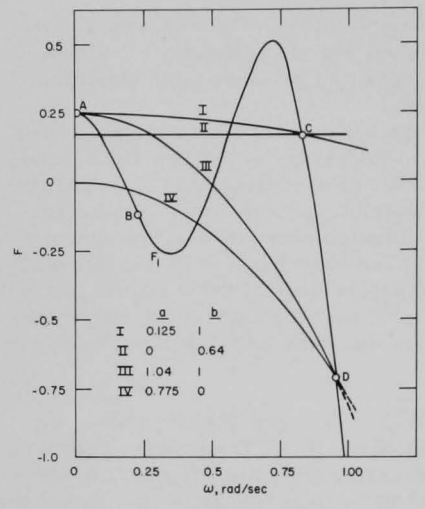

Fig. 16. Allowable F_2 Curves for $c = 0.9$ and $\tau = 3\pi/4$ sec

In this case, the stability boundaries are determined completely by the location of these four points. Because of the growth of F_1 and G_1 with ω, all other intersections are assured. The pairs of points AB and CD form openings like windows. The size of the window CD depends much on the value of c. For example, for the line just tangent to the second peak of G_1, points C and D come together, and the window closes to a single point. On the other hand, there is very little change in the window AB for the same changes in c.

The extrema of a and b are found from the four curves shown in Fig. 16. Each F_2 function has the form $0.25b - a\omega^2$. The corresponding curve must start on the ordinate axis between zero and 0.25. The system under study considers only positive values of a and b. Because of point A, no values of b greater than one are allowed. Curve I sets the minimum value of a when $b = 1$. If a were smaller, the curve would pass above point C. The minimum value of $a = 0$ is permitted only for values of b below that for curve II. Similarly, point D establishes the maximum values of a for $b = 0$ and $b = 1$. For this value of c, point B is not a limitation. If negative values of b were permitted, point B would be a limitation.

The other limiting curves are those that start somewhere between zero and 0.25 on the ordinate and pass through either point C or D. They give the intermediate values of a and b on the stability boundaries. The values of a and b that cause an F_2 curve to pass through a point $[\omega_0, F_1(\omega_0)]$ on the F_1 curve can be found from the relation

$$F_2(\omega_0) = F_1(\omega_0) = 0.25b - a\omega_0^2. \tag{146}$$

But this is an equation for a straight line in the (b,a)-plane. Thus the stability boundaries in this plane are straight lines between the extremum points found previously.

I. Stability Diagrams

If the procedure of Section H above is repeated for different values of c, the various stability boundaries in the (b,a)-plane can be found.

Some of these are shown in Fig. 17. The stable regions are located between the pairs of lines corresponding to the same values of c. The region reduces to a single line for c = 0.99, the tangent line. For c = 0.8 and less, there is no boundary on the left side; therefore, the stable region extends to the a = 0 axis.

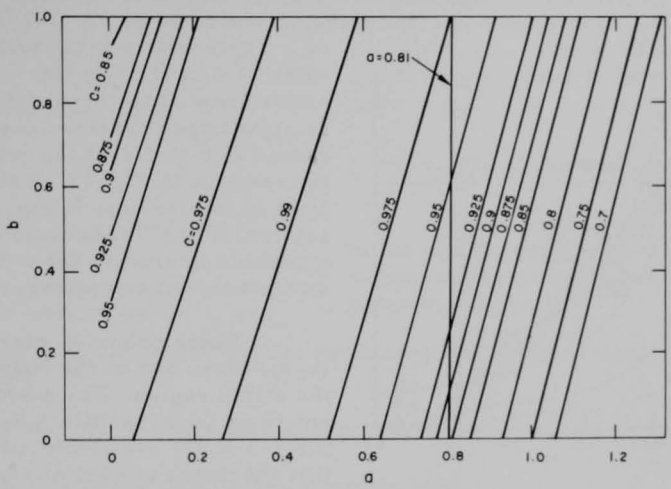

Fig. 17. Stability Diagram for a, b, and c with $\tau = 3\pi/4$ sec

The values of the transmission-gain parameters that result in a stable system can be found from Fig. 17. The gain parameters are related to a, b, and c by Eq. 54, which is repeated here:

$$\left.\begin{aligned} a &= d_1 d_2, \\ b &= k_1 k_2, \\ \text{and} \\ c &= 0.5(k_1 d_2 + k_2 d_1). \end{aligned}\right\} \tag{147}$$

In the case used for comparison throughout this study, $d_1 = d_2 = 0.9$, and the above equations become

$$\left.\begin{aligned} a &= 0.81, \\ b &= k_1 k_2, \\ \text{and} \\ c &= 0.45(k_1 + k_2). \end{aligned}\right\} \tag{148}$$

This case is represented by the vertical line at a = 0.81. For any value of c that crosses this line, all the values of b on the line above the intersection indicate a stable system. The intersection is a stability boundary point.

The points corresponding to the above intersection points can be found in the (k_1,k_2)-plane. In this plane, as indicated by Eq. 148, each value of b represents a hyberbola, and each value of c, a straight line. Figure 18 shows some of the hyperbolas and straight lines corresponding to the values of b and c at the points of intersection in Fig. 17. For each point of intersection in Fig. 17, there are two in Fig. 18, because each hyperbola intersects the corresponding straight line at two points.

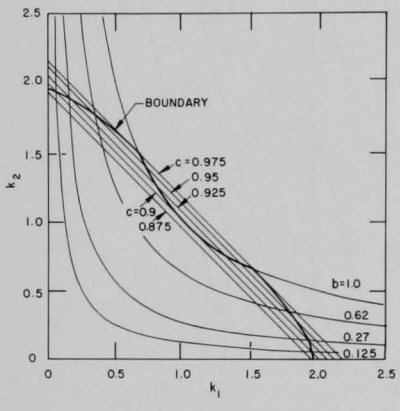

Fig. 18. Stable Region in (k_1,k_2)-plane for $\tau = 3\pi/4$ sec and $d_1 = d_2 = 0.9$

These points of intersection in (k_1,k_2)-plane are on the boundary of the stable region. For example, the points on the hyperbola $k_1k_2 = 0.27$ (or b = 0.27) are stable, provided that the points are located to the left of the straight line for c = 0.925, $0.45(k_1+k_2) = 0.925$. Similar conditions apply for the other hyperbolas. Connecting the corresponding points of intersection gives the stability boundary. The hyperbola $k_1k_2 = 1$ is also part of the boundary. Points on this boundary, however, indicate a zero of the system equation at the origin, which is acceptable as discussed earlier. Figure 18 shows the complete boundary.

In a manner similar to that described in Sections G and H, of this chapter, stability diagrams for other values of time delay can be constructed. Figure 19 shows the stable regions in the (b,a)-plane for different values

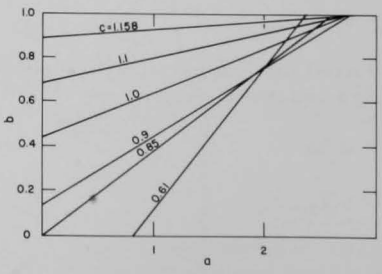

Fig. 19

Stability Diagram for a, b, and c with $\tau = \pi/8$ sec

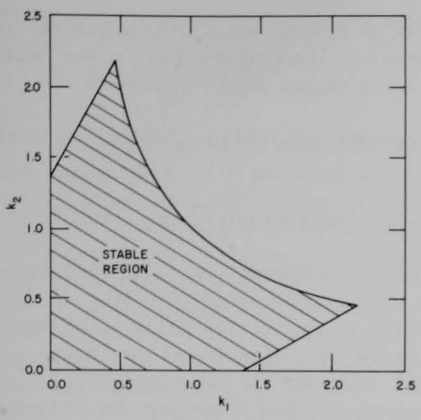

Fig. 20. Stable Region in (k_1, k_2)-plane for $\tau = \pi/8$ sec and $d_1 = d_2 = 0.9$

of c with $\tau = \pi/8 = 0.393$ sec or a real transmission time delay of 3.93 msec. In this case, the stable regions are above the lines for each value of c. The value of $c = 1 + 0.5\tau \approx 1.20$ is a critical value; stability is impossible for a greater value. Figure 20 shows the stable region in the (k_1, k_2)-plane for $\tau = \pi/8$ and $d_1 = d_2 = 0.9$.

J. Summary of the Procedure

A brief summary of the steps in the entire procedure for determining stability, as presented in this chapter, follows:

1. Find the characteristic equation of the system being investigated.

2. Put the equation into the form of an exponential polynomial, $P(z)$.

3. Check that $P(z)$ has a principal term.

4. Find the real and imaginary parts of $P(z)$ for values along the imaginary axis, $P(jy) = F(y) + jG(y)$.

5. Split the real and imaginary parts each into two parts, $F = F_1 - F_2$, $G = G_1 - G_2$, so that the first parts, F_1 and G_1, do not contain any variable parameters and the second parts, F_2 and G_2, are as simple as possible.

6. If necessary, change the independent variable to one that is convenient for computation, such as $y = \omega\tau$.

7. Compute and plot F_1 for an appropriate range of independent variable; compute and plot F_2 on the same graph for nominal values of the variable parameters. Repeat for G_1 and G_2 on another graph.

8. Note the points of intersection of each graph. These are the zeros of F and G.

9. Check that the location and number of the zeros of F and G meet the conditions for stability required by Theorem 1 of the Pontryagin criterion. Or, alternately, check that the angle subtended by the vector

$W = F + jG$, as indicated by the zeros of F and G, equals the value required for stability as stated in Theorem 2 of the criterion or, more basically, as deduced from application of the principle of the argument.

10. If necessary, adjust the parameters to obtain the desired intersections on the F and G graphs.

11. Determine the ranges of parameters required for stability.

Some comments on the procedure are appropriate. The effectiveness of the procedure depends on the success achieved in splitting the functions F and G in step No. 5. With the transmission gains as parameters, the splitting was very effective in the investigation of the force-reflecting servomechanism under study. Chapter VII discusses the application of the procedure to other systems or when other parameters vary If $\tau = 0$, when there is no delay, the procedure can also be applied. In that case, the principal term always exists. Finally, Chapter V discusses the use of another contour path besides the imaginary axis in step No. 4.

CHAPTER V

EXTENSION OF THE CRITERION TO DETERMINE RELATIVE STABILITY

The Pontryagin stability criterion basically requires determining the encirclements of the origin by a plot of P(z) or, what is essentially the same, measuring the change in argument of P(z) as z traverses the given contour. Since this is an application of the principle of the argument that does not require a particular contour, it is appropriate to consider extending the application of the criterion to other contours that could give information about relative stability. Such contours would include some regions of the left half plane in addition to the right half plane. The objective would be to find the values of adjustable parameters such that no zeros of the characteristic equation lie inside these contours. This chapter pursues this objective. Several contours are considered, but some include regions from which it is impossible to exclude zeros. Such a contour is discussed first to illustrate the method, and also to provide results that will be used later.

A. Contour with Radial Boundaries

Figure 21 shows the first contour investigated that includes part of the left half plane. The left boundary consists of two radial lines extending from the origin into the left half plane, each making an angle of 30° with the imaginary axis. The rest of the contour is the same as the one in Fig. 12 with the horizontal lines extended. The objective in using this contour was to try to eliminate any zeros of the system function that had arguments of less than 120° or greater than 240°. Thus, all zeros would have a damping ratio of 0.5 or greater. This value was chosen because it is a commonly used lower limit for a damping factor. With this limit, the system would have no lightly damped time responses.

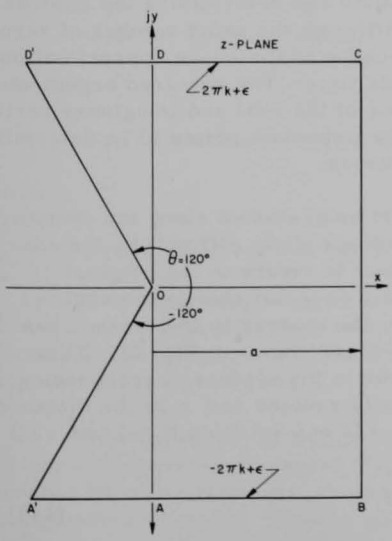

Fig. 21. First Contour for Determination of Relative Stability

The same system function, P(z), of Eq. 123 is used in this chapter. Also, a similar procedure is attempted for evaluating the change in argument of P(z) as discussed in Section IV.D. Therefore, as z traverses the part of the contour from A through B and C to D, as shown in Fig. 20, the change in argument

of P(z) approaches $8k\pi + 4\pi$, because the approximation of $P(z) \simeq (1/\tau^4)z^4e^{2z}$ still applied on this part of the contour. As z traverses the additional horizontal parts A'A and DD', however, the above approximation does not hold because the exponent of e has a negative real part and one of the polynomial terms becomes significant. Although the exact change in argument is not easily determined, limits on its value can be found. The approximation that is valid for these parts of the contour is $P(z) = (z^2/\tau^2)[(z^2/\tau^2)e^{2z} - a]$. The contribution to the change in argument of the term in the brackets as z traverses DD' does not increase indefinitely with k, but has a value between $-\pi$ and $+\pi$ radians. The contribution due to the (z^2/τ^2) term is $\pi/3$. The same changes in argument occur as z traverses A'A. Therefore, the total contribution due to z traversing DD' and A'A is a value between $2\pi/3 - 2\pi$ and $2\pi/3 + 2\pi$ radians. Finally, the total change in argument of P(z), as z traverses A'BCD', lies between $8k\pi + 8\pi/3$ and $8k\pi + 20\pi/3$ radians, or between $4k + 4/3$ and $4k + 10/3$ revolutions, as k approaches infinity.

In order that there be no zeros inside this contour, the change in argument of P(z), as z traverses the whole contour, must be zero as required by the principle of the argument. Therefore, the change in argument as z traverses A'OD' must equal the value found above as z traverses A'BCD'.

The argument of P(z) along contour A'OD' is determined as before by splitting P(z) into real and imaginary parts and determining the number of zeros of each by a graphical method. Although the exact number of zeros required for each function is not known because of the above approximations, establishing a minimum is sufficient at this time. The required argument variation requires no less than $8k + 2$ zeros of the real and imaginary parts, to produce $4k + 4/3$ revolutions. Again, the important points to be determined are that there are no nonreal or multiple zeros.

To carry out the process, P(z) must be evaluated along the contour. Only the part OD' is necessary since the values along A'O will be the conjugates of these. Also, it is again convenient to return to the original variables by substituting $z = s\tau$ for z. This does not change the angle of the radial lines of the contour. Therefore, the contour in the s-plane has the identical shape as the contour in the z-plane shown in Fig. 21. Thus, the values of s along the part of the contour in the s-plane corresponding to OD' are $s = re^{j\theta}$, where $\theta = 120°$ or $2\pi/3$ radians and r is the distance from the origin. Substituting for s in Eq. 122 and splitting $H_p(s)$ into real and imaginary parts yields

$$H_p(re^{j2\pi/3}) = F_r(r) + jG_r(r), \tag{149}$$

where

$$F_r(r) = e^{-\tau r}(-0.5r^4 + 2r^3 - r^2 - 0.5r + 0.25) \cos(\sqrt{3}\,\tau r)$$
$$- e^{-\tau r}\sqrt{3}(0.5r^4 - r^2 + 0.5r) \sin(\sqrt{3}\,\tau r)$$
$$+ 0.5ar^2 + 0.5cr - 0.25b \tag{150}$$

and

$$G_r(r) = e^{-\tau r}\sqrt{3}(0.5r^4 - r^2 + 0.5r) \cos(\sqrt{3}\,\tau r)$$
$$+ e^{-\tau r}(-0.5r^4 + 2r^3 - r^2 - 0.5r + 0.25) \sin(\sqrt{3}\,\tau r)$$
$$+ 0.5\sqrt{3}(ar^2 - cr). \tag{151}$$

Again the real and imaginary parts each can be separated into a complicated trigonometric part without the parameters a, b, or c, and a simpler algebraic part containing the parameters. This yields

$$F_r(r) = F_{r1}(r) - F_{r2}(r), \tag{152}$$

and

$$G_r(r) = G_{r1}(r) - G_{r2}(r), \tag{153}$$

where

$$F_{r2}(r) = 0.25b - 0.5cr - 0.5ar^2 \tag{154}$$

and

$$G_{r2}(r) = 0.5\sqrt{3}(cr - ar^2). \tag{155}$$

The remaining terms are contained in the complicated parts, F_{r1} and G_{r1}, and, as before, can be evaluated on a computer. The simpler parts, though not as simple as before, are still only quadratics and are manageable for variations of a, b, and c.

The objective, as before, is to find zeros of F_r and G_r by finding the points of intersection between F_{r1} and F_{r2} and between G_{r1} and G_{r2}, respectively. There is, however, an essential difference between this case and the imaginary-axis case. The F_{r1} and G_{r1} terms contain negative exponentials, $e^{-\tau r}$, and as r increases to infinity, F_{r1} and G_{r1} approach zero. F_{r2} and G_{r2} however, continue to grow so that for r greater than a certain value, the amplitudes of F_{r1} and G_{r1} will be less than F_{r2} and G_{r2}, respectively,

and there will be no more intersections. But as k increases, more intersections are required to provide the minimum number of zeros, 8k + 2. This means that some of the zeros of F_r and G_r are not real, and some zeros of the system function lie in the wedge between the radial line and the imaginary axis, regardless of the values of a, b, and c. This is the case for any radial line whose angle is greater than $\pi/2$. As shown in Appendix C, there are chains of roots of the system equation far from the origin whose arguments approach $\pi/2$ from values greater than $\pi/2$. Therefore, the zeros cannot be excluded from inside contours of the type shown in Fig. 21.

B. The Composite Contour

A different contour was chosen to include part of the left half s-plane. (The change to the variable s is retained in this section.) Although the arguments of the zeros in chains far from the origin approach $\pi/2$, the real parts of the zeros continue to increase in magnitude proportional to log r so the chains do move away from the imaginary axis. Therefore, it is possible to choose a region to the left of the imaginary axis for the exclusion of zeros. A line parallel to the imaginary axis and to the left of it by σ units was chosen as part of the left boundary, as shown in Fig. 22. With the region between this line and the imaginary axis excluded, any lightly damped time response due to a zero with a large ratio of imaginary part to real part will decay at least as fast as $e^{-\sigma\tau}$. Also, since the magnitude of response due to zeros farther from the origin is generally less, it is more important that the zeros close to the origin be more restricted. The contour was not run straight past the origin since there is often a zero at or very near the origin. Also, any negative real zeros between the σ-line and the origin are acceptable because they do not indicate an oscillatory response. The radial line is run at the angle of 120° as before and is terminated at r = 1. This is about the magnitude of the natural frequency of the system and was chosen so that only oscillatory zeros of greater magnitude are permitted. Therefore, any higher-frequency oscillations would probably have smaller magnitudes and be less significant. The choice of the terminal value of r results in the value of $\sigma = -1/2$.

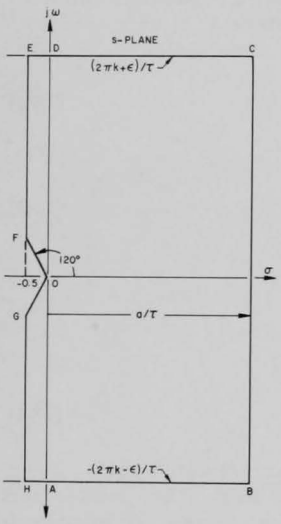

Fig. 22. Composite Contour for Determination of Relative Stability

To evaluate $H_p(s)$ along the vertical line of this contour, the value $s = -0.5 + j\omega$ is substituted into Eq. 122. Splitting H_p into real and imaginary parts, separating the terms containing parameters, and simplifying yields

$$H_p(-0.5 + j\omega) = F_\sigma(\omega) + jG_\sigma(\omega), \tag{156}$$

$$F_\sigma(\omega) = F_{\sigma 1} - F_{\sigma 2}, \tag{157}$$

$$G_\sigma(\omega) = G_{\sigma 1} - G_{\sigma 2}, \tag{158}$$

$$F_{\sigma 1} = e^{-\tau}(\omega^4 - 0.5\omega^2 + 1/16) \cos 2\tau\omega, \tag{159}$$

$$G_{\sigma 1} = e^{-\tau}(\omega^4 - 0.5\omega^2 + 1/16) \sin 2\tau\omega, \tag{160}$$

$$F_{\sigma 2} = 0.25b + 0.25a - 0.5c - a\omega^2, \tag{161}$$

and

$$G_{\sigma 2} = (c - a)\,\omega. \tag{162}$$

The form of Eqs. 159 and 160 is deceptively simple. If a different value of σ were chosen, both sine and cosine terms would occur in each function. Although $F_{\sigma 1}$ and $G_{\sigma 1}$ contain exponentials, their exponents are constant; therefore, intersections for large ω are assured.

The real and imaginary parts of $H_p(s)$ are different functions on the various sections of the part of the contour HGOFE shown in Fig. 22. When the functions are evaluated, only the top half of the contour need be considered since the bottom half produces conjugate values. Therefore, for the line OF, the functions are

$$F = F_r(r), \quad 0 \le r \le 1, \tag{163}$$

and

$$G = G_r(r), \quad 0 \le r \le 1; \tag{164}$$

and for the line FE,

$$F = F_\sigma(\omega), \quad \omega \ge 0.5\sqrt{3}, \tag{165}$$

$$G = G_\sigma(\omega), \quad \omega \ge 0.5\sqrt{3}. \tag{166}$$

The above functions are used to evaluate the change in argument of $H_p(s)$ along the contour HGOFE by investigating the zeros of F and G. The change in argument must equal that for $H_p(s)$ when s traverses the contour between the same points but on the right side; that is, the path HBCE. The change in argument for ABCD has already been evaluated as approaching $8k\pi + 4\pi$ radians or $4k + 2$ revolutions. The contribution due to traversing the segments HA and DE is negligible as k approaches infinity. Therefore, this again leads to the requirement of $8k + 4$ alternating and simple zeros

for F and G on the path HGFOE. Since all the functions of F and G on this path have been split so that the simpler parts contain the parameters, the zeros of F and G are found in the same manner as in Chapter IV, by using the intersections between the plots of the two parts of each function.

C. Example of the Procedure

Figures 23 and 24 are typical plots of the F and G functions for the composite contour for $\tau = \pi/8$. The functions F_{r1}, F_{r2}, G_{r1}, and G_{r2} are plotted against the imaginary-axis component, ω, of their independent variable r. Since $\omega = r \cos 120° = 0.866\ r$, this is equivalent to an abscissa scale change for the interval $0 \leq r \leq 1.0$ or $0 \leq \omega \leq 0.866$. Although this is not necessary and is not done in the next example, it shows that the functions are continuous at the point $\omega = 0.866$. For example, $F_{r1} = F_{\sigma 1}$ and $G_{r1} = G_{\sigma 1}$ at this point.

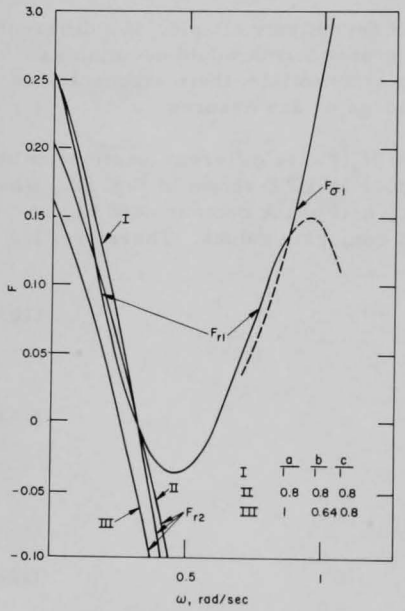

Fig. 23. Relative-stability F Functions for $\tau = \pi/8$ sec

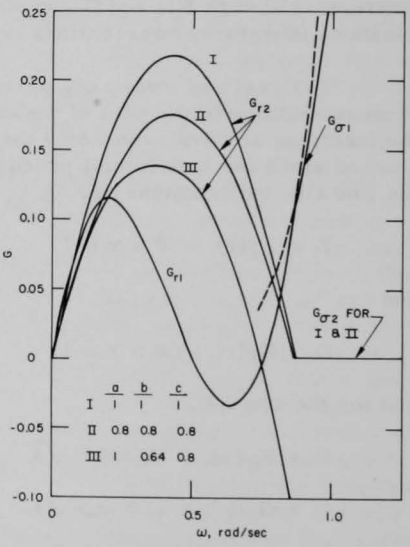

Fig. 24. Relative-stability G Functions for $\tau = \pi/8$ sec

Each of the functions F_2 and G_2 are shown for three sets of values of the parameters, as follows:

No. I: $a = b = c = 1.0$,

No. II: $a = b = c = 0.8$,

and

No. III: $a = 1.0$, $b = 0.64$, $c = 0.8$.

The proper places for intersections are not as obvious as in the examples in Chapter IV. Figure 23 shows, however, that if F_{r2} for parameter set No. II represents a system that meets the conditions for relative stability, F_{r2} for set No. III does not, because it does not intersect this negative peak of F_{r1}. The curve for F_{r2} for set No. I indicates a zero of $H_p(s)$ at the origin. This zero is avoided by indenting the contour around it, as discussed in Appendix D. Therefore, attention is confined to the curves for set No. II.

The important range of ω for the consideration of intersections is that shown in Figs. 23 and 24. Beyond the range of the figures, the values of ω at the points of intersection approach those for the zeros of the functions $F_{\sigma 1}$ and $G_{\sigma 1}$ because the amplitudes of these functions grow so rapidly with ω. Even the next point of intersection between each F_2 curve shown in Fig. 23 and the one F_1 curve lies between $\omega = 2.3$ and 2.4, while the zero of F_1 occurs at $\omega = 2.0$.

From the intersections in Figs. 23 and 24 and the computer data for the values of the functions F_1 and G_1, the locations of the zeros of F and G are found. These zeros are shown on the ω-axes in Fig. 25.

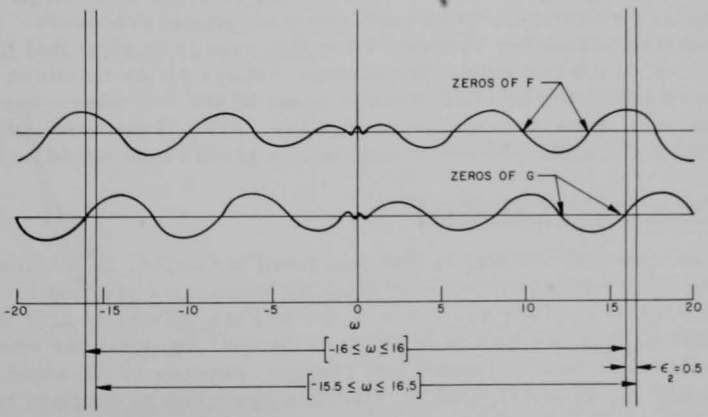

Fig. 25. Zeros of F and G along Relative-stability Contour for $a = b = c = 0.8$ and $\tau = \pi/8$ sec

As for the example in Chapter IV, the zeros are joined by a smooth curve that has no specific amplitude relationship to the actual functions except that it denotes the sign of the function between zeros. The range of ω chosen is that for $k = 2$. Then the range $-2\pi k + \epsilon \leq \omega\tau \leq 2\pi k + \epsilon$ becomes, for $\tau = \pi/8$, $-16 + \epsilon_2 \leq \omega \leq 16 + \epsilon_2$. At the ends of this range and beyond, the zeros of F and G are spaced very regularly. The value of $\epsilon_2 = 0.5$ is chosen as being sufficient to exclude from the range the zero of G at $\omega = -16.0$ and include the one at $\omega = 16.0$.

Each function F and G has the required number of zeros, which is $4k + 4$ or 12 zeros, for the range in Fig. 25. Since these zeros alternate, the vector $H_p(s)$, as s traverses the left side of the composite contour, subtends an angle of $8k\pi + 4\pi + \delta$ radians, where δ is less than $\pi/2$. Also, at each zero, the sign of the other function indicates that the angle increases in the positive direction as ω increases. Therefore, it has been determined that the change in argument of $H_p(s)$, as s traverses the entire composite contour, is zero to within an error of much less than π radians. Since the change must be zero or an integral multiple of 2π, the change is zero. Consequently, no zeros are located inside the contour, and the system with $a = b = c = 0.8$, has the desired relative stability.

In effect, a variation of Theorem 2 has been used, except that the contour has been distorted slightly. The condition of Eq. 126 has not been used because the discontinuities of F' and G' at $\omega = 0$ and $\omega = 0.866$ would require special consideration. Rather, the direction of the angle was found from the signs of the functions shown in Fig. 25. Also, an applicable variation of Theorem 1 was not developed completely because the procedure used here is primarily a graphical one and is very satisfactory. Theorem 1 would be more necessary in an exclusively analytical procedure. The main requirement to establish Theorem 1 for this case is to show that $H_p(s)$, for values of s on the left side of the contour, always yields functions F and G that have a maximum number of zeros equal to $4kv + r$, where v and r are the exponents of the principal term of $H_p(s)$. Then, if the zeros of F and G were real and simple, the exact number in a given range would be known.

D. Relative-stability Diagrams

In a manner similar to that described in Chapter IV for absolute stability, information for relative-stability boundaries are found. Since the F_2 and G_2 curves for $a = b = c = 0.8$ in Figs. 23 and 24 give the correct intersections, the curves are adjusted to the limiting positions where the number of order of zeros would just change. Because of the rapid growth of the functions F_1 and G_1 with ω, attention again can be confined to the range of ω from 0.0 to 0.866 or r from 0.0 to 1.0. Therefore, only the functions F_{r2} and G_{r2} of Eqs. 154 and 155 need be considered for F_2 and G_2. In this case, however, the functions are not so simple, and the parameters a and c appear in both functions. Nevertheless, results can be obtained relatively easily.

The case used for comparison throughout this investigation has $d_1 = d_2 = 0.9$ and, therefore, a fixed value of $a = 0.81$. With this value, Eqs. 154 and 155 become

$$F_{r2}(r) = 0.25b - 0.5cr - 0.405r^2, \tag{167}$$

and

$$G_{r2}(r) = 0.866cr - 0.7015r^2. \tag{168}$$

The function G_{r2} now contains only the one parameter, c. Figure 24 indicates that for a large value of c the G_{r2} curve will be completely above the first hump of G_1 and there will be one less intersection in this range. Also, for a small enough value of c, G_{r2} will be completely below the first hump and there will be two less intersections. In this way, the limits of the allowable values of c are found. Then, for particular allowable values of c, the G_{r2} curves can be drawn. Their intersections with G_1 yield the zeros of G, which then can be indicated on the plot of F_1.

For each value of c, the function F_{r2} has b as the only variable parameter. Since b is in the constant term, the shapes of the F_{r2} curves remain the same as b changes; only their ordinate intercepts change. Furthermore, it is simple to slide the F_{r2} curves up and down to obtain the proper intersections, which are between the zeros of G, and thereby obtain the allowable range of b. In this manner, the region of allowable values of b and c was obtained and is shown in Fig. 26A. It is the area inside the designated boundary.

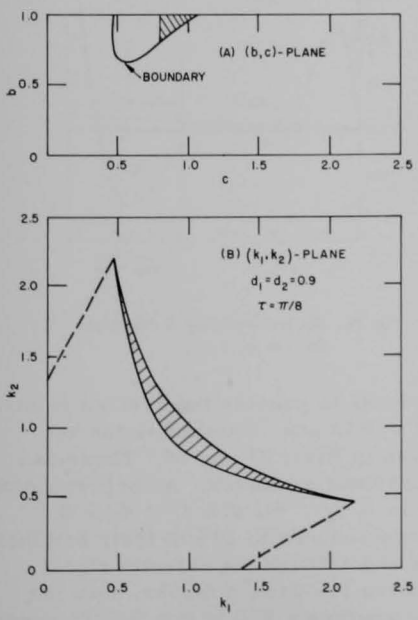

Fig. 26. Relative-stability Diagrams for $\tau = \pi/8$ sec

By the method described in Section IV.I, of using intersections between the hyperbolas and straight lines derived from the values of b and c, respectively, the region of relative stability can be found in the (k_1, k_2)-plane. The region for this case is shown in Fig. 26B. Not all the allowable values of b and c contribute to defining the region in Fig. 26B. This occurs because when b and c are related to k_1 and k_2, they are not completely independent. The region of useful values of b and c is shown shaded in Fig. 26A.

In Fig. 26B, the boundaries of the absolute-stability region are also shown by dashed lines. An interesting feature of this diagram is that the desired relative stability is not achieved for small values of positional gain for these values of d_1 and d_2. On the other hand, if all gains are small, equal to zero, for example, the desired degree of relative stability exists, but the system has poor performance.

E. Another Example

Another example illustrates that, although absolute stability is relatively easy to achieve, the desired amount of relative stability is not. For the same composite contour of Fig. 22, the functions F and G for $\tau = 3\pi/4$ are shown in Figs. 27 and 28. (The comparable curves for determining absolute stability are those in Figs. 13 and 14.) In this case, the F_1 and G_1 curves are such that the F_2 and G_2 curves associated with the nominal values of the parameters do not intersect their second or third humps. For example, if a = 0.81, no curves can be found that provide the required intersections.

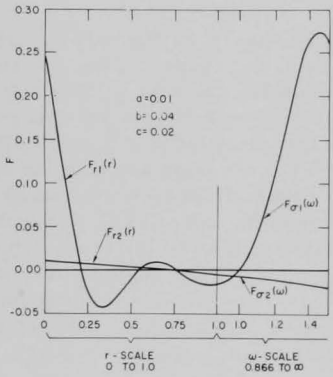

Fig. 27. Relative-stability F Functions for $\tau = 3\pi/4$ sec.

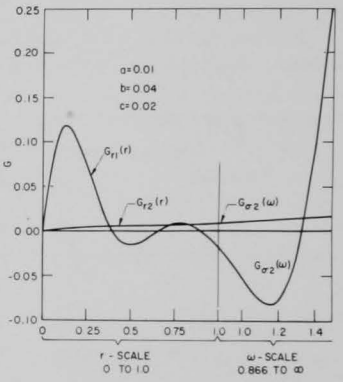

Fig. 28. Relative-stability G Functions for $\tau = 3\pi/4$ sec.

Some sets of parameters can be found to provide the desired relative stability. The trivial case of a = b = c = 0 is one. Another is the set a = 0.01, b = 0.04, and c = 0.02 as shown in Figs. 27 and 28. These can be verified in the same manner as the previous examples. A corresponding set of transmission-gain parameters is $k_1 = k_2 = 0.2$ and $d_1 = d_2 = 0.1$. Therefore, the transmission gains must be reduced to 20% of their nominal values for the positional signal channels and 10% for the velocity signal channels. This is a severe reduction. Even low gain, however, does not ensure relative stability. The set of parameters a = b = c = 0.0225 does not produce the proper intersections.

F. Summary

The procedure developed in this chapter is one for determining the range of gain parameters that produces a certain amount of relative stability in the response of the system under study. The criterion of relative stability is the requirement that the characteristic equation of the system has no zeros inside the contour of Fig. 22, even as k and a go to infinity. The procedure is essentially the same as that pertaining to absolute stability given in Section IV.J, except for small changes in two steps. In Step 4 the real and imaginary parts of $P(z)$, or $H_p(s)$, are found for values along the left side of the contour of Fig. 22 instead of along the imaginary axis. In Step 9, the zeros of F and G are used to determine if the change in argument of $H_p(s)$ along the left side of the contour is sufficient to cancel that due to the rest of the contour. Specific reference to Theorem 1 is omitted because its use has not been completely justified.

CHAPTER VI

ANALYTICAL AND EXPERIMENTAL RESULTS

A. Analytical Results

The main analytical results have already been presented in the form of stability diagrams in the various chapters as they were developed. In this section some are assembled for comparison.

The several stability regions for the case used throughout this report of $d_1 = d_2 = 0.9$ are shown superimposed in Fig. 29. The boundary nearest the origin, labeled "any τ," encloses the region of unconditional stability. The values of k_1 and k_2 for any point inside this region produce a system that is stable for any value of time delay. Successively larger regions are enclosed by the boundaries for $\tau = 0$ and $\tau = \pi/8$. The boundary for $\tau = 3\pi/4$ shows the tendency for the regions to be smaller as τ increases further and to approach that of "any τ." The dashed line is the left boundary of the relative stability region for $\tau = \pi/8$ developed in Chapter V.

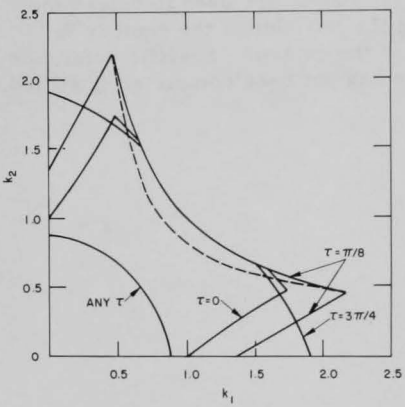

112-9487

Fig. 29. Stability Regions in (k_1, k_2)-plane for $d_1 = d_2 = 0.9$ and Different Values of Time Delay

In all cases, except that for "any τ," the hyperbola $k_1k_2 = 1$ forms part of the boundary. As discussed previously, points on this boundary indicate a zero at the origin and are considered in the stable region. Points on the side borders are not considered in the stable region; they indicate a system response of sustained oscillations. The axes are arbitrary boundaries because negative gains are not permitted. Actually, there are substantial stable regions in the other quadrants.

Some general conclusions can be drawn from Fig. 29. The larger stable region for $\tau = \pi/8$, compared to $\tau = 0$, indicates the stabilizing effects of a time delay under certain conditions. On the other hand, for the symmetrical system with $k_1 = k_2$, the stable range is the same for the two time delays considered. For some larger value of time delay, however, the stable range will be decreased. The region of unconditional stability may be one of poor relative stability. For example, for $\tau = \pi/8$, it is well separated from the region of designated relative stability. Finally, as determined in Chapter V, Fig. 29 has no region in which the required relative stability exists for $\tau = 3\pi/4$.

B. Experimental Results

Some analytical results were checked on the analog computer setup described in Section III.D. Approximately 150 test runs were made with different combinations of parameters. In general, the tests corroborated the analytical results.

The procedure used the setup shown in Fig. 9. The potentiometers were adjusted to give the proper parameter values. The desired time delay was established by selecting the tape speed of the magnetic tape recorder. The recorder amplifiers were adjusted for proper gain and balance. With the tape recorder operating, an initial value was set for the variable $\theta_1(t)$, the input position of the system. After waiting at least a length of time equal to the time delay, we started the problem. The variable $\theta_1(t)$ and the instantaneous error, $\theta_1(t) - \theta_2(t)$, were recorded on a strip-chart recorder. The instantaneous error is not measurable in a physical system because of the time delay, but it is conveniently available in the simulation.

The main difficulties encountered in the testing were due to the drift and offset of the amplifiers of the tape recorder. These are enhanced by a factor of about 60 by the analog-computer amplifiers that follow in the same signal channels. Some of the initial tests gave recorder traces of signals that went off-scale and seemed to indicate unexpected instability. The drift and offset were substantially reduced by providing more warmup time for the amplifiers. However, any errors due to these difficulties are conservative; that is, only stable systems would possibly be identified incorrectly as unstable, but the reverse would not occur.

Most of the tests were performed for the normalized time delays of $\tau = 0$, $\pi/8$, and $3\pi/4$ sec. These correspond to the real time delays of $\lambda = 0$, $\pi/800$, and $3\pi/400$ sec. The time-scale factors and the tape-recorder delays used are discussed in Section III.D. In addition, however, many of the tests for $\lambda = 3\pi/400$ sec were repeated with a different arrangement. The computer is equipped with a feature that allows switching its time scale to speed up the problem by a factor of 10. With this change and the 10-times-faster tape-recorder speed, the same real time delay is simulated. The recorder traces of the repeated tests were almost identical with the originals. Also, with various combinations of the computer time-scale switch and the tape-recorder speeds, several tests were made using time delays not examined analytically. These were equivalent to real time delays of $3\pi/40$, $3\pi/4000$, $\pi/80$, and $\pi/8$ sec.

All the recorded traces of the tests for the time delays of $\lambda = 0$, $\pi/800$, and $3\pi/400$ sec strongly resembled exponential functions or exponentially varying sinusoids. Almost all appeared to be the responses of second-order, or sometimes third-order, systems to a step input. Only for $\lambda = 3\pi/40$ sec and greater were the traces substantially different.

Some results warrant special mention. It was shown early in the development of the F and G curves in Chapter IV that the nominal system with a = b = c = 1.0 was not stable for $\lambda = 3\pi/400$ sec. The tests for this condition showed a slowly growing sinusoid, which indicates a system just barely unstable. When the d's were reduced to 0.9, the tests showed a slowly decaying sinusoid and hence stability. Increasing the time delay to $3\pi/40$ sec again caused instability; reducing the k's to 0.9 did not eliminate it. The latter tests indicate the tendency of the stability boundary in Fig. 29 to shrink toward the "any τ" boundary as the time delay increases.

The point $k_1 = 1.5$, $k_2 = 0.67$ on the stability boundary in Fig. 29 for $\lambda = 3\pi/400$ sec was checked. After careful adjustments and many trials, the results indicated that the system was stable but could easily become unstable with a slight change in parameters. On the other hand, the checking of a point just inside the boundary at $k_1 = 1.8$, $k_2 = 0.2$ indicated stability with no difficulty.

Figures 30-32 are oscillograph traces of test results. Each d and k was set equal to 0.9 for the three time delays of 0, $\pi/800$, and $3\pi/400$ sec. The time scale of the traces depends on the time-scale factors used in the simulation. The factors were 35.7 for the test runs with $\lambda = \pi/800$ sec, and 59.3 with $\lambda = 3\pi/400$ sec. For convenience, the latter was used for $\lambda = 0$. The results were typical. The average value of the error settles to zero relatively quickly, but the input (and output) positions do not.

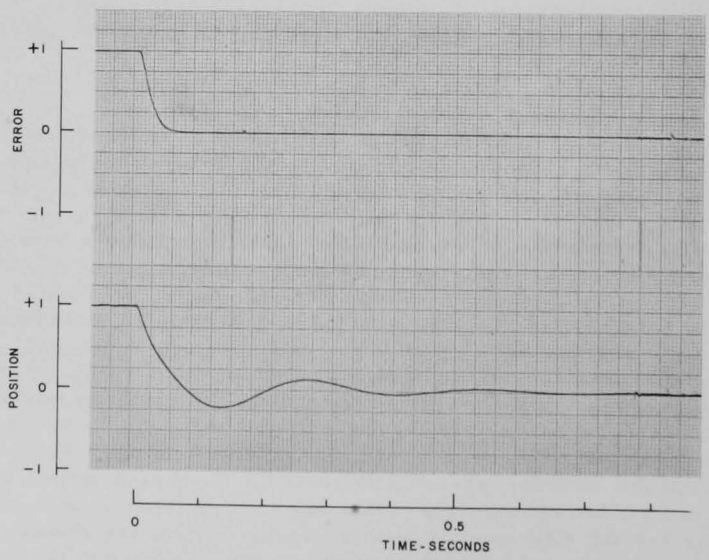

Fig. 30. Oscillograph Traces for Tests with $k_1 = k_2 = 0.9$, $d_1 = d_2 = 0.9$, and $\lambda = 0$

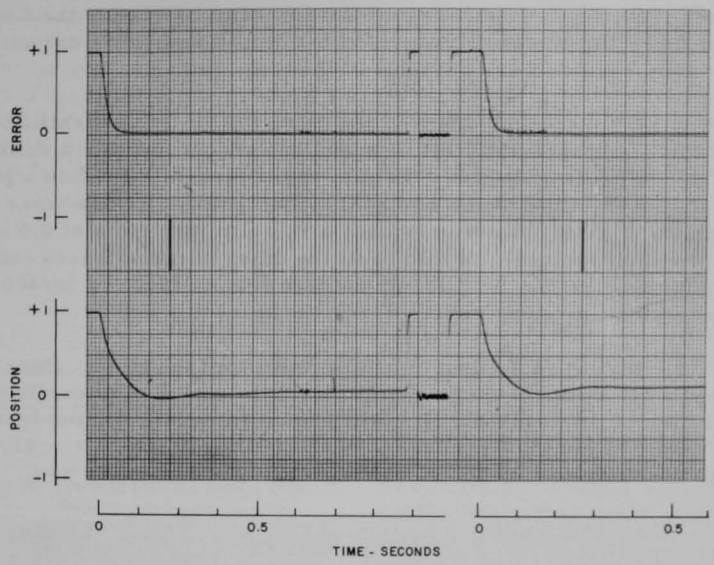

Fig. 31. Oscillograph Traces for Tests with $k_1 = k_2 = 0.9$, $d_1 = d_2 = 0.9$, and $\lambda = \pi/800$ sec

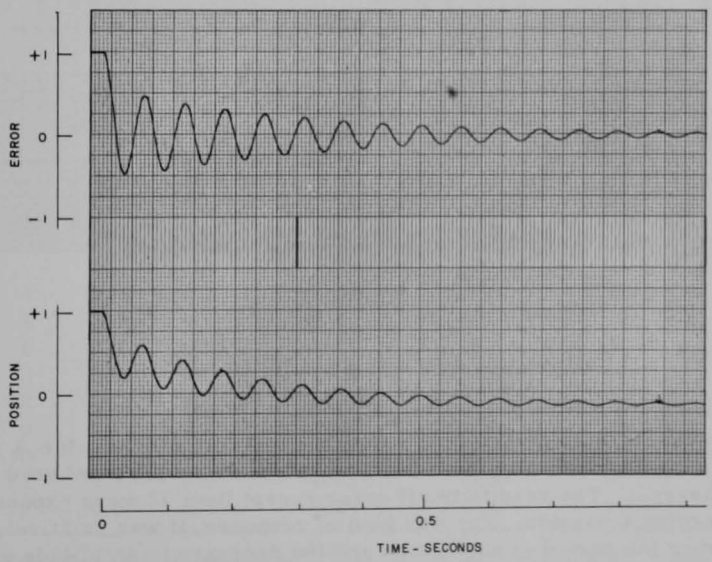

Fig. 32. Oscillograph Traces for Tests with $k_1 = k_2 = 0.9$, $d_1 = d_2 = 0.9$, and $\lambda = 3\pi/400$ sec

The offset of the tape-recorder amplifiers is responsible for the final values of the position signal being different from zero. This did not occur when the tape recorder was not used in the tests with $\lambda = 0$.

Figure 31 shows an effect of time delay on relative stability. The trace of the position signal for $\lambda = \pi/800$ sec should indicate a damping ratio of 0.5 or greater, because the gain parameters used define a point in the relative stability region of Fig. 29. Comparison of this trace with the response of a second-order system with a damping ratio of 0.5 indicates that this is the case. In contrast, the other position traces indicate smaller damping ratios. In fact, all the test results for $\lambda = 3\pi/400$ sec indicated a small damping ratio.

Figure 33 is an excerpt of another oscillograph trace. Here the response is not a simple damped sinusoid. It is a case of unconditional stability with the d's equal to zero and longest time delay of any test, $\lambda = \pi/8$ sec. (The corresponding normalized time delay is $\tau = 12.5\,\pi$sec.) Although the system is stable, it would probably not have any use.

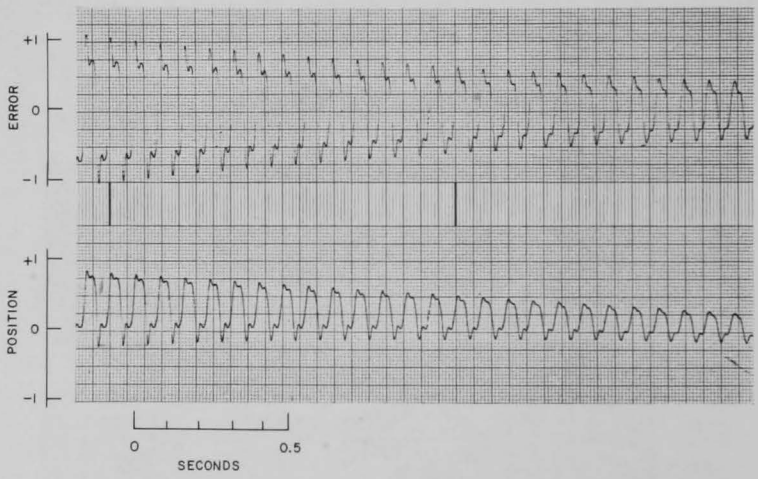

Fig. 33. Oscillograph Traces for an Unconditionally Stable System with $k_1 = k_2 = 1.0$, $d_1 = d_2 = 0$, and $\lambda = \pi/8$ sec

Several tests were run to verify the stability diagram for $\lambda = \pi/800$ sec, redrawn in Fig. 34. Tests were run for every numbered point in the diagram. The results in all cases except Item 12 were exponentially varying sinusoids. For this kind of response, it was relatively easy to measure the period of oscillation and the decrease in amplitude of the peaks. If the form of the response is assumed to be $Ae^{\sigma\tau} \sin(\omega t + \phi)$, the

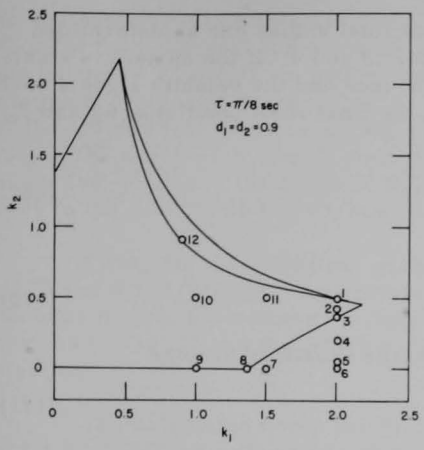

Fig. 34. Points in Stability Region That Were Tested Experimentally

values of σ and ω can be determined from the measured information. Table I lists the values so determined. These values are normalized to be consistent with the normalized values of s and τ used throughout.

All items in Table I agreed with the results predicted from the stability diagram of Fig. 34 except Item 1. The data of Item 1 indicate a damping factor of about 0.28 rather than an expected value greater than 0.5. It was difficult to obtain good tests for this point. This was often the case for points along the k_1k_2 = 1 hyperbola away from the midpoint. For many of the tests, it could not be easily determined if the oscillograph trace was aiming for a constant final value off-scale or infinity. Repeated adjustments of the gain potentiometers, however, usually resulted in the final value being on-scale. Tests for other points away from that hyperbola gave consistent results without much difficulty. In those cases, the responses had a final value of zero, except for small differences due to amplifier offset.

TABLE I. Analog-computer Results for $\tau = \pi/8$ sec and $d_1 = d_2 = 0.9$

Item	k_1	k_2	σ (sec^{-1})	ω (rad/sec)	Comment
1	2.0	0.5	-0.02[a]	0.07[a]	Stable
2	2.0	0.425	-0.01	0.15	Stable
3	2.0	0.35	0.0	0.21	Sustained oscillation
4	2.0	0.2	+0.02	0.28	Unstable
5	2.0	0.05	+0.04	0.34	Unstable
6	2.0	0.0	+0.05	0.35	Unstable
7	1.5	0.0	+0.01	0.39	Unstable
8	1.35	0.0	-0.004	0.41	Stable
9	1.0	0.0	-0.03	0.46	Stable
10	1.0	0.5	-0.09	0.32	Stable
11	1.5	0.5	-0.05	0.21	Stable
12	0.9	0.9	-0.1[b]	0.2[b]	Stable

[a]Data for this item varied. This is the best of several trials.
[b]Difficult to estimate these values.

The effects of amplifier offset on final values can be determined from the equations for motor torque, Eqs. 3 and 4. If the system is stable, it should come to rest with the motor torques and the velocity signals each equal to zero. Under these conditions, the final shaft positions, θ_{1f} and θ_{2f}, appear in these equations as follows:

$$-K_{11}\theta_{1f} + K_{12}\theta_{2f} = 0, \tag{169}$$

and

$$K_{12}\theta_{1f} - K_{22}\theta_{2f} = 0. \tag{170}$$

However, if offset voltages are present, the equations become

$$-K_{11}\theta_{1f} + K_{12}\theta_{2f} + V_1 = 0, \tag{171}$$

and

$$K_{12}\theta_{1f} - K_{22}\theta_{2f} + V_2 = 0. \tag{172}$$

Here V_1 and V_2 represent the combined effects of the offset voltages on motors No. 1 and No. 2, respectively. Solving for the final values yields

$$\theta_{1f} = \frac{V_1K_{22} + V_2K_{12}}{K_{11}K_{22} - K_{12}K_{21}}, \tag{173}$$

and

$$\theta_{2f} = \frac{V_1K_{12} + V_2K_{11}}{K_{11}K_{22} - K_{12}K_{21}}. \tag{174}$$

Since $K_{11}K_{22} - K_{12}K_{21}$ is usually small, the final values are very dependent on offset. When $K_{11}K_{22} - K_{12}K_{21} = 0$, which is the same as $k_1k_2 = 1$, the final values are infinite, if there is any offset.

In addition to the difficulty with Item 1, there was a problem of obtaining any better than rough values for σ and ω from the test results for Item 12. As can be seen from Fig. 31, measuring the amplitude of successive peaks is impossible. The value of σ was based on an estimate of the location of an envelope of the trace. Since there was some doubt about the quantitative results of both tests in the region of relative stability, another method of verification was used.

C. Other Verification

The results of Items 1 and 12 in Table I and some other points were verified by calculating the zeros of the appropriate system equation. Since

no computer program was available for finding the zeros of such equations, some of the programs for previous calculations were used. The values of the functions F and G, in polar-coordinate form, were calculated for incremental values of the modulus r, from zero to two, and the argument θ, of the independent variable s in the upper half plane. From these data, the loci of the zeros of F and G were plotted in the s-plane. The intersections of the loci indicated the zeros of $H_p(s)$. Where necessary to improve accuracy in the vicinity of a zero, smaller increments were used.

First, for the conditions of Item 12, the calculated zeros are at -0.75 and $0.192\angle\pm122.5°$. Apparently the complex pair with its smaller modulus mainly determines the response. These zeros are outside the contour of Fig. 22 and therefore meet the requirements for relative stability.

The calculated zeros for the conditions of Item 1 are 0.0, -0.036, and $1.97\angle\pm162°$. But these are outside the relative stability contour, as they should be. The calculation was repeated with the value of k_2 changed slightly to 0.49. The zeros for this condition are $0.051\angle\pm100°$ and $1.98\angle\pm162°$. The two dominant zeros are now almost on the imaginary axis. Apparently, in this case the location of the dominant zeros is very dependent on only slight changes in parameters. Therefore, the unexpected response in the test of Item 1 was probably due to slight errors in the setting of the parameters. This sensitivity of the response to parameter changes is indicated by the narrowness of the relative-stability region in this vicinity. For Item 2, the calculated values for the dominant zeros are $-0.007 \pm j\,0.13$. These indicate reasonable agreement with the values of σ and ω in Table I.

Zeros were calculated for a few more conditions. Again, since some difficulty was experienced in setting up these parameters, the zeros for a = b = c = 1.0 were found. They are:

for $\tau = 0$: 0, 0, -1, -1 (stable);

for $\tau = \pi/8$: 0, -0.14, -0.73 (stable);

and

for $\tau = 3\pi/4$: 0, -0.33, -0.57, $0.95\angle\pm89°$ (unstable).

Finally, the estimated values of the zeros found from the traces shown in Fig. 32 were compared to the calculated values. They are:

as estimated: $-0.06, -0.03 \pm j\,0.99$;

as calculated: $-0.05, -0.02 \pm j\,0.95, -0.33, -0.57$.

Estimates for the larger zeros at -0.33 and -0.57 were not made because of the rapid decay of the response associated with them. That part of the re- [illegible] than 4% of its initial value with 0.1 sec.

CHAPTER VII

OTHER APPLICATIONS OF THE NEW TECHNIQUES

This chapter briefly discusses other possible extensions or applications of the new techniques developed in the earlier chapters for determining the stability of time-lag systems. Since these topics are beyond the planned scope of the investigation, they will not be developed or demonstrated in complete detail.

A. Load Effects

An important consideration of any force-reflecting servomechanism is its behavior under load. A system with time delay is no exception. In a manipulator application, the system encounters different loads ranging in magnitude from zero to infinity. Of first interest is the effect of simple passive loads on the stability of the system. This could be investigated by the methods already developed, if each load condition is considered individually. This would be a tedious process, however, if carried out for the full range of loads. Therefore, an alternate procedure that avoids this difficulty is developed as outlined below.

The characteristic equation of the system with a general passive load has been already derived in Chapter II. (It is Eq. 55.) The load consists of an inertia, a viscous damper, and a spring whose magnitudes are linearly related to the factors α, β, and γ, respectively, as indicated by Eq. 45. If this equation is multiplied by $e^{2s\tau}$ and evaluated along the imaginary axis, the following expressions for the real and imaginary parts result:

$$\begin{aligned} F(\tau\omega) = {} & [A_0 \cos 2\tau\omega - B_0 \sin 2\tau\omega] + \alpha[A_1 \cos 2\tau\omega - B_1 \sin 2\tau\omega] \\ & + \beta[A_2 \cos 2\tau\omega - B_2 \sin 2\tau\omega] + \gamma[A_3 \cos 2\tau\omega - B_3 \sin 2\tau\omega] \\ & + a\omega^2 - 0.25b, \end{aligned} \tag{175}$$

and

$$\begin{aligned} G(\tau\omega) = {} & [B_0 \cos 2\tau\omega + A_0 \sin 2\tau\omega] + \alpha[B_1 \cos 2\tau\omega + A_1 \sin 2\tau\omega] \\ & + \beta[B_2 \cos 2\tau\omega + A_2 \sin 2\tau\omega] + \gamma[B_3 \cos 2\tau\omega + A_3 \sin 2\tau\omega] \\ & - c\omega, \end{aligned} \tag{176}$$

where

$$\left.\begin{aligned} A_0 &= \omega^4 - 2\omega^2 + 0.25, \\ A_1 &= \omega^4 - 0.5\omega^2, \\ A_2 &= -\omega^2, \\ \text{and} \\ A_3 &= -0.5\omega^2 + 0.25; \end{aligned}\right\} \tag{177}$$

and

$$\left.\begin{aligned} B_0 &= -2\omega^3 + \omega, \\ B_1 &= -\omega^3, \\ B_2 &= -\omega^3 + 0.5\omega, \\ \text{and} \\ B_3 &= 0.5\omega. \end{aligned}\right\} \tag{178}$$

When $\alpha = \beta = \gamma = 0$, Eqs. 175 and 176 reduce to Eqs. 135 and 136, the equations for the system with no load, which were investigated in Chapter IV.

Splitting the equations as in Chapter IV gives

$$F(\tau\omega) = F_1(\tau, \omega) - F_2(\omega), \tag{179}$$

and

$$G(\tau\omega) = G_1(\tau, \omega) - G_2(\omega), \tag{180}$$

where $F_1(\tau, \omega)$ and $G_1(\tau, \omega)$ are the trigonometric parts and, as before,

$$F_2(\omega) = 0.25b - a\omega^2, \tag{181}$$

and

$$G_2(\omega) = c\omega. \tag{182}$$

In this case, $F_1(\tau, \omega)$ and $G_1(\tau, \omega)$ are linear combinations of the terms inside the brackets in Eqs. 175 and 176. But the terms in the brackets do not depend on the load parameters. Therefore, they can be calculated easily on a digital computer, just as the first term was for the data needed in Chapter IV.

With these data, the procedure in this case is to plot the first term of F_1. This results in a curve such as that for F_1 in Fig. 14. Then one or more of the other terms in the brackets are plotted on the same graph. The total ordinate of F_1 at each value of ω is the sum of the ordinates of each part, appropriately weighted by its associated load factor, α, β, or γ. Then intersections with the F_2 curves can be found, which give the zeros of the function F. A similar procedure yields the zeros of the function G. With this information, Pontryagin's criterion can be applied to determine stability.

In practice, it is difficult to work simultaneously with the parts associated with all the load parameters. If each type of load is considered individually, however, the procedure is much easier. It also demonstrates any stabilizing or destabilizing tendency due to increasing a load parameter. In addition, construction of the summation curves is not necessary at all points but only in the vicinity of intersections.

As an example, the system with $\tau = 3\pi/4$ and the nominal value of gain parameters, $a = b = c = 1.0$, was briefly investigated. With no load, this system is unstable. Increasing β, the viscous friction, has the greatest stabilizing effect. The system is stable with $\beta = 0.1$. Increasing α, the inertia, has a similar effect but not as great. The system is not stable when $\alpha = 0.1$, but it is when $\alpha = 1.0$. Increasing γ, the spring, at first does not tend to stabilize the system. With $\gamma = 1.0$, the zeros of F and G are farther out of order than with $\gamma = 0$. When $\gamma = 5.0$, however, the system is stable. As each parameter is increased beyond its stable value above, the system remains stable. Thus, the ranges of values of load parameters that produce stability could be determined.

If the system equation is evaluated along the relative stability contour of Chapter V, there is a similar separation of terms possible as in Eqs. 175 and 176. That is, F_1 and G_1 each will consist of a linear combination of terms weighted by the factors α, β, and γ. Therefore, the procedure of Chapter V can also be used to determine the effects of load parameters on the relative stability of the system.

B. Application to Classical Problems

A classical equation used in an example of the application of Pontryagin's criterion by Bellman and Cooke[28] is

$$H_p(s) = s^2e^s + as + b. \tag{183}$$

This could represent a system with a time lag $\tau = 1$. The objective, as usual, is to determine the values of the parameters a and b for which Eq. 183 has zeros in the left half plane only. To apply the criterion, $H_p(s)$ is evaluated along the imaginary axis. The resulting real and imaginary parts of $H_p(j\omega)$ are

$$F(\omega) = -\omega^2 \cos \omega + b, \tag{184}$$

and

$$G(\omega) = -\omega^2 \sin \omega + a\omega. \tag{185}$$

In Ref. 28, the conformance of these equations with the conditions of the criterion is determined analytically. However, the graphical technique developed in this investigation can also be applied. The parameters are contained in simple functions. Both functions represent straight lines; one of them is horizontal. Either method will yield the same results. The great advantage of the technique developed here is that it can easily be extended to much more complicated problems of similar form. For example, the equation

$$H_p(s) = f(s)e^s + as + b, \tag{186}$$

where f(s) is a polynomial in s of order of two or greater, can be investigated almost as easily as Eq. 183, since a and b still appear in simple terms. Equation 186 could not be treated analytically except when f(s) is simple.

In addition, Eq. 183 or 186 is evaluated along the relative stability contour of Fig. 22, the techniques of Chapter V can be applied. Thus, the effects of the parameters a and b on relative stability can also be found.

Another classical equation is

$$H_p(s) = \alpha e^s + b - se^s. \tag{187}$$

Along the imaginary axis, the real and imaginary parts of $H_p(j\omega)$ are

$$F(\omega) = \alpha \cos \omega + \omega \sin \omega + b, \tag{188}$$

and

$$G(\omega) = \alpha \sin \omega - \omega \cos \omega. \tag{189}$$

Again the procedures developed in this investigation can be applied. In this case, however, the parameter α occurs in the trigonometric terms. Therefore, the procedure discussed in Section A of this chapter would be used.

In addition, by these procedures, a more complicated equation of the similar form could be investigated almost as easily. Such an equation is

$$H_p(s) = \alpha g(s)e^s + f(s)e^s + b, \tag{190}$$

where f(s) and g(s) are polynomials of any order except zero.

C. An Alternate Procedure

Once it has been determined that the system function has a principal term and, therefore, does not have chains of zeros with positive real parts, it can be restored to a form with negative exponentials. This may lead to an advantage in certain cases. For example, if Eq. 187 is multiplied by e^{-s}, the result is

$$H(s) = (\alpha - s) + be^{-s}. \tag{191}$$

When this function is considered on the Pontryagin contour of Fig. 12, the contribution to the change in argument, due to the three sides not including the imaginary axis, results almost entirely from the terms without the exponentials. On these three sides, because $|e^{-s}| \to 0$, the exponential term has very little contribution. Therefore, examination is again required of the behavior of the entire function along the imaginary axis. There, the real and imaginary parts of $H(j\omega)$ are

$$F(\omega) = \alpha + b \cos \omega, \tag{192}$$

and

$$G(\omega) = -\omega - b \sin \omega. \tag{193}$$

Dividing these equations by b puts them into a form for finding their zeros more easily. Thus, the equations become

$$F_b(\omega) = (\alpha/b) + \cos \omega, \tag{194}$$

and

$$G_b(\omega) = -(\omega/b) - \sin \omega. \tag{195}$$

The conditions of the Pontryagin criterion cannot be applied to the equations in this form. The main reason is that the dominant or principal trigonometric terms do not exist in Eqs. 194 and 195. As a result, the number of encirclements of the origin by $H(j\omega)$ is not uniquely related to the number of zeros of $F(\omega)$ and $G(\omega)$. In this case, there are many superfluous zeros of $F(\omega)$.

Nevertheless, the principle of the argument can be applied. And the change in argument of $H(j\omega)$ can be found from an examination of the zeros of Eqs. 194 and 195 and their magnitudes at certain values of ω. The zeros can be found by the usual graphical techniques.

Two main difficulties arise in this procedure. The many extra zeros must be taken carefully into account so that they do not contribute

to errors in the determination of the change in argument. Also, since the trigonometric terms are not dominant, significant changes in the order of intersections can occur at any value of ω. Therefore, the entire range must be carefully examined.

This procedure could be fairly easily applied to Eq. 191, but its range of application appears to be restricted to simple equations. For example, no useful results could be obtained when the procedure was applied to the equations for the system with load parameters investigated in Section A of this chapter. One purpose of the procedure is that it serves as a basis of comparison for the many advantages of the methods based on the Pontryagin criterion.

CHAPTER VIII

CONCLUSIONS, EXTENSIONS, AND RECOMMENDATIONS

A. Summary and Conclusions

The research subject has been the force-reflecting servomechanism of the type currently in use in manipulator applications, but with the addition of time delay in the signal-transmission channels. The absolute and relative stability of the system has been investigated using several techniques. Some of these are new procedures that have been developed.

Conventional techniques for determining stability were useful in obtaining some preliminary and general information. The generalized form of the Nyquist criterion yielded diagrams that demonstrated the instability of the system under certain conditions. However, no general conclusions could be derived from the diagrams as to the dependence of system stability on the values of parameters or even time delay. Almost every case would require a separate diagram.

A more useful and much more easily applied technique was that due to Satche. The Satche diagram easily supplied the critical value of time delay at which instability just occurs for a system with a particular set of parameters. It also indicated the shape of the system characteristic plot that would give higher critical values of time delay up to infinity. Bode diagrams were better, however, for determining the parameter values for which the system has an infinite critical value of time delay and therefore is unconditionally stable. Neither technique, however, was very useful in determining the range of values of parameters for which a system is stable with intermediate values of time delay.

The simulation of the system on the analog computer produced good results conveniently. The use of the magnetic tape recorder to provide the signal time delay was advantageous. Difficulties with the recorder amplifiers due to drift, offset, and a small signal-voltage range were easily overcome. The absence of problems with signal distortion and noise and the convenience of setting the delay provided the advantages over any other method such as Padé approximations. Although the tape speed could be adjusted only by a factor of ten, changing the time scale of the problem enabled the simulation of any delay required for the testing. The simulation brought attention to the special dependence of the stability of the system on the transmission-gain parameters and later helped verify most of the analytical developments.

Routh's criterion provided quantitative information about the dependence on gain parameters of the stability of the system without delay. The other techniques mentioned above or the root-locus method were much less

helpful because of the number of parameters involved or their location in the system equations. For systems with delay, the objective was to find a criterion as useful as Routh's.

The objective was accomplished by an adaptation and extension of the Pontryagin stability criterion for time-lag systems. Since the criterion had not been used for systems of this order (fourth order), a method of application was developed that was not restricted to second- or third-order systems. In the process of developing the new method, the Pontryagin criterion was explained by relating it to a fundamental theorem of complex variable theory, Cauchy's principle of the argument. The criterion is actually an extension of that principle. Therefore, extensions of the criterion could be made, if adherence to the principle was maintained.

Such an extension was accomplished by distorting the contour used in the criterion for enclosing the right half plane, so that it also includes part of the left half plane near the imaginary axis. By employing the principle of the argument, a procedure was developed by which it could be determined if zeros of the characteristic equation of the system were outside this contour. In addition, it was shown how to adjust the gain parameters, to exclude zeros from this region. Thus, the procedure provides a means for checking that a system has a certain amount of relative stability and for adjusting the variable parameters of the system to achieve that relative stability.

The procedure developed for determining either absolute or relative stability involves finding the change in the argument of the system function for values along the appropriate contour. For absolute stability, the Pontryagin criterion reduces this process to an investigation of the zeros of the real and imaginary parts of the system function evaluated along the imaginary axis. For relative stability, the change in argument can also be determined by a similar investigation of zeros. In this case, however, the system function is evaluated along the left side of the relative-stability contour.

In addition, it was shown that the real and imaginary parts of certain system functions can each be split into two parts in such a way as to yield many advantages. The characteristic function of the system under study is one of this class. One part is a complicated trigonometric function; the other is a relatively simple one containing the variable parameters of the system. The complicated parts can easily be calculated on a digital computer and plotted. The simple parts are easily calculated manually and plotted. Their plots are either straight lines or simple quadratic curves. The intersections between the plots of the complicated and simple functions yield the zeros that are sought. A procedure was given for changing the locations of the zeros by moving the simple lines and curves to achieve a desired arrangement of intersections. The new location of the lines and

curves determines the values of the parameters. Thus, a desired condition of stability or relative stability can be produced, provided it can be achieved within the range of adjustment of the parameters.

The stable regions in parameter space were determined by using the above procedures. A set of diagrams was presented showing the regions of stability in the position-gain parameter plane for particular values of time delay. A region of relative stability was also shown in one of the diagrams. Various points in these diagrams were verified by the analog-computer tests or by direct calculation of the zeros of the system functions.

In addition to verifying the analytical results, the analog-computer tests brought attention to important conditions that might have been overlooked in a completely analytical study. The early tests showed that the stability of the system could be sensitive to changes in the values of the gain parameters when separate signal-transmission channels were used. After better stability regions had been established, later tests showed a similar sensitivity to parameter changes under certain conditions. Further investigation revealed the sensitive regions in the stability diagrams, as discussed in Section VI.C. The testing also revealed the undesirable effects of offset voltages in the signal-transmission amplifiers.

Finally, it was shown that the procedures developed for determining stability or relative stability can be extended to other cases. The effects of load variations on the system under study were investigated by an adaptation of the procedures. Their use on classical equations, either directly or with a similar adaptation, was indicated. Other extensions are discussed in Section B below.

The procedures developed in this investigation have been effective in producing the desired results in all cases attempted.

As a result of this research, some general conclusions can be drawn regarding force-reflecting servomechanisms with time delay. For the shorter time delay of about 4 msec ($\lambda = \pi/800$ sec) used in this study, there was some improvement in stability. For the same parameter settings, the system with this short delay displayed a better damping ratio than one without delay. For the longer delay of about 22 msec ($\lambda = 3\pi/400$ sec), however, the system was much less stable. Although absolute stability could be achieved by adjustment of the parameters, the same degree of relative stability that was possible with the shorter delay could not be achieved with the longer delay. Similarly, the few tests made with longer delays also indicated that, even if absolute stability was possible, the system would have a low damping ratio and tend to be very oscillatory. Therefore, there are serious doubts as to whether a system with a delay of more than 25 msec can be made to have anywhere near the normal behavior of a system without delay unless major changes are made in the system.

B. Extension of Application of the Procedure

The procedures developed here can be applied to force-reflecting servomechanisms of much more complexity. In any practical system, additional time constants are associated with the various elements. For example, the torque of a motor, $T_m(s)$, is related to the control current in its field winding, $I(s)$, by the relation

$$T_m(s) = \frac{K}{1 + s\tau_m} I(s), \tag{196}$$

where τ_m is the time constant of torque buildup. Likewise, other time constants are associated with the reactive circuit elements in the motor-field circuit, in the signal and power amplifiers, and in the filters of any demodulating amplifiers. In each case, the input, $X_1(s)$, and the output, $X_2(s)$, can be related by

$$X_2(s) = \frac{1}{1 + s\tau_i} X_1(s), \tag{197}$$

where τ_i is the appropriate time constant.

The characteristic equation of such systems is more complex. Its order increases by two for each additional time constant. However, the complexity increases only in the already complicated part of the equation. When put into the form of an exponential polynomial, the system function has the form

$$H_p(s) = f(s)e^{2s\tau} - (as^2 + cs + 0.25b), \tag{198}$$

where $f(s)$ is a higher-order polynomial. For example, with one additional time constant on each side of the system, the order of $f(s)$ would be six. But, when the function is split into its real and imaginary parts, the additional complexity occurs only in the trigonometric parts. More algebraic manipulation and computer programming are required, but no additional manual computation, since the terms containing the parameters are the same. Therefore, the new procedures can be applied directly.

However, if any changes in the system are made that increase the order of the terms containing the parameters, the procedure could become difficult. In that case, additional digital computation would probably be helpful.

Only the term representing twice the time delay, $e^{2s\tau}$, occurs in Eq. 198. If the term $e^{s\tau}$ had appeared, the system function could still be an exponential polynomial. And, if the function had a principal term, the

procedures developed could be used. Therefore, a general form of the system equation to which the procedures can be applied is

$$H_p(s) = f(s)e^{2s\tau} + g(s)e^{s\tau} + h(s), \tag{199}$$

where f(s), g(s), and h(s) are polynomials, where the order of h(s) is two or less and the equation has a principal term. It is preferable, however, that the order of f(s) be at least one or two greater than the order of h(s) so that the important intersections occur at low values of ω. Finally, higher-order exponential terms could also be included, provided they were integral powers of $e^{s\tau}$, but these would occur in systems beyond the scope of this study.

C. Recommendations for Future Research

Adequate means for investigating the stability of a linear force-reflecting servomechanism with time delay have been developed. However, this is only the beginning of a long series of problems that must be resolved before a practical system can be evolved. One next major area requiring investigation is that involving the quality of force reflection or feel. This could possibly be carried out by using the impedance or admittance parameters discussed in Chapter II. Another area includes the effects of the operator and the system on each other. This probably involves a consideration of nonlinear impedances and additional time lags and time constants to account for the dynamic response of the operator. An experimental model of the system would be necessary for this investigation.

Other smaller but important practical problems require investigation. For example, the nonlinear characteristics of nonideal components could produce undesirable effects. Also, a practical transmission system using some form of pulse-code modulation could change the system behavior due to its sampling and filtering action.

Finally, there are many other possible extensions, modifications, and applications of the Pontryagin criterion. For example, one application could result in a digital-computer program for solving for the complex roots of exponential polynomials. Some attention in this area would be beneficial.

APPENDIX A

Complete Nyquist Diagrams

Figure 35A shows the complete contour used for the Nyquist criterion. The contour consists of the semicircle with the large radius R, the imaginary axis, and the semicircular indentation around the origin of radius r. In application of the criterion, the entire right half plane is enclosed by letting R approach infinity and r approach zero. Therefore, approximations can be used in evaluating the system characteristic equation on these semicircles. The value of the equation along the positive imaginary axis is determined as in Section III.A, and its complex conjugate is the value along the negative imaginary axis.

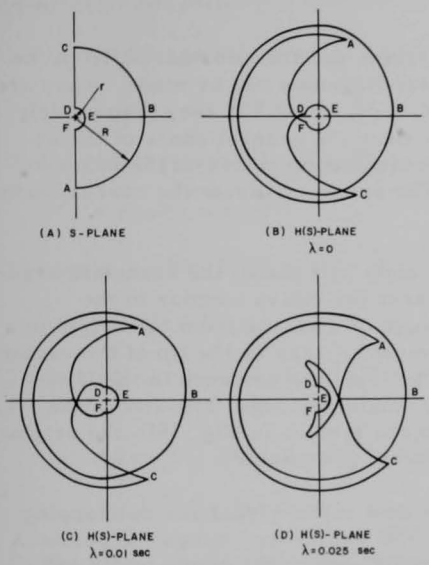

Fig. 35. Complete Nyquist Diagrams

For large values of s, Eq. 65 becomes

$$H(s) \simeq s^4. \tag{A.1}$$

Along the large semicircle, $s = Re^{j\phi}$; therefore,

$$H(Re^{j\phi}) \simeq R^4 e^{j4\phi}. \tag{A.2}$$

For small s, the series expansion for the exponential term is used. It is

$$e^{-2s\tau} = 1 - 2s\tau + \frac{4s^2\tau^2}{2!} - \dots . \tag{A.3}$$

Substituting this into Eq. 65 gives

$$H(s) = 0.25 - 0.25(1 - 2s\tau + 2s^2\tau^2 - \dots) + s - s(1 - 2s\tau + \dots)$$
$$+ 2s^2 - s^2(1 - 2s\tau + \dots) + 2s^3 + s^4. \tag{A.4}$$

For small s, the equation becomes

$$H(s) \simeq 0.5s\tau + s^2(1 + 2\tau - 0.5\tau^2). \tag{A.5}$$

Along the small semicircle, $s = re^{j\phi}$, and the equation becomes

$$H(re^{j\phi}) \simeq 0.5\tau re^{j\phi} + r^2e^{j2}(1 + 2\tau - 0.5\tau^2). \tag{A.6}$$

If $r \ll \tau$, the equation becomes

$$H(re^{j\phi}) \simeq 0.5\tau re^{j\phi}. \tag{A.7}$$

If, however, $\tau = 0$, the equation becomes

$$H(re^{j\phi}) \simeq r^2 e^{j2\phi}. \tag{A.8}$$

With the use of these approximations and the information from the diagrams in Fig. 4, the complete Nyquist diagrams can be made. They are shown in Figs. 35B, C, and D for $\lambda = 0$, 0.01, and 0.025 sec, respectively. The axis scales are highly distorted to show the general shape of the entire diagram. The letters show the corresponding points on the contours in the s-plane and in the H(s)-plane. The arrows indicate the corresponding directions of traversal.

For there to be no zeros in the right half plane, the change in argument of H(s) must be zero as s traverses the entire contour in the s-plane. That is, the total change in angle of a vector from the origin to a point on the contour in the H(s)-plane must be zero as the tip of the vector traces the entire contour. For this to be true, the contours in the H(s)-plane must not completely encircle the origin. In Figs. 35B and C, the origin is not encircled and the systems are stable; in Fig. 35D, the origin is encircled twice and therefore the system is unstable.

The encirclements are more evident if one visualizes unwrapping the contours from the origin. In Figs. 35B and C, the "wings" at points A and C can be brought around to completely expose the origin on its left. This cannot be done in Fig. 35D.

APPENDIX B

Complete Satche Diagram

The same contour in the s-plane, shown in Fig. 35A, used for the Nyquist diagram, is used for the Satche diagram. Also, similar approximations on the large and small semicircles are used as in Appendix A.

For large values of s, Eq. 70 becomes

$$F_1(s) \simeq s^2. \tag{B.1}$$

On the large semicircle, Eq. 70 becomes

$$F_1(Re^{j\phi}) \simeq R^2 e^{j2\phi}. \tag{B.2}$$

For large s, Eq. 71 yields

$$|F_2(s)| \leq 1. \tag{B.3}$$

Therefore, for values of s on the large semicircle, the points of $F_2(s)$ lie on or in the unit circle.

After Eq. 70 is divided out, the approximation for small s becomes

$$F_1(s) \simeq 1 + 4s^2. \tag{B.4}$$

On the small semicircle, this equation becomes

$$F_1(re^{j\phi}) \simeq 1 + 4r^2 e^{j2\phi}. \tag{B.5}$$

From its series expansion, the approximation of Eq. 71 for small s is

$$F_2(s) \simeq 1 - 2s\tau, \tag{B.6}$$

which, on the small semicircle, becomes

$$F_2(re^{j\phi}) \simeq 1 - 2\tau re^{j\phi}. \tag{B.7}$$

With the use of these approximations and the information from the plot in Fig. 5, the distorted but complete Satche diagram is drawn as shown in Fig. 36. The objective again is to find any change in argument of a vector, in this case $F = F_1 - F_2$, as s traverses the entire contour in Fig. 35A. The angular orientation of F can be determined by drawing a line from each unprimed point to the corresponding primed point in the figure.

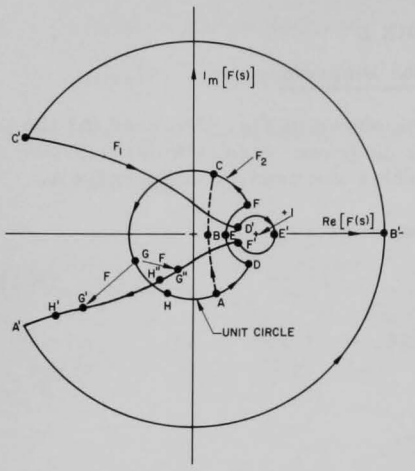

Fig. 36. Complete Satche Diagram

For τ less than the critical value and starting with EE', the angle of the vector F can be traced. It is zero at EE', becomes about $-\pi/2$ at FF', and approaches $-\pi$ for GG', HH', and AA'. At BB', the angle is back to zero. On the rest of the contour, it ranges to $+\pi$ and back to zero. Therefore, the net change is zero, and the system is stable.

When τ is greater than the critical value, the points G" and H" apply, and the angles are different. At GG", the angle returns to zero but continues in a positive direction through $+\pi/2$ at HH", $+\pi$ at AA', and to $+2\pi$ at BB'. The rest of the contour contributes another 2π; in this case, therefore, the total change is 4π. This indicates two zeros in the right half plane and instability.

APPENDIX C

Asymptotic Zeros of System Equation

From Eq. 122, the system equation is

$$H_p(s) = (s^4 + 2s^3 + 2s^2 + s + 0.25)\, e^{2s\tau} - (as^2 + cs + 0.25b). \tag{C.1}$$

For very large values of s, the equation can be approximated by

$$H_p(s) \simeq s^4 e^{2s\tau} - as^2. \tag{C.2}$$

As s becomes large, the zeros of $H_p(s)$ asymptotically approach those of the right side of Eq. C.2. Therefore, the problem is reduced to finding the zeros of

$$P(s) = s^2 e^{2s\tau} - a. \tag{C.3}$$

The double zero at $s = 0$ is discarded because this is not a large value of s.

If the substitution

$$w = se^{s\tau} \tag{C.4}$$

is made, Eq. C.3 becomes

$$W(w) = w^2 - a. \tag{C.5}$$

The zeros of this equation are

$$w_{1,2} = +\sqrt{a},\ -\sqrt{a}. \tag{C.6}$$

If only the first zero is considered,

$$w = \sqrt{a}\, e^{j0}. \tag{C.7}$$

Then

$$\log w = \log\sqrt{a} + j(0 + 2\pi n), \tag{C.8}$$

where

$$n = 0, \pm 1, \pm 2, \ldots .$$

From Eq. C.4,

$$\log w = s\tau + \log s. \tag{C.9}$$

Therefore

$$s\tau + \log s = \log \sqrt{a} + j(0 + 2\pi n). \tag{C.10}$$

The solution of this equation gives one chain of asymptotic zeros of $H_p(s)$. The equation for the other chain comes from the other zero of w in Eq. C.6 and is

$$s\tau + \log s = \log \sqrt{a} + j(\pi + 2\pi n). \tag{C.11}$$

Since

$$s = \sigma + j\omega = re^{j\phi}, \tag{C.12}$$

the real and imaginary parts of Eq. C.10 give

$$\sigma\tau + \log r = \log \sqrt{a} \tag{C.13}$$

and

$$\omega\tau + \phi = 0 + 2\pi n. \tag{C.14}$$

From Eq. C.13,

$$\sigma = -\frac{1}{\tau} \log \frac{r}{\sqrt{a}}, \tag{C.15}$$

and, since $\sigma = r \cos \phi$,

$$\cos \phi = -\frac{1}{\tau r} \log \frac{r}{\sqrt{a}}. \tag{C.16}$$

But since r is very large,

$$\phi = \pm(\pi/2 + \epsilon), \tag{C.17}$$

where $\epsilon \to 0$ as $r \to \infty$. Therefore, from Eq. C.14,

$$\omega\tau = 0 + 2\pi n \mp (\pi/2 + \epsilon). \tag{C.18}$$

Since $\omega = r \sin \phi$, $\sin \phi \to 1$, and r must be positive,

$$r = \frac{1}{\tau}\left|0 + 2\pi n \mp (\pi/2 + \epsilon)\right|. \tag{C.19}$$

Substituting this into Eq. C.15 gives

$$\sigma = -\frac{1}{\tau} \log \left| \frac{0 + 2\pi n \mp (\pi/2 + \epsilon)}{\tau\sqrt{a}} \right|. \tag{C.20}$$

From Eq. C.18,

$$\omega = \frac{1}{\tau} [+2\pi n \mp (\pi/2 + \epsilon)]. \tag{C.21}$$

Thus, Eqs. C.20 and C.21 give the real and imaginary parts of the asymptotic zeros of one chain. The values for the other chain are

$$\sigma = -\frac{1}{\tau} \log \left| \frac{\pi + 2\pi n \mp (\pi/2 + \epsilon)}{\tau\sqrt{a}} \right|, \tag{C.22}$$

and

$$\omega = \frac{1}{\tau} [\pi + 2\pi n \mp (\pi/2 + \epsilon)]. \tag{C.23}$$

The derivation could have been made in the same way if τ was a negative quantity. Then the real parts of the zeros would be positive. Thus, this demonstrates that an equation without a principal term has an infinite number of zeros with positive real parts.

APPENDIX D

Adapting the Procedure for a Zero at the Origin

This appendix demonstrates the method of applying the criterion to the case where the system equation has a zero at the origin. Attention is confined to a small region around the origin where $|s\tau| << 1$. Using the series expansion for $e^{2s\tau}$ in the system equation, Eq. 122, gives

$$H_p(s) = 0.25(1 - b) + (1 - c + 0.5\tau)\, s$$

$$+ (2 - a + 2\tau + 0.5\tau^2)\, s^2 + \text{higher terms}. \tag{D.1}$$

If $b = 1$, there is a zero at the origin. For this case and small values of s, the equation can be approximated by a single term,

$$H_p(s) \simeq (1 - c + 0.5\tau)\, s. \tag{D.2}$$

The zero at the origin is excluded from inside either the absolute- or relative-stability contours by indenting each contour onto a circular path of small radius, r_1, around and to the right of the origin. On this path, Eq. D.2 becomes

$$H_p(r_1 e^{j\phi}) \simeq (1 - c + 0.5\tau)\, r_1 e^{j\phi}. \tag{D.3}$$

The real and imaginary parts of the right side of this equation are

$$F(\phi) = (1 - c + 0.5\tau)\, r_1 \cos\phi, \tag{D.4}$$

and

$$G(\phi) = (1 - c + 0.5\tau)\, r_1 \sin\phi. \tag{D.5}$$

The range of ϕ depends on the type of contour. If it is the one for determining absolute stability, ϕ ranges from $-\pi/2$ to $\pi/2$; if, for relative stability, ϕ ranges from $-2\pi/3$ to $2\pi/3$. In either case, the zeros of F and G no longer occur together; a double zero of F at the origin has separated into two. Therefore, with this identation, these alternating zeros can be considered along with those for the rest of the contour in determining system stability or relative stability.

ACKNOWLEDGMENTS

Acknowledgment is made to Professor A. G. Vacroux for his advice and helpful suggestions in the latter stages of the research and during the preparation of this report; to Professor C. H. Hoffman, who is now on assignment at Kabul University, Afghanistan, for his advice and guidance in the formulation of the research problem; and to Professor E. R. Whitehead for his advice and encouragement to continue with the program.

I wish to acknowledge the use of the facilities and equipment at Argonne National Laboratory. I am indebted to Mr. R. C. Goertz, former Director, Remote Control Engineering Division, and Mr. L. J. Koch, Director, Reactor Engineering Division, for their interest in this endeavor. Moreover, I express my appreciation to Mr. E. Hutter, Mr. W. C. Lipinski, and many others in both divisions, for their cooperation; and to Mr. R. Grench for his assistance in computer programming.

REFERENCES

1. Ray Goertz, *Manipulator Systems Development at ANL*, Proc. 12th Conf. Remote Syst. Tech., American Nuclear Society, p. 117 (Nov 1964).

2. R. C. Goertz and F. Bevilacqua, *Force-Reflecting Positional Servomechanisms*, Nucleonics *10*, No. 11, pp. 43-45 (Nov 1952).

3. R. C. Goertz, J. R. Burnett, and F. Bevilacqua, *Servos for Remote Manipulation*, National Convention Report, Institute of Radio Engineers, New York, N. Y., Part 9, pp. 103-109 (June 1953).

4. R. C. Goertz and W. M. Thompson, *Electronically Controlled Manipulator*, Nucleonics *12*, No. 11, pp. 46-47 (Nov 1954).

5. J. R. Burnett, R. C. Goertz, and W. M. Thompson, *Mechanical Arms Incorporating a Sense of Feel for Conducting Experiments with Radioactive Materials*, Proceedings of the International Conference on the Peaceful Uses of Atomic Energy, Geneva, 1955, Paper No. 712, United Nations, Vol. 14, p. 116 (1956).

6. W. M. Thompson and R. C. Goertz, *Master-Slave Servo-Manipulator, Model 2*, Fourth Annual Symposium on Hot Laboratories and Equipment, TID-5280, Dept. of Commerce, Office of Technical Services, Washington, D.C., p. 1 (1955).

7. R. C. Goertz *et al.*, *ANL Mark E4A Electric Master-Slave Manipulator*, Proc. 14th Conf. Remote Syst. Tech., American Nuclear Society, p. 115 (Nov 1966).

8. R. S. Mosher, *Force-Reflecting Electrohydraulic Servomanipulator*, Electro-Technology *66*, No. 6, pp. 138-141 (Dec 1960).

9. S. Barabaschi, S. Cammarato, C. Mancini, A. Pulacci, and F. Roncaglio, *An Electronically Controlled Servo-Manipulator*, Proc. 9th Conf. Hot Labs. Equip., American Nuclear Society, pp. 143-153 (Nov 1961).

10. R. C. Goertz, R. A. Blomgren, J. H. Grimson, G. A. Forster, W. M. Thompson, and W. H. Kline, *The ANL Model 3 Master-Slave Electric Manipulator -- Its Design and Use in a Cave*, Proc. 9th Conf. Hot Labs. Equip., American Nuclear Society, pp. 121-142 (Nov 1961).

11. R. Weiss, *Transportation Lag -- An Annotated Bibliography*, IRE Trans. on Automatic Control *AC-4*, pp. 56-64 (May 1959).

12. N. H. Choksy, *Time Lag Systems -- A Bibliography*, IRE Trans. on Automatic Control *AC-5*, pp. 66-70 (Jan 1960).

13. D. A. Pierre, *Transient Analysis and Synthesis of Linear Control Systems Containing Distributed-Parameter Elements*, Ph.D. thesis, The University of Wisconsin (1962).

14. M. N. Oguztoreli, *Time-Lag Control Systems*, Academic Press, New York and London (1966).

15. N. H. Choksy, *Time Lag Systems*, Progress in Control Engineering *1*, Heywood and Company, Ltd. (1962).

16. A. M. Krall, *Stability Criteria for Feedback Systems with a Time Lag*, J. Soc. Indust. Appl. Math., Series A: Control, Vol. 2, No. 2 (1965).

17. M. G. Spooner and C. H. Weaver, *An Analysis and Analogue Computer Study of a Force-Reflecting Positional Servomechanism*, Trans. AIEE *74*, Part 2 (Applications and Industry), No. 22, pp. 384-387 (Jan 1956).

18. C. Mancini and A. Pulacci, *Design of a Force-Reflecting Servomechanism with Magnetic Particle Clutches*, (in Italian), CNI-14, Comitato Nazionale per le Ricerche Nucleari, Milan, Italy, (June 1959).

19. W. J. Chalmers, *Bilateral Force-Reflecting Servomechanism Research-Servomechanism Synthesis Through Network Parameters*, Ph.D. thesis, Purdue University (1955).

20. L. E. Weaver, *A Study of Dead Time Delay in Feedback Control Systems*, Ph.D. thesis, Purdue University (1958).

21. R. C. Arzbaecher, *Servomechanisms with Force Feedback*, Ph.D. thesis, University of Illinois (1960); also, ANL-6157 (May 1960).

22. E. M. Schmidt, *Effective Reduction of Inertia and Friction in a Positional Servomechanism*, M.S. thesis, Purdue University (1957).

23. J. R. Burnett, *Force-Reflecting Servos Add "Feel" to Remote Controls*, Control Engineering *4*, No. 7, pp. 82-87 (July 1957).

24. T. B. Sheridan and W. R. Ferrell, *Remote Manipulative Control with Transmission Delay*, IEEE Trans. on Human Factors in Electronics *HFE-4*, pp. 25-29 (Sept 1963).

25. W. R. Ferrell, *Remote Manipulation with Transmission Delay*, IEEE Trans. on Human Factors in Electronics *HFE-6*, No. 1, pp. 24-32 (Sept 1965).

26. W. R. Ferrell, *Remote Manipulation with Transmission Delay*, NASA Tn D-2665 (Feb 1965).

27. T. B. Sheridan and W. R. Ferrell, *Progress Report*, Engineering Projects Lab., M.I.T., NASA N66-16394 (Jan 1966).

28. R. Bellman and K. L. Cooke, *Differential-Difference Equations*, Academic Press, New York, N. Y. (1963).

29. N. H. Choksy, *Analytic Determination of the Stability of Servomechanism and Other Automatic Control Systems Having Transcendental Characteristic Equations*, Ph.D. thesis, The University of Wisconsin (1955).

30. L. S. Pontryagin, *On the Zeros of Some Elementary Transcendental Functions*, American Mathematic Society Translations, Series 2, Vol. 1, pp. 95-110 (1955); translation of the paper in Izvestiya Akademii Nauk, SSSR, Ser. Mat., Vol. 6, pp. 115-134 (1942).

31. R. Bellman, *A Survey of the Mathematical Theory of Time-Lag, Retarded Control, and Hereditary Processes*, Rand Corporation Report R-256 (March 1954).

32. S. J. Bhatt and C. S. Hsu, *Stability Criteria for Second-Order Dynamical Systems with Time Lag*, J. Appl. Mech. *33*, Series E, No. 1 (March 1966).

33. C. S. Hsu and S. J. Bhatt, *Stability Charts for Second-Order Dynamical Systems with Time Lag*, J. Appl. Mech. *33*, Series E, No. 1 (March 1966).

34. A. Jeffrey, *The Stability of Interacting Control Systems*, Automatic and Remote Control *1*, pp. 126-131, Butterworths, London (1961).

35. L. Hsun-Ching, *On the Absolute Stability of Systems with Time Lags*, Chinese Mathematica *4*, No. 4, pp. 609-626 (1963); translation of Acta Mathematics Sinica *13*, No. 4 (1963).

36. I. M. Repin, *Quadratic Liapunov Functionals for Systems with Delay*, Journal of Applied Mathematics and Mechanics *29*, pp. 669-672 (Aug 1966); translation of Prikladnaya Matematika i Mekhanika, PMM *29*, No. 3, pp. 564-566 (1965).

37. Chin Yuan-Shun, *Unconditional Stability of Systems with Time-Lags*, Chinese Mathematics *1*, No. 1, pp. 138-155 (1960); translation of Acta Mathematica Sinica *10*, No. 1 (1960).

38. L. Eisenberg, *Stability of Linear Systems with Transport Lag*, IEEE Trans. on Automatic Control *AC-11*, No. 2, pp. 247-254 (April 1966).

39. R. Bellman and R. Kalaba, ed., *Selected Papers on Mathematical Trends in Control Theory*, Dover Publications, New York (1964), Paper 5: "Regeneration Theory," by H. Nyquist.

40. L. S. Dzung, *The Stability Criterion*, Automatic and Manual Control, pp. 13-22 and pp. 35-44, Butterworths Scientific Publications, London (1952).

41. C. H. Hoffman, *How to Check Linear System Stability, III--Locating the Roots Graphically*, Control Engineering *12*, No. 6, pp. 71-78 (June 1965).

42. M. Satche, discussion, Journal of Applied Mechanics *16*, pp. 419-420 (Dec 1949).

43. H. S. Tsien, *Engineering Cybernetics*, Chapter 8, McGraw-Hill, New York (1954).

44. G. J. Murphy, *Basic Automatic Control Theory*, Second Edition, D. Van Nostrand Company, Princeton, New Jersey (1966).

45. Y. Chu, *Feedback Control Systems with Dead-Time Lag or Distributed Lag by Root-Locus Method*, Trans. AIEE *71*, Part II, pp. 291-296 (Nov 1952).

46. E. Pinney, *Ordinary Difference-Differential Equations*, University of California Press, Berkeley, California (1959).

47. E. Hille, *Analytic Function Theory*, Volume 1, Chapter 9, Ginn and Company, Boston (1959).

ARGONNE NATIONAL LAB WEST
3 4444 00011303 5